Journal of Energy Storage 27 (2020) 101082

Contents lists available at ScienceDirect

Journal of Energy Storage

journal homepage: www.elsevier.com/locate/est

Melting and solidification of PCMs inside a spherical capsule: A critical review

Murat M. Kenisarin*, Khamid Mahkamov, Sol Carolina Costa, Irina Makhkamova

Department of Mechanical and Construction Engineering, Northumbria University, Newcastle upon Tyne, NE1 8ST, United Kingdom

ARTICLE INFO

Keywords:
PCM
Melting
Solidification
Heat transfer
Latent heat storage

ABSTRACT

To date, numerous phase change materials (PCM) have been developed for application in latent heat storage systems. There are many issues in the process from the development of PCM to using them in storage systems, which should be resolved. The problem of heat transfer in PCMs during the phase change process is the most important one. Latent heat storage containers usually have simple geometrical forms such as a sphere, cylinder, cylindrical annulus, rectangular enclosure, etc. A large number of papers were published on melting and solidification processes in PCMs. Therefore, there is a pressing necessity for generalizing the art of the state in this field and establish how accumulated knowledge meets practical requirements. The present review considers the current state in investigations of heat transfer in a spherical shell. Heat transfer in PCMs during constrained melting (solid PCM fixed inside the vessel), unconstrained (unfixed) melting and solidification, and phase change in finned shells are analyzed. It is shown that currently, there is no satisfactory description of the constrained melting process. For unconstrained melting and solidification, some correlations are suggested, describing these processes. The applicability range of the proposed correlations, as well as their accuracy were investigated and established. To intensify the process of phase change inside the spherical container, the use of orthogonal fins is appropriate option compared to the employ of circumferential fins.

1. Introduction

Currently, latent heat storage systems (LHSS) with the use of phase change materials (PCMs), are at the focus of numerous research projects. The developments in the latent heat storage technology, using PCMs, have been reported in [1–6]. In comparison with traditional sensible heat storage systems, latent heat TESs have significantly higher specific energy capacity per mass or volume. Moreover, the charging and discharging processes in LHSS take place in the narrow temperature range, close to the melting temperature of PCMs. It should be noted that most prospective PCMs have low thermal conductivity, and this restricts the speed of charging and discharging processes. Every LHSS contains at least the following three components. First, it has a suitable PCM with the desired melting/solidification temperature range. Second, the suitable container should be used for housing PCM. Third, a suitable heat exchanger is required for transferring the heat effectively from a heat transfer fluid (HTF) to the PCM and vice versa. There is the large number of phase change materials, which produced by the leading companies [7–14]. For encapsulating the PCMs, such materials as plastics, aluminum, copper, stainless steel are used. Presently, the most studied geometrical configurations of containers for housing PCMs are spheres, cylindrical tubes, annulus, rectangular plates, and pouches [15, 16].

A typical LHSS serves as a buffer between energy sources and a consumer, and it transfers thermal energy at certain rates at times when the consumer requires it. Usually, during such energy discharging periods, there is no direct supply of the heat from a source. For meeting consumer's heat demand, the storage system should also provide the required rate of heat transfer between the PCM and HTF during the charging and discharging process. In General, during heat transfer process between HTFs and PCMs there are at least the following two problems. The first one is related to enhancing heat transfer from the body of PCM to surfaces, which separate PCMs from HTFs. This problem is solved by deploying many suitable types of heat exchangers. The second problem is the heat transfer inside the envelope containing the PCMs.

The results of experimental, analytical, and numerical studies of phase-change heat transfer performed up to 2000 have been discussed in [17–21]. The investigations results presented in these reviews had mainly the academic character. In one way or another, the practical aspects of phase change heat transfer were considered in review papers [3–5, 22–25]. As it is known that the heat transfer in PCM containers

* Corresponding author.
E-mail address: murat.kenisarin@northumbria.ac.uk (M.M. Kenisarin).

https://doi.org/10.1016/j.est.2019.101082
Received 6 August 2019; Received in revised form 8 November 2019; Accepted 16 November 2019
Available online 29 November 2019

Nomenclature

Ar	Archimedes number ($(\rho_s - \rho_l)gD^3/\rho_s\nu^2$)
Bi	Biot number (Lh/k)
c_p	Specific heat (kJ/kg•K)
f_m	Molten PCM mass fraction
Fo	Fourier number (k/ρ c_p) t/R^2)
f_s	Solid PCM mass fraction
g	gravity vector (m/s^2)
Gr_R	Grashof number (gβ(T_{pcm}-T_m) $R_i^3\rho^2/\mu^2$)
MF	Molten fraction
H	fin height (m)
H_m	heat of fusion (kJ/kg)
HTF	Heat transfer fluid
k	thermal conductivity (W/mK)
k_{eff}	effective thermal conductivity (W/mK)
N_c	conduction-to-radiation parameter $[k/\sigma(T_w - T_m)r_o]$
P	Pressure (N/m^2)
Pr	Prandtl number of the fluid (μ c_p/k)
r	radius (m)
r*	dimentionless radius (r/R_i)
Ra_R	Rayleigh number $(g\beta(T_s - T_{cf})R^3/\alpha\upsilon)$
r_f	radius of the solid-liquid interface (m)
R_i	inner radius of the spherical shell (m)
s	shift of reference point fixed in solid core (m)
Ste	Stefan number (c_p (T_{pcm}-T_m)/H_m)
t	time (s)
T	temperature (˚C)
T_w	wall temperature (˚C)
T_∞	temperature of entering HTF (˚C)
U	dimensionless temperature ($U = T/(T_\infty - T_m)$

Greek symbols

β	thermal expansion coefficient (1/K) or $1/Bi$
θ	Dimensionless temperature
μ	dynamic viscosity (kg/m s)
ξ	Dimensionless position of solid-liquid interface
ρ_l	Liquid density (kg/m^3)
ρ_s	Solid density (kg/m^3)
σ	Stefan-Boltzmann coefficient (W/(m^2K^4)
τ	Dimensionless time
τ_f	Dimensionless time of complete freezing
τ_m	Dimensionless time of complete melting

Subscripts

eff	Effective value
f	freezing
l	Liquid
m	Molten
s	Solid

can be enhanced with fins, heat pipes, metal honeycombs, metal matrices (wire mesh), rings, high conductivity particles, metal fibers or graphite, etc. and relevant publications were considered in [25–26].

From the reviews mentioned above follows that there is still several practical issues, for which the developers of LHSSs do not have recommendations, and these include heat transfer issues in PCMs. It can be explained by existence of a significant diversity of studied objects and their geometries. On another hand, there are many publications, results of which cannot be used on a larger scale due to particularities of studied individual cases. Currently, active LHSSs are become increasingly attractive for researchers and developers. For such systems, the LHSS with certain dynamic characteristics should be deployed. The improved dynamic performances may be only achieved by the substantial increase in the heat transfer surface and enhancing the thermal conductivity of the PCM. In previously cited review papers, problems of heat transfer in PCMs and enhancing their thermal conductivity were discussed. For analysis of heat transfer problems in PCMs contained in a storage unit with complex geometry, it is required firstly to apply existing advanced knowledge on examining similar processes in containers with simple forms and without any additional inclusions.

The rapid development of research in the field of latent heat storage stimulated the development of various TES designs for particular applications. Following recent studies [27–35], the spherical capsules with PCM, are very perspective in the packed bed TES devices for solar heating and cooling systems. For instance, Cristopia Energy Systems [36] builds packed bed latent thermal energy storage systems for air conditioning of big buildings around the world. As known, some practical success achieved in using the spherical encapsulation of PCMs. Despite of many publications, there is no general approach developed for the solution during melting and solidification heat transfer inside spherical shells. The present paper critically considers analytical, numerical, and experimental studies of heat transfer during the phase change of PCMs inside such spherical containers.

The primary purpose of the present review is the detailed analysis of the state of investigations and developments in the field of the phase change heat transfer in latent heat storage materials encapsulated into spherical enclosures. The applicability of results of considering studies for engineering methods of calculation of TES performances (energy stored or released) depending on the size of a spherical capsule, initial and operational conditions, a PCM material, and other factors is in the focus of the present analysis.

Among investigations performed in last two decades, there are very interesting experimental and numerical works. Thus, the effect of Stefan, Bio, Prandtl numbers, as well as other factors on intensity of melting and solidification processes have been observed. Unfortunately, the qualitative results obtained in such studies [37–43, etc.] repeat the facts, which were obtained by previous researchers. Therefore, we believe that it is necessary to give the basic theory of PCM melting and solidification processes and to note the great researchers who made a significant contribution in this field.

2. Basic theory of PCM melting and solidification processes

Before the analysis of issues in achieving the large heat transfer surfaces between PCM and HTF, it is necessary to clearly understand the physical processes of heat supply and removal during PCM melting and solidification processes. To achieve such a goal, all major factors, which affect the dynamics of these processes, should be considered. There is a large number of applications in which a material undergoes a phase change, e.g. melting and freezing (solidification). Heat conduction in these processes is accompanied by a moving interface, separating two phases. Such a problem is called "moving boundary problem" or Stefan's problem. The formulation of the problem and its solution can be found in [44]. Stefan considered a simplified model with the following assumptions: (1) one-dimensional conduction, (2) constant properties of the liquid and solid phases, (3) no changes in the fusion temperature and (4) quasi-steady state with the Stefan number less than 0.1. Solidification of the matter in a one-dimensional liquid region shown in Fig. 1. Initially, the liquid is at the melting temperature Tf. Then the surface at $x = 0$ suddenly assumes the temperature $T_o < T_f$, while the opposite surface of the slab at distance L (thickness of the slab) is maintained at T_f. The time required for complete solidification is found in [44] as

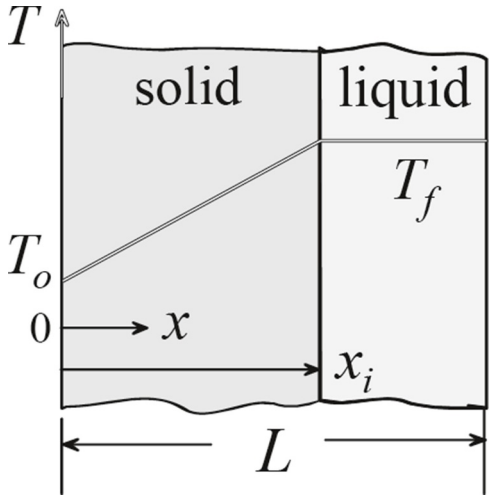

Fig. 1. Solidification of one-dimensional slab at the fusion temperature [44].

$$t_o = \frac{\rho_s H_m L^2}{2k_s(T_f - T_o)}, \quad (1)$$

where ρ_s is the density of solid phase, k_s is the thermal conductivity, H_m is the heat of fusion. From this formula, it follows that the solidification time depends linearly on the volumetric heat of fusion (ρH_m) of the PCM and squared value of the layer's thickness. The solidification time also inversely depends on the thermal conductivity and the difference between the PCM's freezing temperature and HTF's temperature.

Due to the constancy of melting heat, the solidification time critically depends on such the physical property as thermal conductivity, the design parameter (the thickness of PCM layer), and the operational parameter as ($T_f - T_o$). These highlighted crucially important factors should be the subject of optimization in any LHSS. For low-temperature solar heating systems combined with the latent heat storage system, it critically important to provide the optimal differences between the HTF temperature and the PCM temperature ($T_f - T_o$) during the charge and discharge of the LHSS. Due to the significant variation of HTF temperature in solar collectors, the HTF maximum temperature at charging process is restricted by the efficiency of the solar collector. On the other hand, the HTF temperature at discharge process is restricted by the minimum permissible temperature of the HTF.

During the melting process, heat transfer is as a result of the combination of thermal conduction and natural convection mechanisms. Research groups headed by Profs E. M. Sparrow and R. Viskanta at Minnesota and Purdue Universities respectively made a significant contribution to understanding the processes of melting and solidification. Thus, Viskanta [17] has made the fundamental review of works performed before 1983. Unfortunately, this review book was published in small numbers and therefore was not widely accessible to the research community. The book of G.A. Lane is recently reprinted. Other comprehensive reviews such as [18–21] also remained mostly unknown to researchers in the field. On the other hand, over the last 20 years, a great number of research studies were published in which it was concluded that the natural convection had a dominant role in the melting process. Interestingly, this dominant role of natural convection in melting processes was already established in classical works of Sparrow et al. [45] and Hale and Viskanta [46], which were published about 40 years ago.

3. Heat transfer during melting of PCM inside a spherical enclosure

3.1. Constrained melting

Khodadadi and Zhang [47] were the first to perform the computational and experimental study of buoyancy-driven convection on the constrained melting within a spherical enclosure. The physical model considers a spherical container of radius R, which houses a solid PCM (silicon) at temperature T_i lower then T_m. The phase change material is initially subcooled. For time $t > 0$, a constant temperature (T_o), which is greater than the melting temperature, was imposed on the surface of the sphere, i.e., To > Tm. To validate the computational findings, a set of melting experiments were conducted. Paraffin wax was used as the PCM with the melting point of 62–64 °C and Prandtl number of about 57. Spherical bulbs with outside diameters of 51.5, 78.1, 94.0 and 123 mm were used in experiments. The PCM with a starting temperature of 60 °C was placed into the water bath with a temperature of 73 °C. The process of paraffin wax melting was photographed, and these are presented in Fig. 2. The parameter t^* in this figure is the dimensionless time (*Fo•Ste*). For instance, the actual time needed to melt the PCM to the state, shown at the dimensionless time $t^* = = 0.0293$, corresponds to 134 min. Analysis of taken photographs demonstrated that the dominant role of buoyancy-driven convection occurs starting at $t^* = = 0.0164$. The numerical study and visual observations of the constrained melting carried out in [45] were summarized by authors as follows:

- The conduction mode of heat transfer is dominant at the early stages of melting;
- Melting process is much faster at the top region of sphere, compared to its bottom part;
- The Rayleigh number determines the magnitude of natural convection effect in the melting process to a greater extent than the Stefan number;
- The Prandtl number also has a significant effect on the melting process;
- The observed intensive melting process at the top region of the

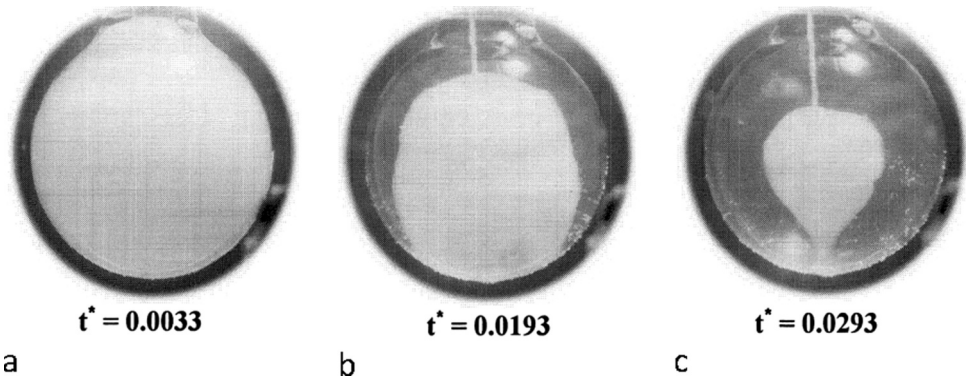

Fig. 2. Instantaneous photographs of melting of wax inside a spherical bulb [47].

sphere is caused by natural convection, which determined by the buoyancy forces (the difference between densities of PCM in solid and liquid phases).

Tan [48] carried out the experimental study of constrained and unconstrained melting of PCM inside a spherical enclosure. N-octadecane was used as the PCM for investigations. The spherical flask with a diameter of 101.66 mm and a volume of 550 cm^3 was filled with the molten PCM. For constrained melting, three experiments were performed at three different initial sub-cooling levels of 1, 10, and 20 °C for a constant temperature of 40 °C at the surface of the sphere. The typical experimental results for the constrained melting are presented in Fig. 3. In experiments with the initial sub-cooling level of −10 °C, it was observed that the natural convection starts to play a dominant role in the heat transfer process after 30 min from the beginning of the experiment. This period corresponds to $t^* \approx 0.046$ (our estimation), which is significantly higher than 0.0164, obtained in [47]. The contours of melting process shown in photographs in [47] and [48], also significantly differ. It is worth noting that under the same experimental conditions, the unconstrained melting inside the sphere occurs at a faster rate than during constrained melting. Thus, the time required for constrained melting was 130 min, whereas only 80 min were required for the unconstrained melting. During the constrained melting, heat conduction plays a role only at the beginning of melting process. This effect causes the PCM to melt inwards in almost concentric manner. An oval shape-melting pattern is formed at the top half of the solid PCM but the profile at the bottom remains relatively unchanged. The oval shape phase front is caused by the natural convection when the liquid layer increases. Natural convection occurs because of the warm liquid PCM rises along the hot wall while the cooler liquid in the center flows down to replace the warmer fluid. This creates an unstable fluid circulation inside the sphere, known as buoyancy-driven convection. The top part of PCM melts at a faster rate than its bottom half. Natural convection also occurs at the bottom half of the vessel, thus resulting in the wavy profile of the bottom part of PCM.

Tan with colleagues [49] conducted a comparative study of experimental results, presented in [46], and numerical simulations on the constrained melting of PCM. Fig. 4 shows the instantaneous values of the liquid fraction within the spherical capsule found numerically and experimentally. It can be seen, that the computational technique predicts a faster rate of constrained melting. Experimental data was obtained using the digitalization of the photographs with the solid-liquid interface (similar to those in Fig. 3). Three-dimensional melting effects, which were not accounted for in the modeling, cause the observed differences in sets of results.

Khot et al. [50] carried out an experimental investigation of constrained and unconstrained melting of paraffin wax inside a spherical capsule. In the study, the sample of paraffin wax was used with the melting point of 59.8 °C and the heat of fusion of 190 J/g. The borosilicate glass spherical capsules with a diameter of 85 mm was used for

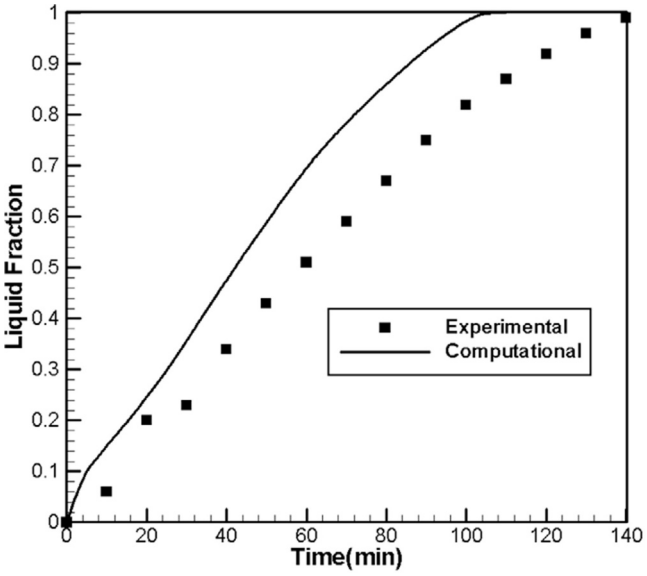

Fig. 4. Computational and experimental variation of the liquid fraction as a function of time [49].

melting process observation. Preliminarily, capsules were maintained at a constant initial temperature of 27 °C. When the water reached the required temperature, the capsules were placed into the test water tank, and the melting process was started. A digital camera captured the process of melting by taking photos with 10 min intervals. The tests were conducted for four HTF temperatures of 62, 70, 75 and 80 °C for both constrained and unconstrained melting of the PCM inside the capsule. Fig. 5 presents the instantaneous photographs of wax melting during one of the experiments. The effect of Stefan number on forming molten fraction during the constrained melting was studied. At the Stefan number of 0.227, paraffin wax completely melted within 55 min compared to 60, 80, and 115 min for Stefan numbers equal to 0.171, 0.114, and 0.024, respectively. The higher Stefan number (i.e. higher ΔT) results in, the shorter time, required for complete melting in both constrained and unconstrained modes of melting. It is easy to note that the contours of the solid-liquid interface observed in [45] differ from those presented in [46].

In 2015, Galione et al. [51] presented the results of the fixed-grid numerical modeling of melting of n-octadecane inside a spherical capsule. A comparison of predicted values with data of Tan et al. in [49] demonstrated that only three-dimensional simulations provide a close approximation to the experiment, see Fig. 6.

Li et al. [52] reported results of another numerical study on the constrained melting of PCM inside a spherical capsule. For validation of the mathematical model, the experimental observation of the constrained melting of paraffin wax inside the spherical glass flask was

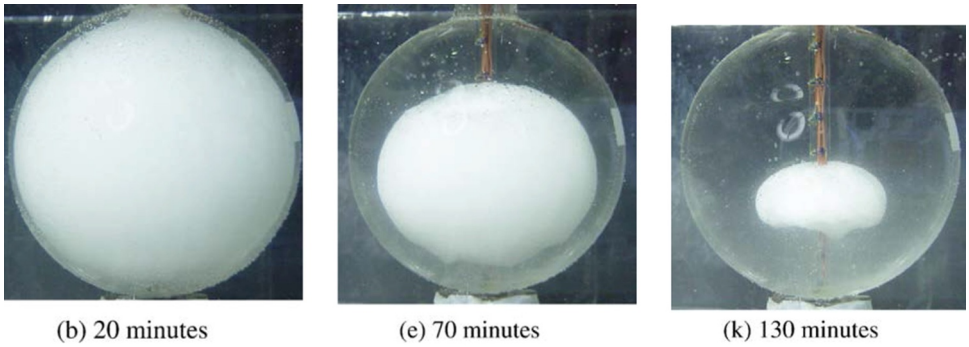

Fig. 3. Constrained melting phase fronts at 40 °C with the initial sub-cooling of 10 °C [48].

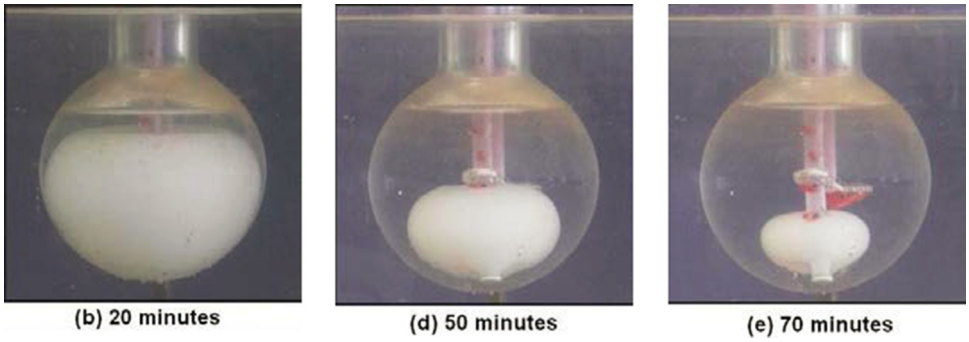

Fig. 5. Constrained melting phase front at 70 °C [50].

conducted, see Fig. 7. The paraffin melts in the range of 45.8 and 50.3 °C and has a latent heat of 129 kJ/kg. Its specific heat capacity in solid/liquid state is 2/1.5 kJ/kgK, thermal conductivity in solid/liquid state is 0.27/0.15 W/mK and density in solid/liquid state is 916/776 kg/m^3. For solving the governing equations, the SIMPLE method within Fluent software was used. The effects of the sphere radius (4, 5, and 6 cm), the PCM thermal conduction coefficient (0.2, 2, and 5 W/mK), the spherical shell material (aluminium, steel, plastic) and the external (bath) temperature (50, 55, 60 °C) on the molten fraction of PCM inside a sphere were investigated. Based on the results presented,

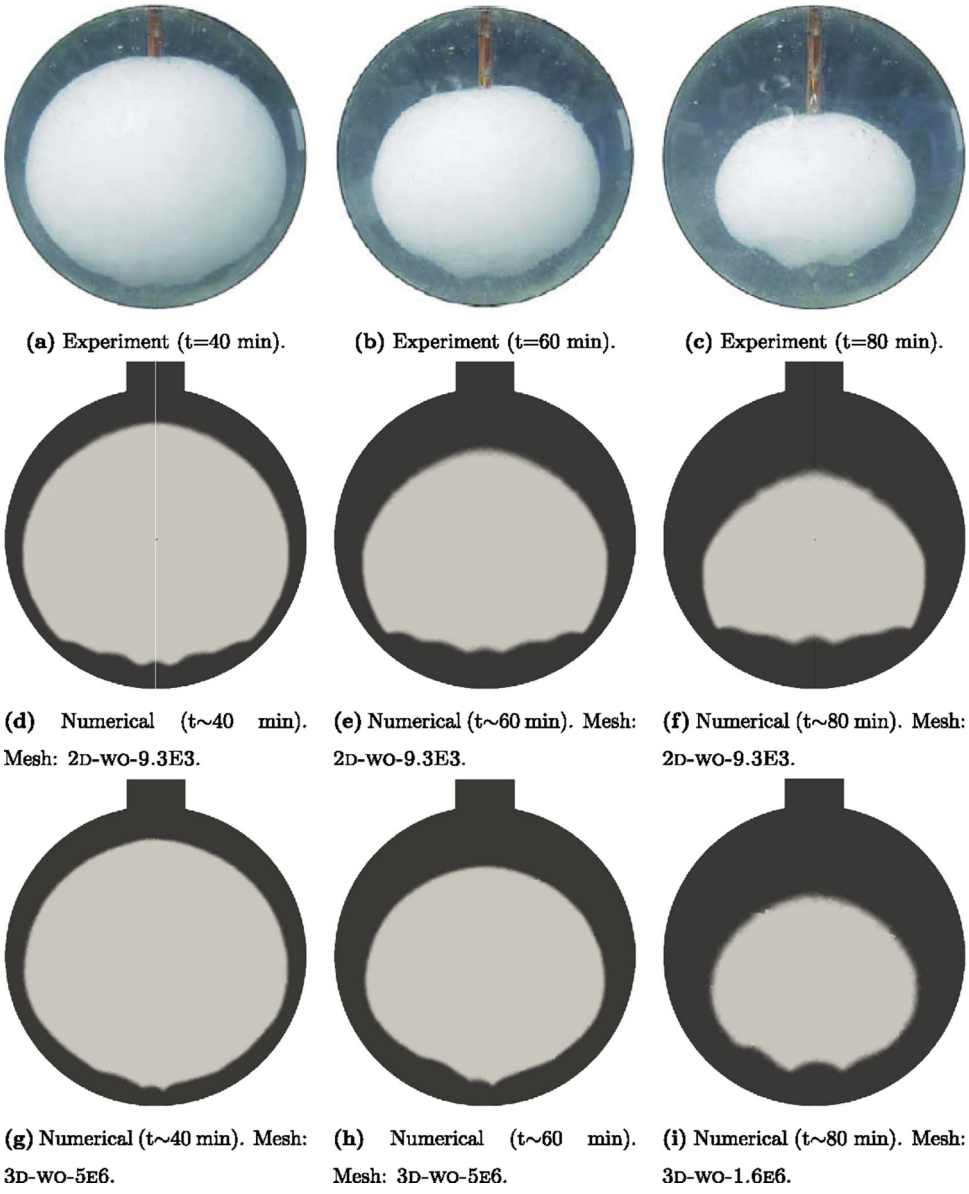

Fig. 6. Comparison of the experimental photographs of Tan et al. [49] and numerical results for the case C, using variable properties, with 2D and 3D meshes. Liquid fraction map (dark - liquid; light - solid) is shown for the numerical results [51].

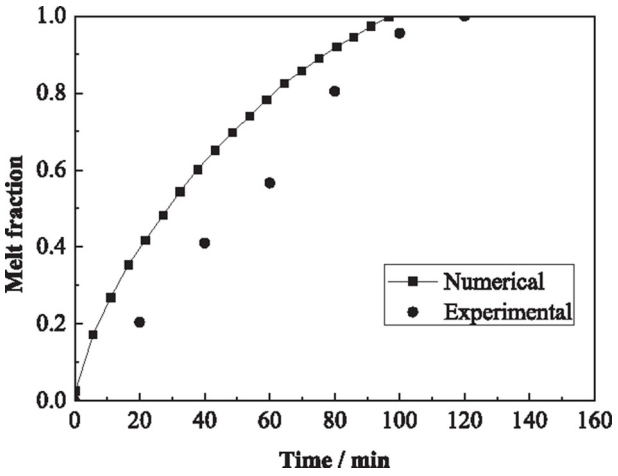

Fig. 7. Comparison of the experimental and numerical molten mass fractions [52].

the following conclusions were made:

- With the same initial temperature and bath temperature, the smaller the sphere is, the faster the PCM melts. To intensify charging and discharging process in a LTSS, small diameter spheres are preferred;
- The bath temperature has a great effect on the melting of PCM inside a sphere. The PCM melts faster in spheres with the same radius if the bath temperature is increased;
- The higher thermal conductivity of PCM results in faster melting process;
- The metal shells with high thermal conductivity are preferred for accelerating the melting process if conditions are non-corrosive; the plastic shells can be used for corrosive conditions.

In fact, the above general conclusions could be drawn without particular experiments and numerical simulations. Despite conducting comprehensive numerical simulations, no empirical dimensionless correlations were proposed.

Sattari et al. [53] performed the CFD simulation of the constrained melting process of n-octadecane inside the spherical container with the same geometrical parameters as in [49]. The variation of the solid-liquid interface with time is shown in Fig. 8. The comparison of these computational results with experimental data of Tan et al. in [49] is presented for the same period in Fig. 6, which shows that the mathematical model used by Sattari et al. [53] describes the melting process less accurately than the model developed by Galione et al. [51]. In the study, no correlations were proposed for engineering evaluations

Soni et al. [54] performed a numerical investigation of constrained melting for identifying the reasons in the discrepancy between numerical predictions and experimental results. The study considered three cases. Case 1 analyzed a sphere with a diameter of 101.66 mm without thermocouple tube placed in the shell. Case 2 reproduced experimental conditions in tests by Tan et al. [47], while Case 3

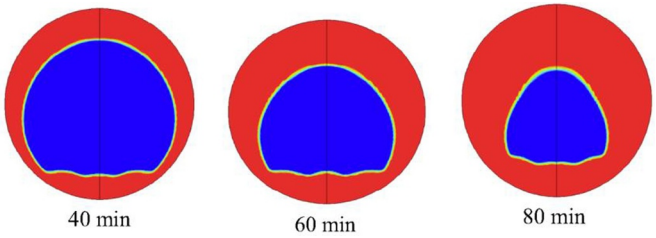

Fig. 8. Constrained melting phase front at different times for the wall temperature of 40 °C and initial temperature of 27.2 °C [53].

considered differences in thermal conductivity of the liquid and solid PCM. The computational results for variation of the solid-liquid interface with time and experimentally measured results [47] are presented in Fig. 9. Despite some differences in geometrical forms of experimental and computational interface, the predicted liquid fractions are in very good agreement with experimental data (see Fig. 10). The main conclusion from the numerical simulations was that Case 3, which considers different solid and liquid phase properties, produced the most accurate predictions. However, the developed model was not used for derivation of the dimensionless correlation for calculation of variations in the liquid fraction.

Prabakaran et al. [42] studied experimentally the constrained melting behaviour of OM 08 PCM (Pluss Advanced Technology, India) modified with graphene nanoplatelets (GnP). The PCM is based on fatty acids composition with melting temperature of 8 °C. The volume percentage of the GnPs varied from 0.1 to 0.5%. The thermal conductivity and viscosity of all tested samples were preliminarily measured. The experiments were carried out using the spherical aluminum flask with an inner diameter of 80 mm and a thickness of 1.6 mm. Five resistance temperature sensors fixed the temperature distribution within PCM. The measurements showed that the addition of 0.5 vol.% of GnP increases the thermal conductivity of the PCM nanocomposite from 0.228 to 0.444 W/mK, as well as rises the melting rate significantly. Experiments demonstrated that the conduction heat transfer dominates at the initial stage of melting, whereas the natural convection heat transfer prevails at the more late stage. Melting of the PCM in the upper part of the spherical shell is faster than that in the bottom part due to the natural convection currents.

3.2. Unconstrained melting

Moore and Bayazioglu [55] studied the heat transfer for unconstrained melting inside a spherical capsule computationally and experimentally. The solid's density was assumed to exceed that of the liquid, the implication being that the solid will continually descend as the material melts away from its underside. This movement generates a fluid motion, which contributes to a convective term in the energy equation, written for the liquid region. Tests were conducted in a well-insulated 10-gallon water bath using glass spheres with radii of 3.272 and 2.789 cm and the average wall thickness of 1.5 mm. The cut in the insulation of the water bath made it possible to observe and take photographs of the process. Octadecane was used as the PCM. The surplus in the PCM's volume (about 5–6%), generated during the melting of the solid substance, was stored at the top region of the sphere. The typical results from calculations of the interface position are presented in Fig. 10. The comparison of numerical simulations and experimental data shows a reasonable agreement, see Fig. 11.

Bahrami and Wang [56] considering a sphere of the radius R, containing the PCM, which initially was in the solid phase at the melting point, and then the temperature was suddenly risen. It was found that the correlation between the dimensionless time τ and dimensionless downwards distance travel of solid ξ can be presented as

$$\tau = \left(\frac{Ste}{\mathrm{Pr}Ar}\right)^{1/4}\left(\frac{\rho_s}{\rho_l}\right)(1.56\xi + 0.279\xi^2 + 0.261\xi^3 - 0.0686\xi^4 \quad (2)$$

Assuming that the entire mass of PCM is molten when $\xi = =1$, the melting time takes the form of

$$\tau_f = 2.03\left(\frac{\rho_s}{\rho}\right)\left(\frac{Ste}{\mathrm{Pr}Ar}\right)^{1/4} \quad (3)$$

The parameter τ/τ_f is the relative time and is equal to the ratio of current time elapsed and time, required for complete melting, and can be expressed in terms of ξ. Fig. 13 illustrates the correlation between these values and it can be seen that the relationship is almost linear. This fact implies that the solid fraction descends during the melting

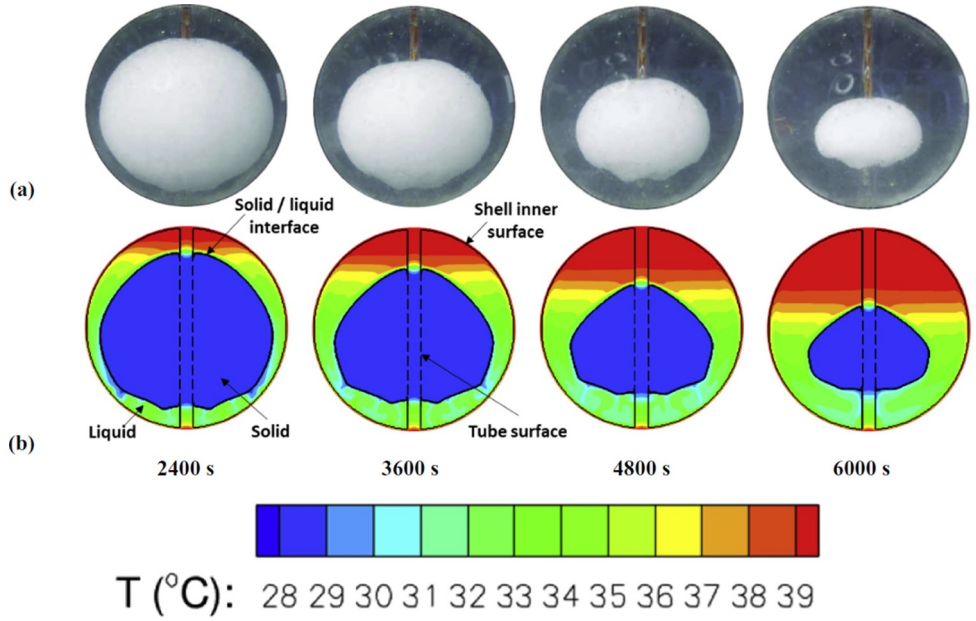

Fig. 9. Comparison of the predicted melting behaviour of PCM for Case 3 with the experimental results (a) Experimental snapshots (Tan et al. [49]) (b) Temperature map [54].

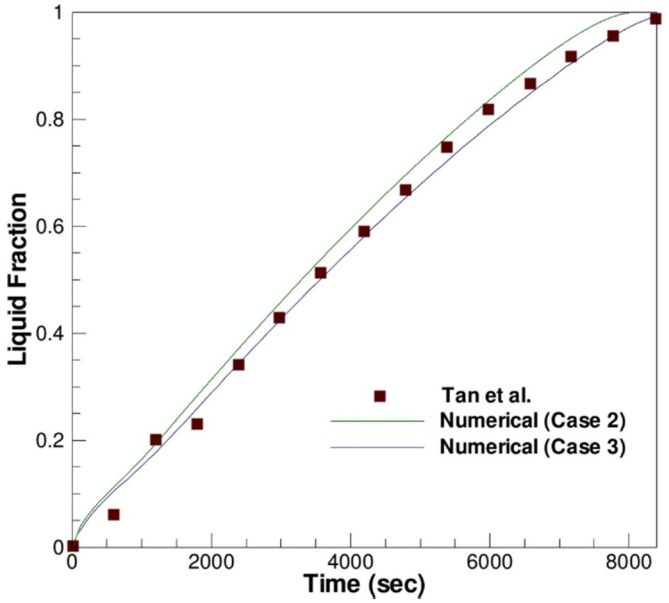

Fig. 10. Solid-liquid interface position at various stages of melting [55].

process at a relatively constant speed. A comparison of the correlation with experimental data of Moore and Bayazitoglu [55] shows a good agreement only for FoSte less than 0.001. For *FoSte* greater than 0.001, theoretical values are greater than experimental data by about 20%.

By studying the unconstrained melting process within the spherical shell, Roy and Sengupta [57] improved the method of Bareiss and Beer [58] by eliminating their assumption, made for the film thickness, and used for analysis of melting process in cylindrical capsules. The suggested correlation for the calculation of the solid PCM motion downwards (drop) was derived numerically, and results are shown in Fig. 13. A comparison of computational and experimental data by Moore [59] indicated that the theory predicts the greater melting rate. The maximum deviation from the experimental results is about 16%. The

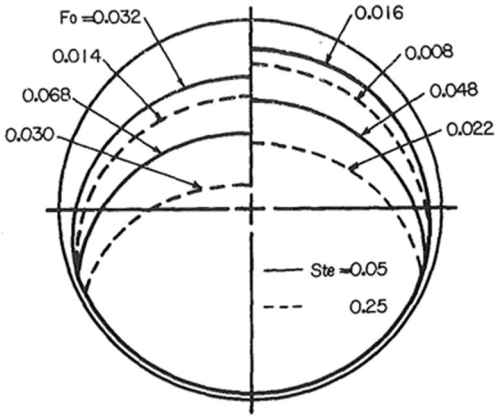

Fig. 11. Comparison of interface positions with experimental data for R = 32.72 mm, θ = =0, Ste = =0.05 and 0.1 [55].

performed analysis indicates that:

- The temperature differences have a greater effect with the downwards motion (drop) rate being proportional to $(\rho^{*}Ste/Pr)^{3/4}$;
- The melting rate increases with a rise in the temperature difference between the wall and solid PCM, the size of the enclosure and the difference between the solid and liquid PCM densities;
- The melting rate decreases with an increase in the latent heat of melting and viscosity of the fluid. It was shown that the film thickness increases with time owing to the solid volume decreases at a faster relative rate than the supporting surface area, resulting in a slower melting rate.

Toksoy and İlken [60] obtained primary data, which could be useful for determination of the charge time during PCM melting in a spherical container. They performed the experiments with melting of calcium chloride hexahydrate ($CaCl{\cdot}6H_2O$, the melting point is 27.22 °C) in the spherical enclosure exposed to the flow of hot air. Fig. 15 shows the

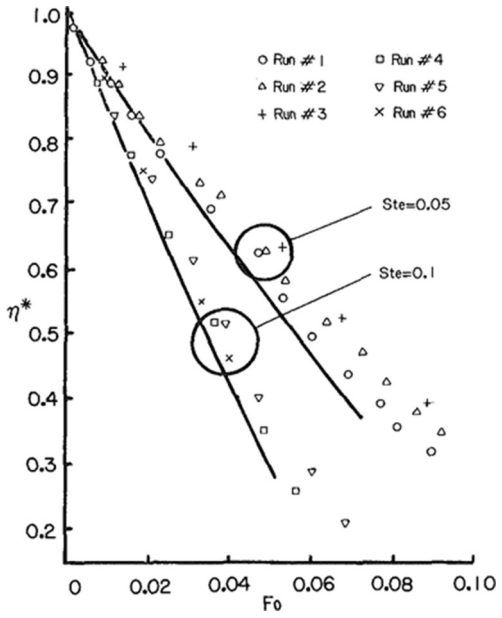

Fig. 12. Ratio of the solid PCM travel distance to sphere diameter as a function of the relative time [56].

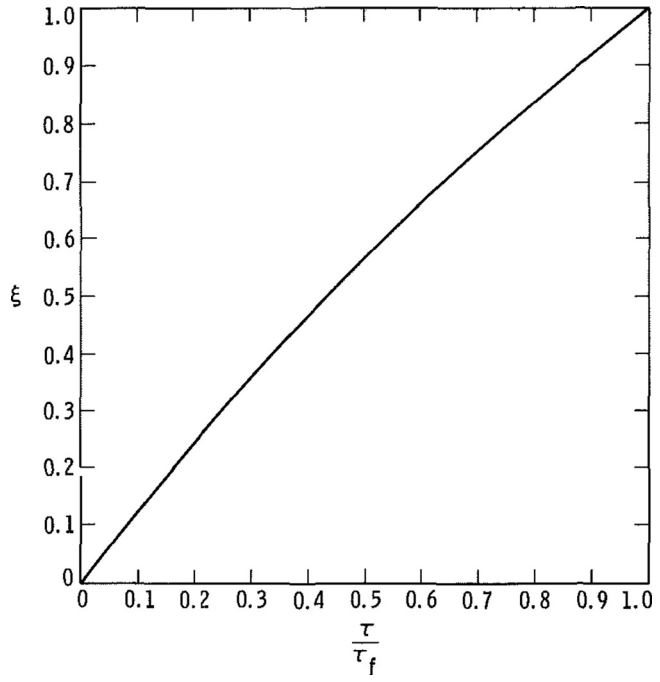

Fig. 13. Ratio of solid travel distance to sphere diameter as a function of normalized time [57].

schematic of an experimental setup used in that study. In seven experiments, they used two glass spheres with the inner radii of 3.93 and 2.34 cm, connected with expanding plastic tubes. The results of their experiments are presented in Table 1. The stored energy was calculated by using the relation given by Carlsson and Wettermark [61]:

$$Q_{stor} = \frac{H_m}{\Delta V_z}\frac{d(\Delta V)}{dt} \quad (4)$$

where ΔV is the amount of volumetric expansion of the PCM during melting, ΔV_z is the difference in specific volume between the liquid and solid phase of PCM. The volumetric expansion was measured during experiments and the stored energy was calculated using Eq. (4). The

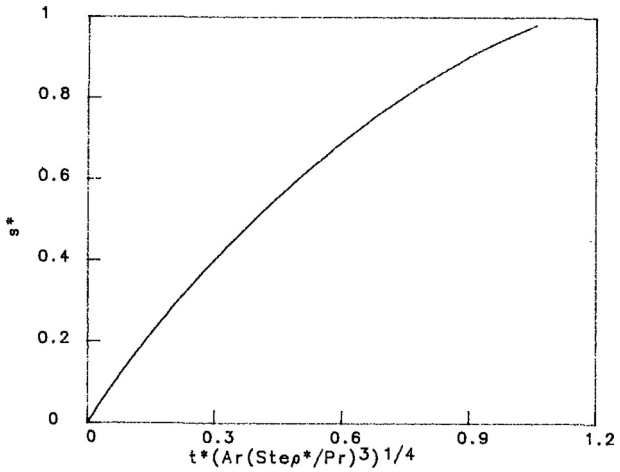

Fig. 14. Experimental set-up for study of PCM melting process in single spherical container [57].

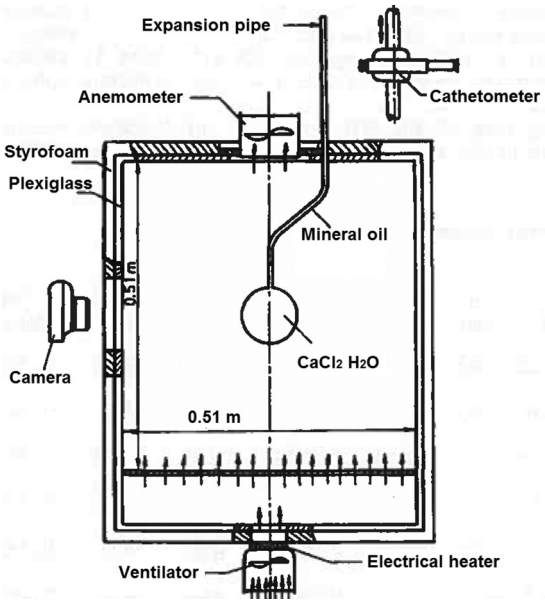

Fig. 15. Molten mass fraction versus dimensionless time [60].

comparison of the experimental results with Solomon's [62] and Moore's [59] solutions showed that analytical solutions provide significantly overestimated values.

Saitoh et al. [63] performed the theoretical analysis for combined

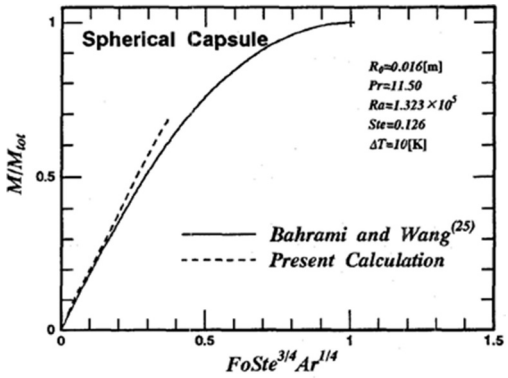

Fig. 16. Comparison of results for the solid PCM descending distance versus time (Ste = =0.05, 0.10) [64]. In the graph, [2] corresponds to Bahrami & Wang [56]; [5] – to Moore & Bayazitoglu [55].

Table 1
Experimental parameters and results obtained by Toksoy and İlken [60].

Experiment number	T_{air} (°C)	PCM mass (gram)	Container radius (cm^2)	Sphere surface area (m^2)	Stefan number	Complete melting time (s)	Stored energy (kJ)	Heat flux (kW/m^2)
1	39.9	424.85	3.93	0.0194	0.0946	16080	49.47	0.1586
2	40.0	424.85	3.93	0.0194	0.0950	14488	46.0	0.1614
3	40.3	434.11	3.93	0.0194	0.0976	17317	58.09	0.1730
4	39.9	434.11	3.93	0.0194	0.0946	16223	54.23	0.1723
5	40.3	82.81	2.34	0.0069	0.0976	8391	11.5	0.1987
6	39.7	82.81	2.34	0.0069	0.0930	8981	12.8	0.2605
7	45.0	82.81	2.34	0.0069	0.1327	7800	13.17	0.2446

close-contact and natural convection melting in the ice storage spherical container. The following assumptions were made for the analysis: the flow is laminar; customary Boussinesq approximation can be used; properties are constant and there is a constant volumetric expansion rate during the melting process. The fixed boundary method was used to evaluate the interface position. Numerical simulations were performed for melting ice, which initially was packed in a shell with an inner diameter of 32 mm. Calculations were made for two different temperatures of the spherical capsule: 3 and 10 °C. As it can be seen in Fig. 15, at the early stage of unconstrained melting, the calculated molten mass fraction was in a good agreement with data of Bahrami and Wang [56]. As the process progressed, the increasing discrepancy in time was observed. These differences were caused by intensification of the natural convection flows.

Considering the configuration of unconstrained melting, Hu and Shi [64] developed a mathematical model describing the close-contact melting of PCM inside a spherical shell. The calculation was performed for two sets of experimental conditions, studied by Moore and Bayazitoglu [55], namely the first set: $Ste = =0.05$, $Pr = =54.7$, $Ar = =7.36 \times 10^5$; the second set: $Ste = =0.1$, $Pr = =41.8$, $Ar = =1.26 \times 10^6$. Fig. 17 shows data produced by Hu and Shi [64] in comparison with the results of Moore and Bayazitoglu [55], Bahrami and Wang [56]. It can be seen, that there is a good agreement between theoretical and experimental data.

Fomin and Saitoh [65] investigated the close-contact (unconstrained) melting within a spherical capsule numerically and analytically. Equations of their mathematical model were solved numerically by using the fixed boundary method. For constructing an approximate analytical model of contact melting in a sphere with non-isothermal wall, the original approach was developed and applied by Bareiss and Beer [58]. The use of the perturbation technique allowed to obtain an analytical solution for the evaluation of interface position,

$$\tau = [(\sqrt{2} - A) + (\sqrt{2} - A - B)Ste/4]\frac{s^2}{2} + [A + (A + B)Ste/4]s \quad (5)$$

and for the complete time of melting,

$$\tau_m = \frac{(\sqrt{2} + A)}{2} + \frac{(\sqrt{2} + A + B)Ste}{8}, \quad (6)$$

where

$$A = \left(\frac{3}{2a^3}\right)^{\frac{1}{4}}\left[a + \frac{a}{1+a} - 2\ln(1+a)\right]^{\frac{1}{4}}; \quad (7)$$

$$B = \left(\frac{24}{1+a}\right)^{1/4}\frac{-6a - 5a^2(6 + 8a + 2a^2)ln(1+a)}{a(2a + a^2 - 2(1+a)\ln(1+a))^{3/4}}. \quad (8)$$

Here a is the coefficient in capsule's wall temperature equation: $T_w = =a\sin^2\theta$. In accordance with the experiments, a varies from 0 to 0.4 and for the most cases, a can be chosen as 0.2.

Assuming that the capsule wall was isothermal ($a = 0$) and the heat transfer was dominated by heat conduction across the molten layer only, the comparison was conducted between the computed solid shift, as a function of relative time, and the results of Bahrami and Wang [56]. As it can be seen in Fig. 17, for these conditions the theoretical values completely coincide with experimental ones. The following conclusions were made by the authors:

- The approximate analytical solutions of close-contact melting, obtained by the perturbations technique, were found to be in a good agreement with the numerical solution of the complete mathematical model. The discrepancy in results did not exceed 10 ± 15%;
- The assumption, which was used in the previous research works on the temperature in the wall of capsule being constant, can lead to results, which significantly differ from those obtained for the real conditions of melting, in which the wall of the capsule is non-isothermal.

Eames and Adref [66, 67] carried out a comprehensive experimental study of freezing and melting of water inside a spherical shell. This type of shells is usually used in ice storage systems. The test apparatus is shown schematically in Fig. 18. The first sphere acted as the test object and was filled to 80% of its volume with de-ionized water. The air space in the test sphere was connected to the second sphere by a plastic tubing. The second sphere contained only air. During the freezing process, the air pressure in the two spheres would rise due to the increase in the volume of water as it freezes in the first sphere. The pressure was measured using a manometer. The purpose of the second sphere was to set the initial air volume contained by the two spheres. Once freezing had been completed the resulting air pressure would not exceed the strength of the glass spheres or the maximum pressure range of the manometer. The measurements of air pressure were used to estimate the quantity of ice produced at any point in time during the freezing process. Using this date, the position of the water/ice interface could be estimated. The experiments showed that at least 90% of the energy was discharged in 70% of the time needed to complete the full discharge from the spherical storage element. For practical purposes, it is important to know the rate of melting or solidification. The

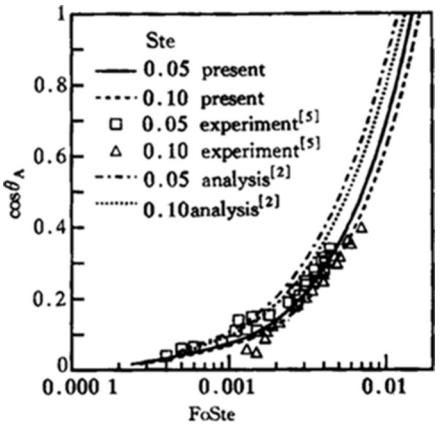

Fig. 17. The solid PCM travel distance as a function of ratio between current time elapsed and the time required for complete melting (τ/τ_m) [65.

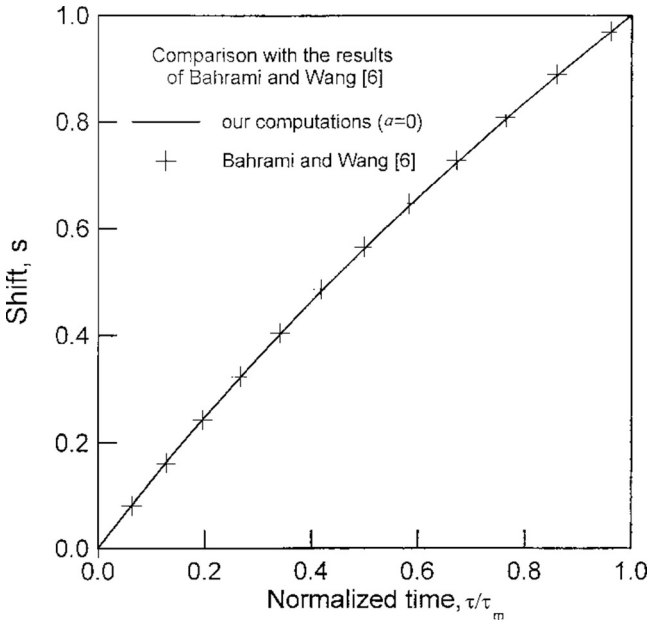

Fig. 18. Schematic view of experimental apparatus [66].

experimental data allowed to derive the following empirical equations for calculation of rates of storing and discharging energy (in Watts, not in W/m):

$$\dot{Q}_{charging} = -1.44 k_{ice} T_{HTF} \left(0.12 \frac{FoSte}{R_o} - 1\right)^2 \rightarrow \text{for } FoSte < 0.2 \text{and} T_{HTF} < 0°C \quad (9)$$

and

$$\dot{Q}_{discharging} = 4 k_{water} T_{HTF} \left(0.3 \frac{FoSte}{R_o} - 1\right)^2 \rightarrow \text{for } FoSte < 0.07 \text{and} T_{HTF} > 0°C \quad (10)$$

Ettouney et al. [68] carried out the experimental study of heat transfer during the phase change of paraffin wax with the melting point of 48.5 °C and heat of fusion at 210 kJ/kg inside spherical capsules. Measurements were conducted in a glass column with the diameter of 20 cm and a height of 40 cm, using air as the HTF and copper spheres with diameters of 2, 3, 4, and 6 cm. The detailed temperature field was obtained within the spheres, using 10 thermocouples. The values of the air velocity and temperature used in the experiments were 4–10 m/s and 60–90 °C, respectively. The inlet air temperature of 24 °C was maintained during the solidification process. Measured melting and solidification times varied over a range of 5–15 and 2–5 min, respectively. The specific melting or solidification times were calculated as the time, required for melting or solidifying a unit mass of the PCM. Experiments showed that the highest specific melting time was obtained for the smallest diameter of sphere. The specific melting time decreases with an increase in the sphere diameter. The reason was that in the small diameter sphere the conduction plays a dominant role in the heat transfer process. However, natural convection effects were more pronounced in spheres with larger diameters. That enhances the heat transfer process and reduces the specific melting. It should be noted that variations in the specific solidification time did not correspond to the real experiments. As mentioned previously, the solidification process was investigated only with the inlet air temperature of 24 °C. Because of the conducted experiments, correlations were suggested, characterizing the heat transfer during melting and solidification inside a spherical capsule, using air as the heat transfer fluid. Thus, for melting

$$Fo_m = 0.199\ Ste^{-0.56} Bi^{-0.212}, \quad (11)$$

(Correlation is valid for $0.08 < Ste < 0.38$; $1.89 < Bi < 6$; $60\ °C < T_{air} < 90\ °C$) and

$$Nu_m = 0.022\ Fo^{-068} Ste^{0.62} Ra^{0.22}, \quad (12)$$

(Correlation is valid for $0.007 < Fo < 0.2$; $0.08 < \text{Ste} < 0.38$; $50{,}000 < Ra < 28{,}000{,}000$; $60\ °C < T_{air} < 90\ °C$).

For solidification

$$Fo_s = 0.344\ Ste^{0.62} Bi^{-2.01}, \quad (13)$$

(Correlation is valid for $0.08 < Ste < 0.38$; $1.89 < Bi < 6$; $23\ °C < T_{air} < 43\ °C$) and

$$Nu_s = 0.023\ Fo^{-0.36} Ste^{0.28} Ra^{0.21}, \quad (14)$$

(Correlation is valid for $0.003 < Fo < 0.04$; $0.08 < Ste < 0.38$; $1{,}100{,}000 < Ra < 28{,}000{,}000$; $23\ °C < T_{air} < 43\ °C$).

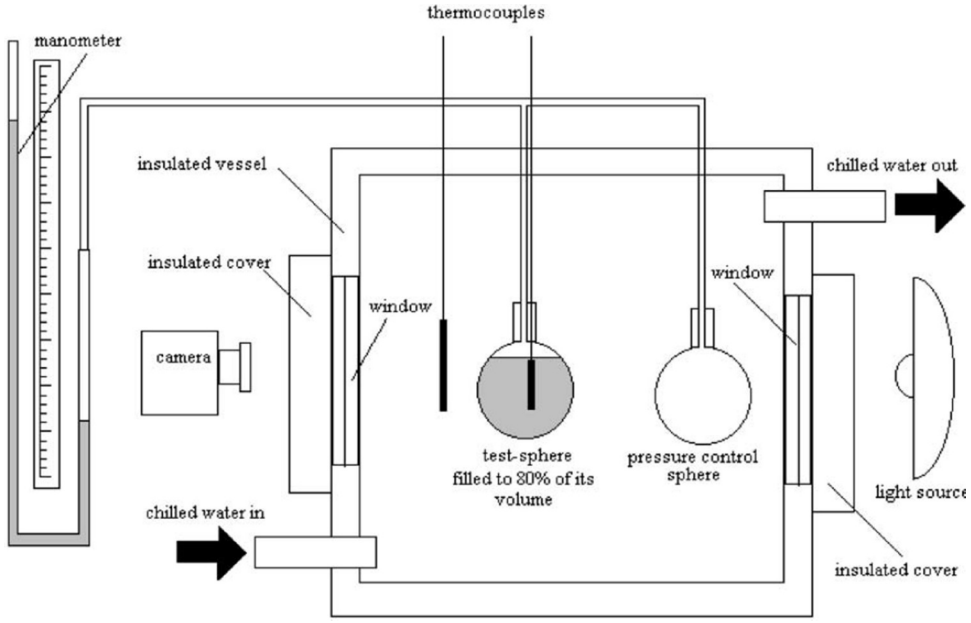

Fig. 19. Typical instantaneous photographs during melting of paraffin wax inside the spherical capsule at the HTF temperature of 78 °C (Ste = =0.2048) [69].

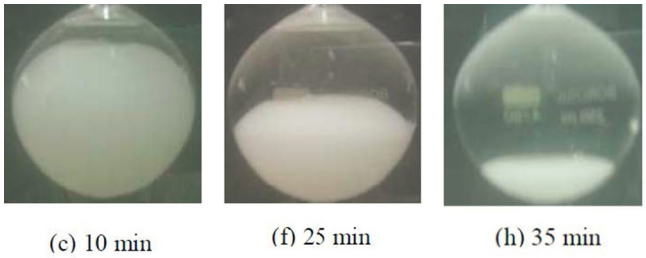

Fig. 20. Variation of the molten fraction with time (a) and the time, required for complete melting, as a function of the sphere radius (b) [69].

In conclusion, it should be noted that there are some contradictions in data presented by Ettouney et al. in [68], related to solidification. Thus, it was reported that the solidification process was studied at the inlet air temperature of 24 °C. At the same time, it was recommended to use the correlations (13) and (14) for 23 °C < T_{air} < 43 °C.

Regin et al. [69] carried out an experimental and numerical investigation of melting of the PCM inside a spherical capsule. Numerical analysis was conducted by using the enthalpy method. For experimental study, a spherical glass capsule with a diameter of 98 mm was placed in a convective environment. The temperature distribution inside of wax was measured with nine thermocouples. Paraffin wax with the melting temperature between 52.9 and 61.6 °C was selected as the PCM. The temperature of the heat transfer fluid (water) used in this experiment were 70, 75, 78 and 82 °C. The results of the observations are shown as photographs in Fig. 19. Fig. 21a presents the experimental and predicted values of molten fraction depending on the time and Stefan number, whilst Fig. 21b shows the effect of capsule radius on time, required for complete melting. An additional experiment was performed to validate the numerical model using thermocouples inside the capsule. The test was conducted using a spherical transparent capsule made of glass with a wall thickness of 1.5 mm and an outside diameter of 80 mm. As a result, it was concluded that there was a reasonable agreement between experiments and numerical simulations.

Bulunti and Arslantürk [70] carried out the numerical investigation of inward spherical melting of a solid, which initially was at the fusion temperature, and then exposed to convection and radiation. The governing equations for the liquid phase and interface, expressed in the dimensionless form, showed that there was a dependence between the rate of interface movement and Biot number, Stefan number, conduction-radiation parameter, and dimensionless temperature. One of the main results obtained is presented in Fig. 21.

Assis et al. [71] carried out the comprehensive numerical and experimental investigation of unconstrained melting in a spherical capsule. A detailed parametric analysis was performed using Fluent 6.0 software for PCM melting in spherical shells with diameters of 40, 60,

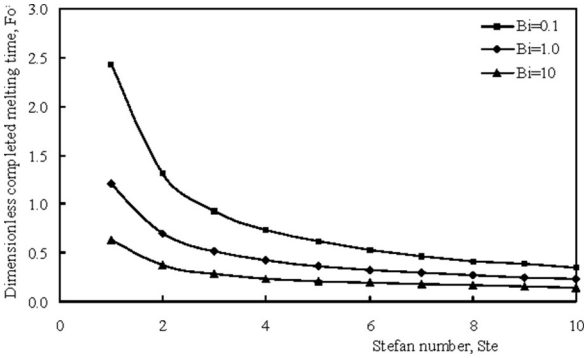

Fig. 22. Variation in the molten fraction with time: a – comparison of experimental and numerical data; b – generalized results for all simulated cases [71].

and 80 mm. The cases when the wall-temperature was uniform and varied from 2 to 20 °C above the mean melting temperature of the PCM were considered. Assis et al. [71] also conducted an experimental investigation with visual observation to validate the numerical simulation. The paraffin wax RT27 (Rubitherm GmbH) was used as the PCM (melting temperature of 28–30 °C, the heat of fusion at 179 kJ/kg). The solid phase initially occupied 85% of the volume in a vessel, which had a flat top. The comparison of numerical simulation results with experimental data is shown in Fig. 22a. As can be seen, the melting time, obtained in the simulations, was slightly shorter than in experiments. This was also observed by Roy and Sengupta in [57]. All numerical simulation results are summarized in Fig. 22b. It can be seen that all curves, except that for *Ste* = =0.2, practically merge into a single curve. It can be concluded that the generalization is full for Ste ≤ 0.1, which corresponds to $\Delta T \leq 10$ °C. Analysis of results presented in Fig. 23b leads to the following correlation

$$MF = 1 - \left(1 - \frac{FoSte^{\frac{1}{3}}Gr^{\frac{1}{4}}}{1.9}\right)^{\frac{3}{2}}. \quad (15)$$

The above correlation for molten fraction allows to evaluate *MF* for any time and to estimate the time of complete melting in the spherical capsule for the case in which MF is equal to 1.

The experimental study [48] of the constrained melting of n-octadecane inside a spherical flask was considered in Section 3.1. Below in Fig. 23, the typical results from observations of unconstrained melting, obtained by Tan [48], are shown as photographs. The amount of melting liquid fraction was estimated from the digital images captured at different time instances. Fig. 24 illustrates the liquid fraction versus time for different surface temperatures. It can be seen that the high surface temperature of 45 °C provides complete melting in 80 min, compared to 90 and 160 min for the surface temperatures of 40 °C and

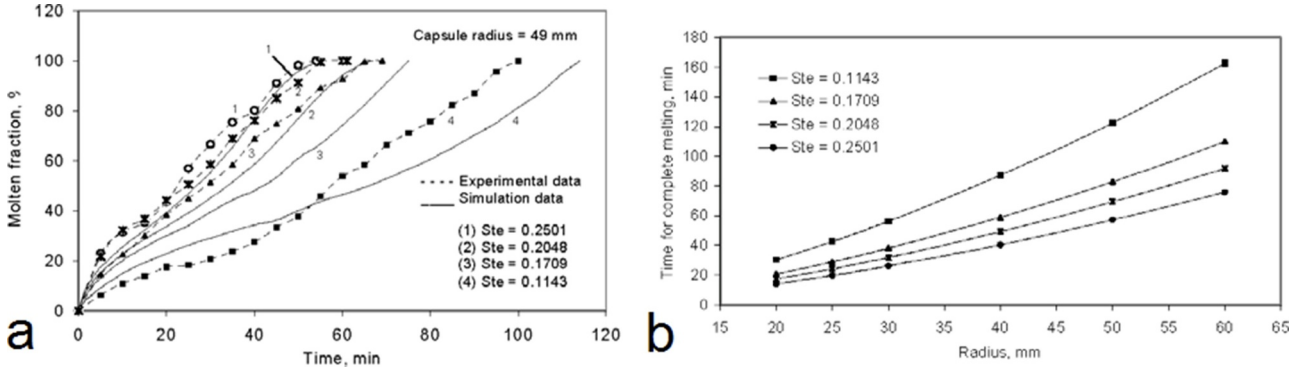

Fig. 21. Variation of the molten fraction with time (a) and the time, required for complete melting, as a function of the sphere radius (b) [67].

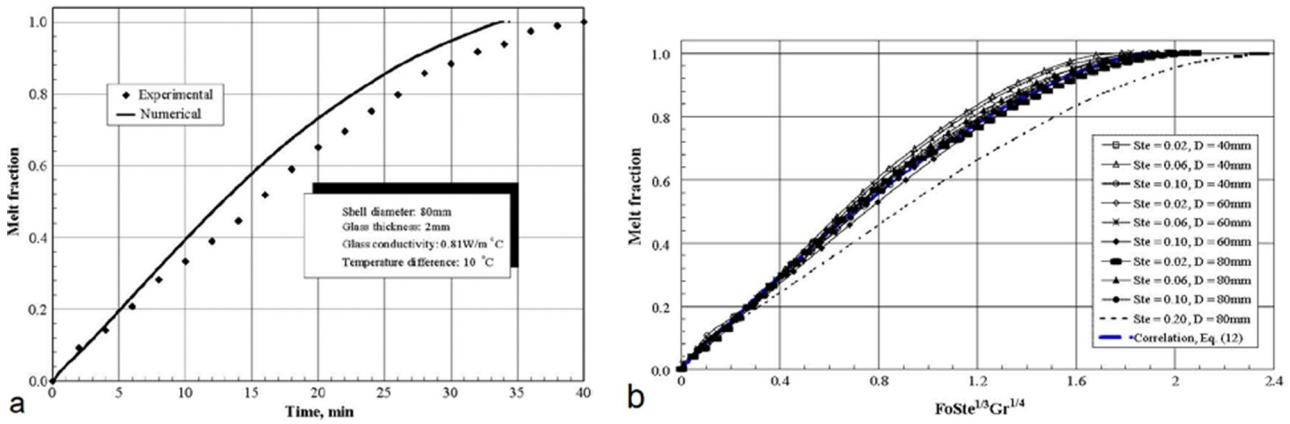

Fig. 23. Unconstrained melting phase front at 40 °C with an initial sub-cooling of 1 °C [48].

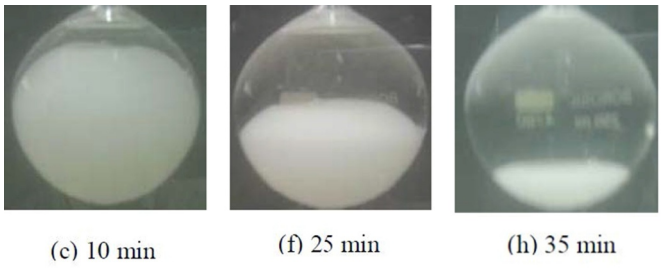

Fig. 24. Liquid fraction versus Stefan number in unconstrained melting [48].

35 °C, respectively. Melting occurs almost instantaneously for the surface temperatures of 40 and 45 °C. In the case of surface temperature of 35 °C, a 30 min delay before the start of melting was observed. A low surface temperature resulted in an opposite effect on the melting rate. Low surface temperatures decrease the creation of the centers of crystallization on the sphere wall and affect the heat transfer rate through the natural convection. It causes a significant slowdown in the melting rate.

Veerappan et al. [70] studied the heat transfer during phase change of the PCM in a spherical enclosure as a combination of conduction and natural convection process. They developed the analytical correlations for evaluating the dimensionless position of the solid-liquid interface in melting and solidification processes. Particularly for melting, the following correlation was suggested

$$(6 + \beta - 3\beta_{eff}s^2 + 2\beta_{eff}s^3)(1 - SteFo\beta_{eff}) = 6, \quad (16)$$

where $\beta = \frac{R^2 q_v}{k(T_o - T_m)}$; $\beta_{eff} = \frac{R^2 q_v}{k_{eff}(T_o - T_m)}$; $\frac{k_{eff}}{k_l} = 0.202\, Ra_L^{0.228}(\frac{L}{r_{eqv}})^{0.252} Pr^{0.029}$; r_{eqv} is equivalent radius of the melting solid; $L = R - r_{eqv}$; $s = \sigma/2R$ is the dimensionless position of the interface. Assuming $s = 1$ and taking into account that *SteFo* is the dimensionless time τ, the time for complete melting can be estimated as

$$\tau_f = \frac{1}{\beta_{eff}}\left(1 - \frac{6}{6 + \beta - \beta_{eff}}\right). \quad (17)$$

For solidification, the transient position of the interface for $\beta < 6.0$ was expressed as

$$SteFo = \frac{6}{\beta}(s - 1) + \frac{6}{\beta}\sqrt{\frac{6}{\beta} - 1}\left[tan^{-1}\left(\sqrt{\frac{\beta}{6 - \beta}}\right) - tan^{-1}\left(s\sqrt{\frac{\beta}{6 - \beta}}\right)\right] + \frac{5.3753}{\beta} - \frac{3}{\beta}ln(6 - \beta + \beta s^2) \quad (18)$$

The obtained correlation was verified using experimental data of Adref and Eames in [67]. The deviations were found to be within 20% for the melting process. It was shown that the diameter of sphere and temperature difference ($T_o - T_m$), were the main factors affecting the melting rate.

Koizumi et al. [73] used the enthalpy method for numerical simulations. They proposed a stream function, in which a solid sphere was moving in a stagnant viscid fluid for elucidation of the unconstrained melting process of a solid PCM in spherical capsule. In the analysis of the melting process, authors of [73] considered the effect of Stefan number (*Ste*) and capsule diameter (*D*). In the numerical simulations and experiments, the initial conditions were applied in the form of constant and uniform temperature at 25 °C with a sub-cooling of 3 °C, and the isothermal boundary conditions (58 °C, *Ste* = 0.27) were used. The experiment was performed in a transparent plastic tank, filled with water at 58 °C (Gr = =4 × 108). The spherical capsule was made of plastic with 2 mm thickness and with an outer diameter (D) of 100 mm. The solid PCM initially occupied 85% of the enclosed space. The PCM was placed in stagnant water at about 58 °C, which is 30 °C higher than the PCM melting temperature of 28.1 °C. The inner diameter of the sphere was 96 mm, and the internal volume of the capsule was 463 cm^3. The melting process was monitored and recorded with the use of a video-camera. The PCM, used in the experiment, was nOctadecane. The obtained results are presented in Fig. 25.

Archibold et al. [74] performed the comprehensive parametric investigation of melting of sodium nitrate in an aluminum spherical container with a diameter of 10, 20, 30, and 40 mm. The numerical investigation was based on applying the finite-volume and enthalpy porosity technique for solving Navier-Stokes and energy equations. The results of the comprehensive study are illustrated in Fig. 26. As it can be seen, all curves practically merge into a single curve. Data obtained using the correlation (12) of Assis et al. [71] was used for the comparison purpose. As it was noted previously, that correlation had been derived for the low-temperature PCM (RT-27) and produces melting times, which are not significantly shorter than the experiments.

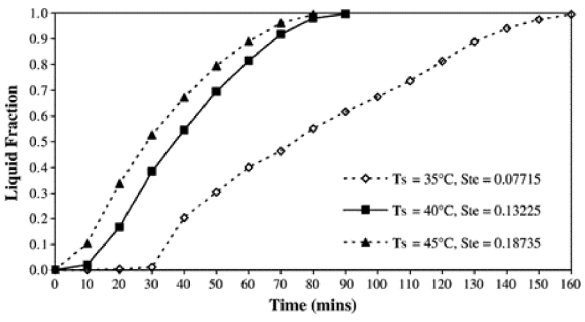

Fig. 25. Comparison of predicted results with experiments: a – variation of molten fraction with time; b – variation of the solid-liquid front with time in visual observations and numerical study [73].

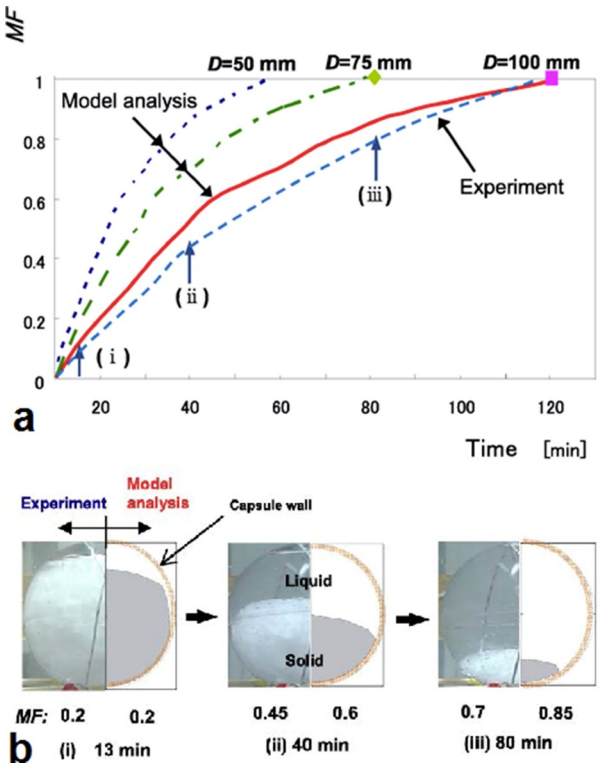

Fig. 26. Generalized results for the melting process (Ref. 13 in the Figure corresponds to [71]) [74].

Therefore, the correlation, obtained in the considered work and presented in Eq. (15) for the liquid mass fraction, produces an accurate prediction of characteristics of the storage system, based on the deployment of the spherical container.

$$LMF = 1 - \left(1 - \frac{FoSte^{\frac{1}{3}}Gr^{\frac{1}{4}}}{2.9}\right)^2. \tag{19}$$

The correlation (19) was valid for the range of parameters used in simulated cases: $0.047 < Ste < 0.1$; $1.2 \times 10^4 < Gr < 1 \times 10^5$; and $7.2 < Pr < 9.1$.

Rizan et al. [75] conducted an experimental study of n-octadecane melting inside a spherical shell immersed in a water tank. The spherical samples subjected to the power flux of 690, 850 and 950 W. About 643.6 cm^3 of solid n-octadecane were housed in a Pyrex spherical flask with the outer diameter of 110 mm, 1.5 mm thickness and neck's length of 168 mm. The flask was placed into an acrylic tank and suspended using a support stand. The tank had external dimensions of 30 cm (L) × 30 cm (W) × 50 cm (H). The thickness of its walls was 10 mm. The spherical flask was immersed into the 37.8-liter water volume with the Risheng Electrical Air Pump SP-780, secured at the center of its base floor. The flask was exposed to upward airflow to regulate heat distribution. The results of the experiments are presented in Fig. 27 and Table 2. The tabular data can be used for validation of the numerical modelling of the PCM melting heat transfer inside a spherical enclosure with constant heat flux applied.

Hosseinizadeh et al. [76] carried out numerical investigations of unconstrained melting of paraffin wax RT-27, which was enhanced by adding nano-size particles of copper. The developed mathematical model was verified by comparison with the data of Assis et al. [71]. As can be seen from Fig. 28a, there is a good agreement between calculated values and experimental data presented by Assis et al. [71]. The typical temporal variations in the liquid fraction are shown in Fig. 28b. The thermophysical properties of the nano-enhanced composition used in simulations. They could be confirm the assumed values of

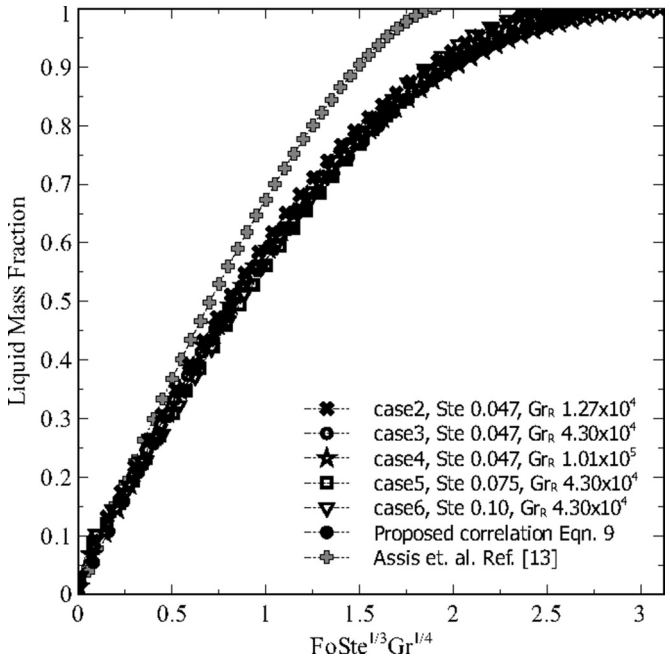

Fig. 27. Variation in the temperature of the water tank, containing PCM spherical shell, as a time function [75].

Table 2
Variation of the Stefan number and the Liquid fraction with time for different heater powers [75].

Time (min)	Stefan number			Liquid volume fraction (%)		
	690 W	850 W	950 W	690 W	850 W	950 W
0	0.0000	0.0000	0.0000	0.00	0.00	0.00
10	0.0237	0.0405	0.0293	2.14	2.65	2.72
20	0.0488	0.0776	0.0652	2.71	4.18	3.48
30	0.0795	0.1168	0.1056	5.33	13.79	13.69
40	0.1078	0.1506	0.1437	17.78	29.89	29.73
50	0.1376	0.1856	0.1779	26.28	48.60	50.76
60	0.1649	0.2225	0.2133	48.59	66.22	70.74
70	0.1937	0.2553	0.2511	67.83	81.07	88.05
80	0.2210	0.2859	0.2893	81.08	90.86	99.61
90	0.2458	0.3193	–	91.07	99.76	100.00
100	0.2729	–	–	99.70	100.00	100.00

thermophysical properties. It was also assumed that both solid and liquid phases were homogeneous and isotropic. This last assumption is difficult to justify due to considerable differences in densities of copper and paraffin wax. There are evidences that the viscosity of compositions, enhanced with nanoparticles, exceeds that of the pure PCM more than ten times. The trivial conclusion, made by the authors, was that their simulation results indicated an enhancement in the melting rate of nano-enhanced composition, compared to conventional RT27.

In the next paper, Hosseinizadeh et al. [77] reported the results of the comprehensive numerical and experimental investigations on unconstrained melting of n-octadecane inside a spherical capsule. PCM melting observation was made in the spherical glass flask with a diameter of 101.66 mm. The experiments were carried out at three different wall temperatures, namely 35, 40, and 45 °C, with a sub-cooling of 1 °C. Numerical simulations were performed using Fluent 6.3 software for different values of Stefan numbers and different capsule diameters (40, 60, 80, and 101.66 mm). The mushy zone constant to be employed in Fluent software was determined from their experimental results. A comparison of the current results with data of Assis et al. [71] is presented in Fig. 29a. As it can be seen, a good agreement between results is observed. Fig. 29 presents the generalized results for different Stefan numbers and shell diameters. The statistical analysis of

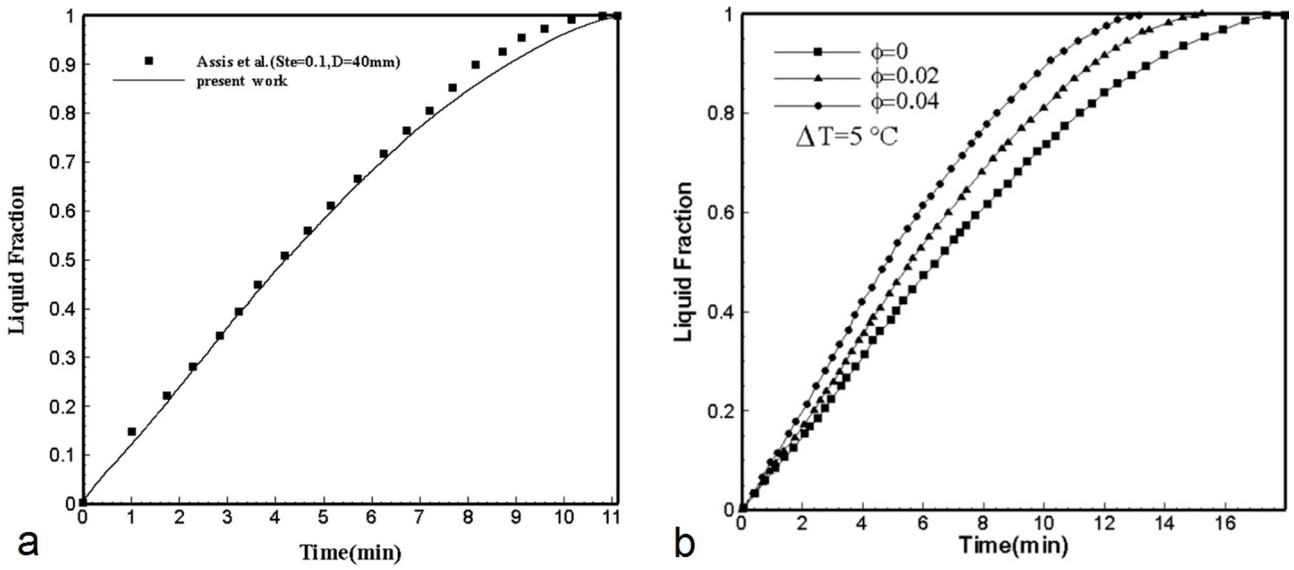

Fig. 28. Variation of the molten fraction with time: a – comparison with results by Assis et al. in [71]; b – generalized results for all analysed cases [76].

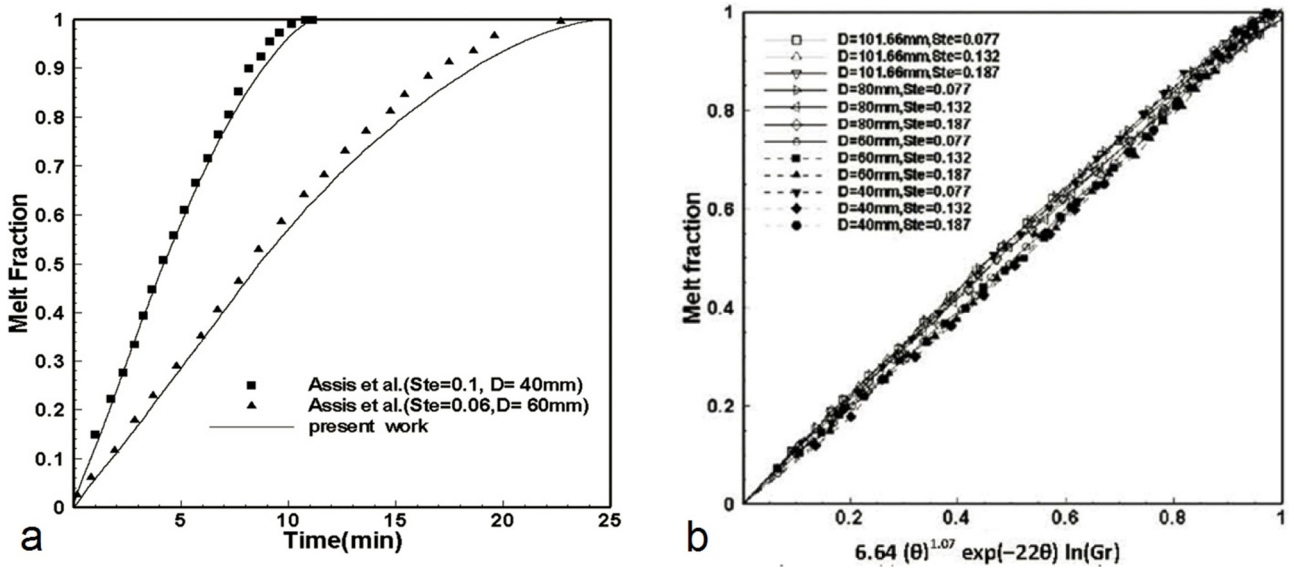

Fig. 29. Variation of the molten fraction as a function of controlling parameters: a – comparison with data of Assis et al. [71]; b – comparison of numerical data with Eq. (17) [77].

numerical simulation data produced the following correlation for the molten fraction

$$MF = 6.64\ \theta^{1.07} exp(-22\theta)\ lnGr, \tag{20}$$

where $\theta = = FoSte$ is the dimensionless time.

The correlation (20) allows easy calculation of the molten fraction as a function of time. However, it cannot be directly used for determination of the time required for complete melting. Therefore, for practical applications, correlations are preferable, which have the form of Eqs. (12) and (15).

The correlation (21) is valid in the range of experimental parameters used in simulations: $0.048 < Ste < 0.194$; $1.32 \times 10^4 < Gr < 2.06 \times 10^5$; $8.73 < Pr < 9.05$.

In 2014, Archibold et al. [78] reported the results of the numerical study of the melting process of sodium nitrate inside a nickel spherical shell. To provide the enough space for molten PCM, the test sphere was partially filled with solid $NaNO_3$. The remaining volume was occupied by air at pressure of 1 bar. Validation of the mathematical model was performed by comparing it with experimental data obtained by Assis et al. [71], see Fig. 33a. The plot of generalized correlation for molten fraction as a function of dimensionless parameters is given in Fig. 30b. A dimensionless equation for calculation of changes in the molten fraction (MF) was presented as:

$$MF = 1 - \left[1 - \frac{FoSte^{0.37} Gr^{0.25}}{2.8}\right]^{2.35}. \tag{21}$$

The results of the study, similar to [78] (considered above), were reported by Archibold et al. [79] in the same year. In this paper, the mathematical model was validated using experimental data of Tan [48]. The comparison demonstrated that the largest deviation (27.5%) of predicted values from experimental data was observed at the early stages when the thermal conduction was dominant. As the melting process progressed, the deviation gradually reduced to a very small number at the end of the process. The main results were decided to describe the melting process as $MF \approx FoSte^a Gr_R^b Pr^c \chi^d \xi^e$. The

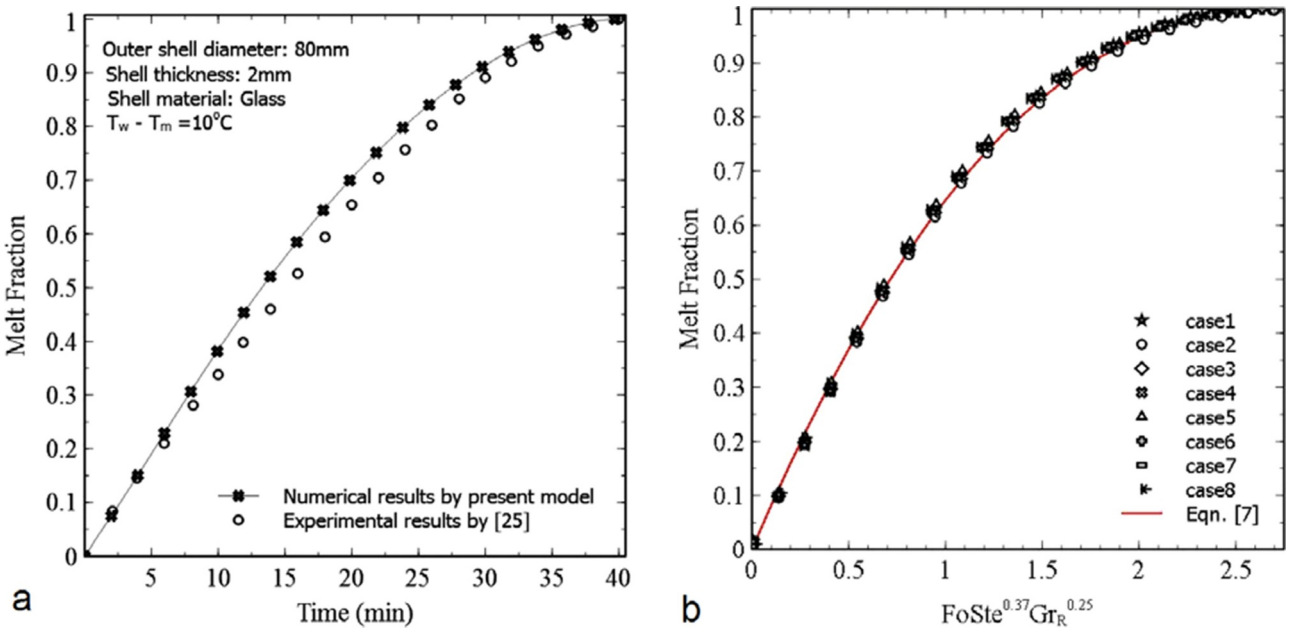

Fig. 30. Variations of the molten fraction measured with the use of all three samples [78].

numerical simulation results were approximated by the following correlation for the molten fraction:

$$MF = 1 - \left[1 - \frac{FoSte^{0.33} Gr_R^{0.27} Pr^{0.37} \chi^{0.72} \xi^{-0.02}}{9.5}\right]^{1.8}, \quad (22)$$

where $\chi = = 1 - k_{pcm}/k_{shell}$; $\xi = = T_{in}/T_m$.

Eq. (22) is valid for the range of parameters used in simulations: $0.048 \le Ste \le 0.145$; $1.32 \times 10^4 \le Gr \le 4.21 \times 10^5$; $8.90 \le Pr \le 35.0$; $0.6709 \le \chi \le 0.9945$; $0.00259 \le \xi \le 0.0259$.

Li et al. [40] conducted the experimental study of melting and solidification processes of the paraffin with melting interval 45.8 - 50.3 °C and paraffin-aluminum composition with 1 and 2 wt.% of aluminum powder. The experimental setup consists of two isothermal water baths, a spherical glass 100 mm in diameter filled with tested material. Five thermocouples placed along the centreline of the sphere are served for temperature control. Experiments demonstrated that the PCM in the upper part of the sphere melts faster than that in the lower part. Adding aluminum powder can accelerate the heat transfer of the PCM inside a sphere during melting and solidification processes.

Fan et al. [80] published results of the comprehensive experimental study on unconstrained melting of a nano-enhanced PCM. Pure 1-dodecanol with the melting point of approximately 22 °C and its blends with 0.5 wt.% and 1.0 wt.% expanded graphite nanosheets were used as the PCM. The specific heat, heat of fusion, melting point, thermal conductivity, density, viscosity was measured for both solid and liquid states. The spherical container was made of stainless steel with the inner diameter and the wall thickness of 48.5 mm and 0.75 mm, respectively. To quantify the value of molten fraction in a transient process, a transparent, straight glass tube with an inner diameter of 5 mm and a height of 300 mm was connected to the top of the spherical container. This calibrated glass was used to measure the expansion volume and to monitor the variation of molten fraction in time. Before performing melting experiments with various nano-enhanced PCM samples, experimental data for pure PCM was validated against Eq. (15), reported by Assis et al. [71]. Generally, good consistency was observed with the correlation, suggested in [71], with the maximum deviation being below 20%. Based on such a comparison, it was concluded that the measured results for molten fraction are also correct. Fig. 34 demonstrates the variations of molten fraction, produced using data in [80]. As a result, the following correlation for determination of the molten mass fraction was suggested:

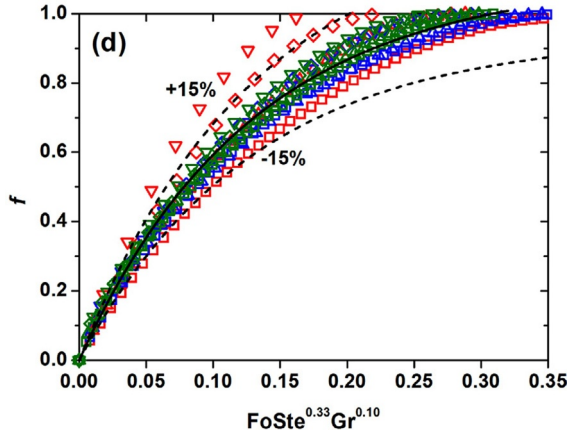

Fig. 31. The experimental images matched with simulated density contours [80].

$$MF = 1.102 - 1.101 exp\left(-\frac{FoSte^{0.33} Gr^{0.1}}{0.129}\right). \quad (23)$$

The range of parameters, for which the correlation (23) is valid, were not identified.

Hariharan et al. [81] carried out the computational and experimental study of melting and solidification behaviour of the paraffin PCM with the melting point of 61–63 °C, encapsulated in a stainless-steel spherical container. The numerical simulations were performed for a sphere with a diameter of 88 mm using commercial modeling software ANSYS ICEM CFD. It was anticipated that the role of natural convection in both melting and freezing processes would be insignificant. The experimental investigations were performed in the cylindrical chamber, which contained the spherical shell with PCM. The flow of hot and cold air with temperature of 75 and 36 °C, respectively, was used as the heat transfer fluid for melting and solidification of PCM. The CFD analysis showed that the time required for solidification and melting is longer by 33 and 30%, respectively, compared to the respective experimental results. The other conclusion from this study was that the solidification rate is higher than the melting rate.

Ghosh and Guha [82] performed numerical and experimental investigations of the effect of container material on the phase change process in a spherical shell. The melting process of the paraffin wax RT27 was studied for different boundary conditions. The shell with diameter of 80 mm was partially filled (85%) with the PCM. The initial PCM material was at the temperature, which was one degree below of the solidus temperature. The study was performed for container materials with three different thermal diffusivities (a): aluminium ($a_{Al} = = 8.5 \times 10^{-5}$ m^2/s), copper ($a_{Cu} = = 11.3 \times 10^{-5}$ m^2/s) and glass ($a_{glass} = = 3.42 \times 10^{-7}$ m^2/s). Commercial software Ansys Fluent 16.2 was used for numerical simulations. The simulations were run for three values of Stefan number: 0.13, 0.18, and 0.28. Results were obtained during the experiment with melting of PCM in the spherical cavity of 80 mm in the diameter and the water-bath at the temperature of 47 °C. Density contours from simulation results are shown in Fig. 32. The major findings of that study can be summarized as follows:

- The properties of the cavity materials affect the phase change process significantly;
- The ratio of height and breadth (aspect ratio) of the solid phase was higher in the copper cavity (high thermal diffusivity) than in the glass cavity during a transient simulation of the melting process. The higher aspect ratio results in an unstable shape of the solid, which increases the bouncy effect.
- Higher Stefan numbers during melting indicate the dominance of the natural convection, as the velocity reaches the maximum values.

Recently, Gao et al. [83] conducted the experimental study of the unconstrained melting process of paraffin RT27 addressing the effect of void inside the spherical shall with using a digital camera. The effect of such factors as the diameter of the spherical container (20.05–70.30 mm), filling ratio of PCM (0.8–0.98), heating temperature (32–47 °C) and initial temperature (7–22 °C) have been studied. These experiments showed that there is a new unconstrained melting mode (so-called floating melting), which takes place before the close-contact melting. The existence of voids in the solid PCM causes the floating melting. Generalizing all influencing factors studied in the present study by fitting the experimental data (Fig. 33) allows expressing the correlation of liquid fraction in form:

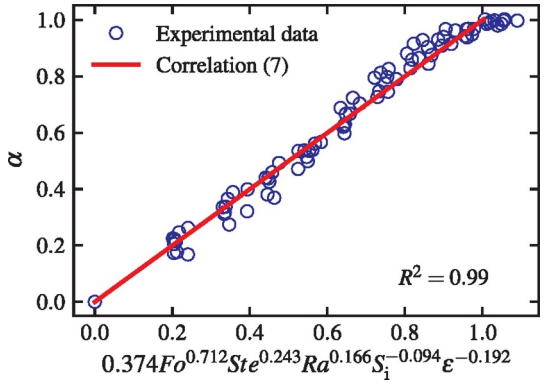

Fig. 33. Generalized results for the liquid fraction [83] (Correlation (7) is corresponds to (22a) of this review).

$$\alpha = 0.374Fo^{0.712}Ste^{0.243}Ra^{0.166}S_i^{-0.094}\varepsilon^{-0.192}. \quad (24a)$$

Correlation (22a) is applicable for $1.00 \times 10^5 \leq Ra \leq 2.70 \times 10^6$, $0.050 \leq Ste \leq 0.151$, $0.85 \leq \varepsilon \leq 0.95$, $0.134 \leq Si \leq 0.268$, and

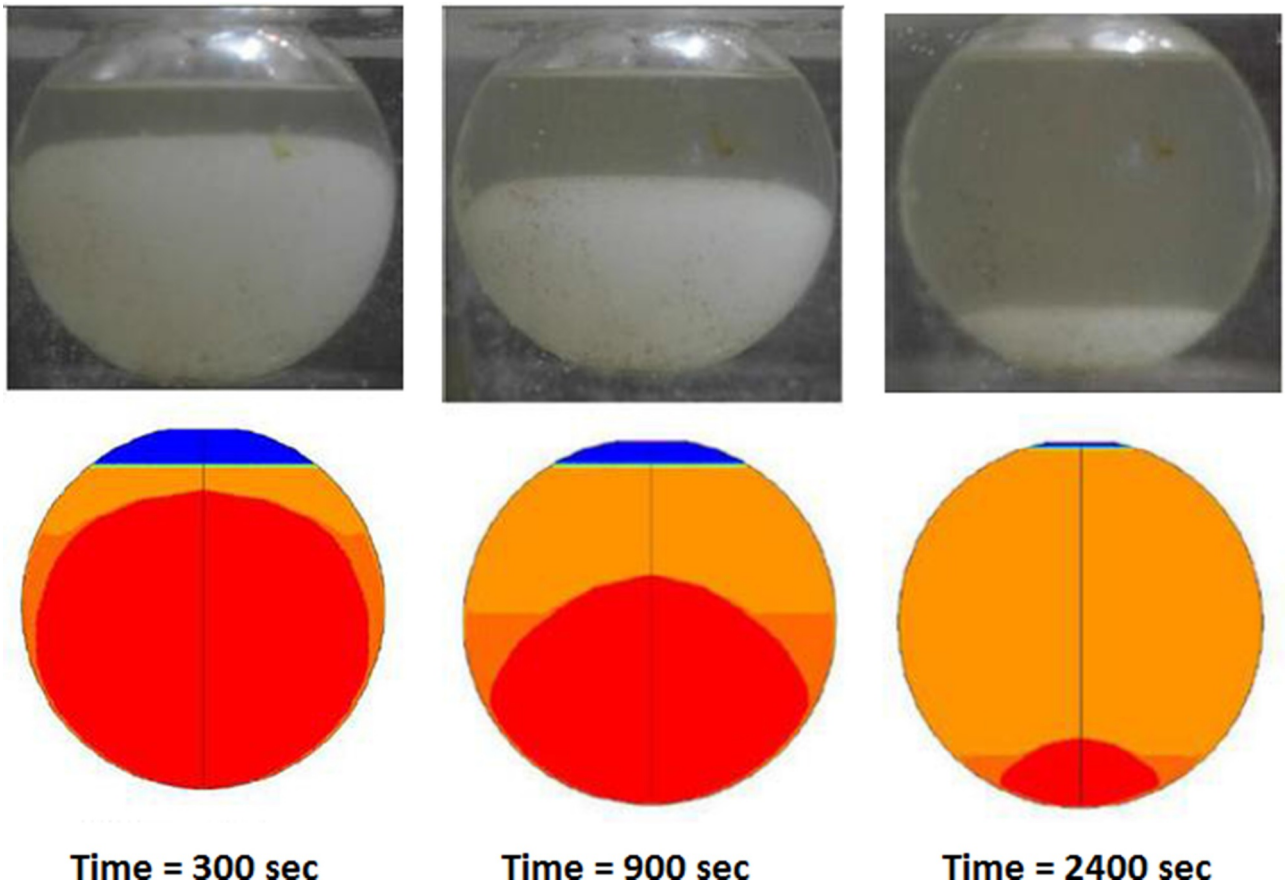

Fig. 32. Generalized solidification time (t^* = = FoSte; β = = 1/Bi; γ = = Ste) [82].

Table 3
Operating conditions and experimental parameters [84].

Parameters	Value
Temperature (during the charging process)	−5 °C, −10 °C, −12 °C, −15 °C, −18 °C, −20 °C, −25 °C
Temperature (during the discharging process)	10 °C, 14 °C,18 °C, 22 °C, 25 °C
Volume flow rate	0.003 m^3/minute
Diameter of spherical container	0.131, 0.106, 0.076, 0.035 m
Spherical shell material	Plastic
Thickness of spherical shell	0.002 m
Density of spherical shell	2.16 g/cm^3
Thermal conductivity of spherical shell	0.35 W/mK
Specific heat of spherical shell	0.960–1.03 J/g °C
Thermal capacity of spherical shell	46.74–1393.14 J/.K

$0 \le Fo \le 0.491$.

Just recently, Lago at al. [84] reported on results of comprehensive experimental investigation of melting and solidification duration of water and water-polyethylene glycol mixtures inside a spherical container. Phase change experiments are conducted under operating conditions and experimental parameters presented in Table 3. Refrigerant fluids R-22 and ethanol were used as heat transfer fluids. The statistical processing of empirical data on the complete melting time gave the following correlations

$$t_{complete\ melting} = 4.7 \times 10^5 D^{0.99}(1 - W)^{2.34}|T_{ini}|^{0.033}T_{bath}^{-0.53}, \quad (24b)$$

where D is diameter (m), W – percentage of polyethylene glycol (decimal number), T_{ini} – initial temperature (°C), T_{bath} – thermal bath temperature (°C), t – time for complete melting (s).

This correlation is applicable in the range of variables:

0.076 m $\le D \le$ 0.131 m, 0.1 (10%) $\le W \le$ 0.5 (50%), −20 °C $\le T_{ini} \le$ −5 °C, 10 °C $\le T_{bath} \le$ 25 °C.

The comparison of predicted values with experimental fixed time of complete melting of water or water-polyethylene glycol mixtures showed that the error does not exceed 7.2%.

3.3. Solidification inside a spherical container

The publication in 1943 of the paper by London and Seban [85] stimulated further investigations into the Stefan problem. Considering the idealized system, they suggested a general approximation method for the solution of freezing problems with applications to ice formation on spherical, cylindrical, and plane boundaries. Particularly, for the spherical container the resulting solution was presented as

$$\tau = FoSte = \frac{1}{3}\left(\frac{1}{Bi} + 1\right)(r^{*3} - 1) - \frac{1}{2}(r^{*2} - 1), \quad (24c)$$

where $r^* = = r/r_o$ is dimensionless radius. Assuming $r^* = = 0$, the time for complete solidification takes the form

$$\tau_f = FoSte = \frac{1}{6} + \frac{1}{3Bi}. \quad (25)$$

Considering the problem of solidification of saturated liquid with a constant thermal conductivity and density inside cylinder and sphere, Tao [86] produced the numerical solution and such the generalized solution obtained for the dimensionless solidification time $t^* = = \tau = = FoSte$ is shown in Fig. 34. For $Ste \to 0$, the solidification time can be calculated analytically using a steady state transport equation

$$t^* = \tau = (1 - r^{*2})\frac{1}{2} + (1 - r^{*3})(\beta - 1)/3 \quad (26)$$

Assuming $r^* = = 0$, the time of complete solidification takes the same form as in Eq. (25)

Shih and Chou [87] suggested the solution for freezing of saturated liquid inside or outside spherical shells using an analytical iteration technique. Comparison of the solution found with the numerical solutions of Tao [86] showed good agreement only for very low Stefan numbers when the third-order approximation was applied. For the higher values of Stefan number, the deviation was significant.

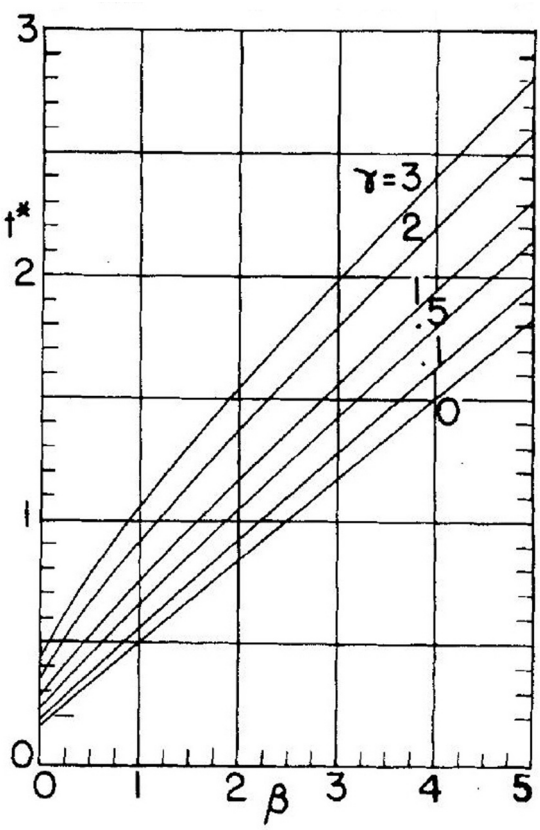

Fig. 34. The time required to freeze the center [86].

Pedroso and Domoto [88, 89] applied the method of strained coordinates to obtain a perturbation solution for solidification inside a spherical shell. It was assumed that the wall temperature is constant. The comparison of the solution with the numerical solution of Tao [86] demonstrated a very good agreement. This solution has the following form

$$\tau = FoSte = \frac{3(r^* - 1)^2 + 2(r^* - 1)^3}{6} + \frac{(r^* - 1)^3 Ste}{6} - \frac{1}{45}\frac{(r^* - 1)^2 Ste^2}{r^*} \quad (27)$$

Riley et al. [90] proposed an analytical solution of the inward solidification in a sphere or circular cylinder using the perturbation method. It was assumed that at the initial stage the PCM was fully melted and maintained at the melting temperature, when the outside surface was suddenly cooled. The complete solidification time τ of the PCM inside the spherical shell was presented as

$$\tau_f = FoSte = \frac{1}{6} + \frac{Ste}{6} - \frac{Ste^{\frac{3}{2}}}{3(2\pi)^{\frac{1}{2}}} + \ldots \quad (28)$$

Kern and Wells [91] suggested a physical model, which can be solved analytically for the most common types of boundary conditions. Assumptions were that the temperature of the wall was constant or there was the finite rate heat transfer to the coolant. It was also assumed that there was a linear temperature profile in the shell with a corresponding differential removal of internal energy. As a result, the solution for the complete inward spherical solidification time was proposed as

Table 4
Comparison of numerical values of the approximate time of complete solidification obtained by using Eqs. (34) and (35) for $Bi = 0.2$ and various values of the *Ste* number (Hill and Kucera [92]).

Ste	1st order approximation	2nd order approximation	3rd order approximation	t^*_{fmin}	t^*_{fmax}
2	1.55	1.42	1.17	0.92	2.75
1	2.53	2.55	2.38	1.83	3.67
0.5	4.40	4.51	4.47	3.67	5.550
0.2	9.92	10.09	10.17	9.17	11.00
0.1	19.09	19.28	19.41	18.33	20.17
0.01	184.1	184.3	184.5	183.3	185.2

$$Fo = F_1(Ste,\ Bi) + F_2(Bi) + C \tag{29}$$

where

$$F_1 = \frac{1}{Ste}\left(\frac{1}{3Bi} + 0.122\right), \tag{30}$$

$$F_2(Bi < 1 + \sqrt{2}) = \frac{2}{3}Bi - \frac{0.146}{Bi} - \frac{4Bi^3 - 6Bi^2 - 3Bi - 1}{6Bi}\ln(Bi + 0.5) + \frac{4Bi^4 - 10Bi^3 - Bi^2 + 4Bi + 1}{3Bi\sqrt{2 - (Bi - 1)^2}} \times cos^{-1}\left\{\frac{Bi + 1}{2\sqrt{Bi + 0.5}}\right\} \tag{31}$$

$$F_2(Bi > 1 + \sqrt{2}) = \frac{2}{3}Bi - \frac{0.146}{Bi} - \frac{4Bi^3 - 6Bi^2 - 3Bi - 1}{6Bi}\ln(Bi + 0.5) - \frac{4Bi^4 - 10Bi^3 - Bi^2 + 4Bi + 1}{6Bi\sqrt{(Bi - 1)^2 - 2}} \times ln\left\{1 - \frac{2}{\frac{Bi + 1}{\sqrt{(Bi - 1)^2 - 2}} + 1}\right\}, \tag{32}$$

$C = -0.439$.

It should be noted that Eq. (29) is valid for dimensionless thickness of the solidified layer $(r_o\text{-}r)/r_o < 1$. The complete time for solidification was found from quasi-stationary solution

$$Fo_f(Ste \to 0) = \frac{1}{Ste}\left(\frac{1}{3Bi} + \frac{1}{6}\right) \tag{33}$$

Hill and Kucera [92] proposed a new semi-analytical method for description of the solidification of PCM inside a spherical capsule. The approximation expression suggested is

$$t^* = -\alpha\beta\left\{(y - 1) + (1 + 2\gamma - \delta)\frac{(y - 1)^2}{2\alpha\beta} + (\gamma^2 + 3\gamma - 1 - \gamma\delta)\frac{(y - 1)^3}{3\gamma^2\beta^2} + (4\gamma - \gamma^2 - \delta)\frac{(y - 1)^4}{3\alpha^2\beta^2} + \frac{(5\gamma^3 - 52\gamma^2 + 28\gamma - 5 - 5\delta^2 - 2\delta + 25\gamma\delta}{15\alpha^4\beta^4} + \ldots\right\}, \tag{34}$$

where $\alpha = \frac{1}{Ste}$; $\beta = \frac{1}{Bi}$; $\gamma = \alpha(\beta - 1)$; $\delta = 2 - \alpha$; $y = R(t)$; $t = Fo$.

The comparison of Eq. (34) with results of Tao [86] and Shih and Chou [87] demonstrated a good agreement between these two sets of data. The approximate time of complete solidification t_f^* was found from Eq. (34) by setting y value to 0. Applying the further simplifications, the minimal and maximum of the first order estimates of t_f were suggested as

$$t^*_{fmin} = Fo_{fmin} = \left(\frac{2}{Bi} + 1\right)/6Ste \text{ and } t^*_{fmax} = Fo_{fmax} = \left(\frac{1}{Ste} + 1\right)\left(\frac{2}{Bi} + 1\right)/6 \tag{35}$$

Table 4 presents the comparison of numerical values of estimates of complete solidification time. It can be seen that the difference between 1st and 3rd order approximations for Stefan number less than 0.5 does not exceed 2%. Consequently, the 1st order approximation can be used for many practical cases.

Milanez and Ismail [93] suggested a simplified solution for calculation of the solidification time during freezing process inside the spherical shell assuming that the temperature profile in the solidified layer is linear:

$$\tau = FoSte = \left[\frac{(1 - r^*)^3}{3}\left(\frac{1}{Bi} - 1\right) - (1 - r^*)^2\left(\frac{1}{Bi} - \frac{1}{2}\right) + \frac{(1 - r^*)}{Bi}\right]. \tag{36}$$

Assuming $r^* = 0$ in Eq. (36), the complete solidification time takes the same form as in Eq. (25)

A more precise solution was obtained using a second-degree polynomial representation for the temperature profile.

In order to solve the solidification problem of PCM inside a spherical shell, Caldwell and Chan [94] used the enthalpy method. In considering this problem, the same assumptions were applied which were used previously in other reviewed studies. Data obtained using the enthalpy method was compared to calculation results determined by using the heat balance integral method (HBIM). The comparison results are shown in Fig. 35. It can be seen that the applied enthalpy method agrees very well with the HBIM, except for very small Stefan numbers.

Ismail and Henriquez [95, 96] performed a numerical study of the

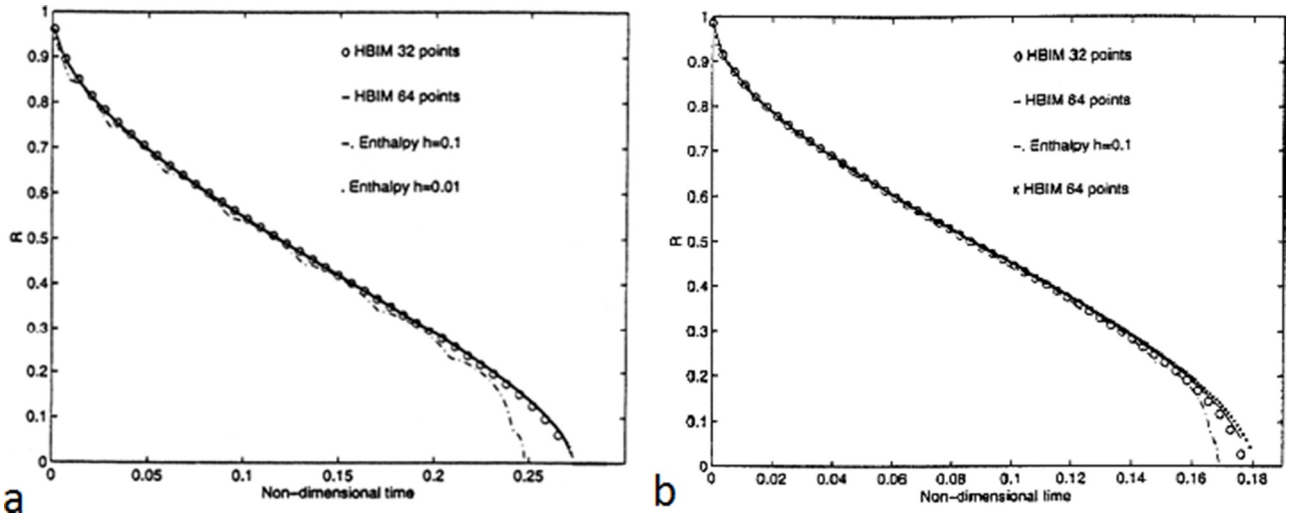

Fig. 35. Position of the solid-liquid interface versus non-dimensional time (here $\tau/\alpha = FoSte$ for a: $\alpha = 1/Ste = 1$; b: $\alpha = 1/Ste = 10$) [94].

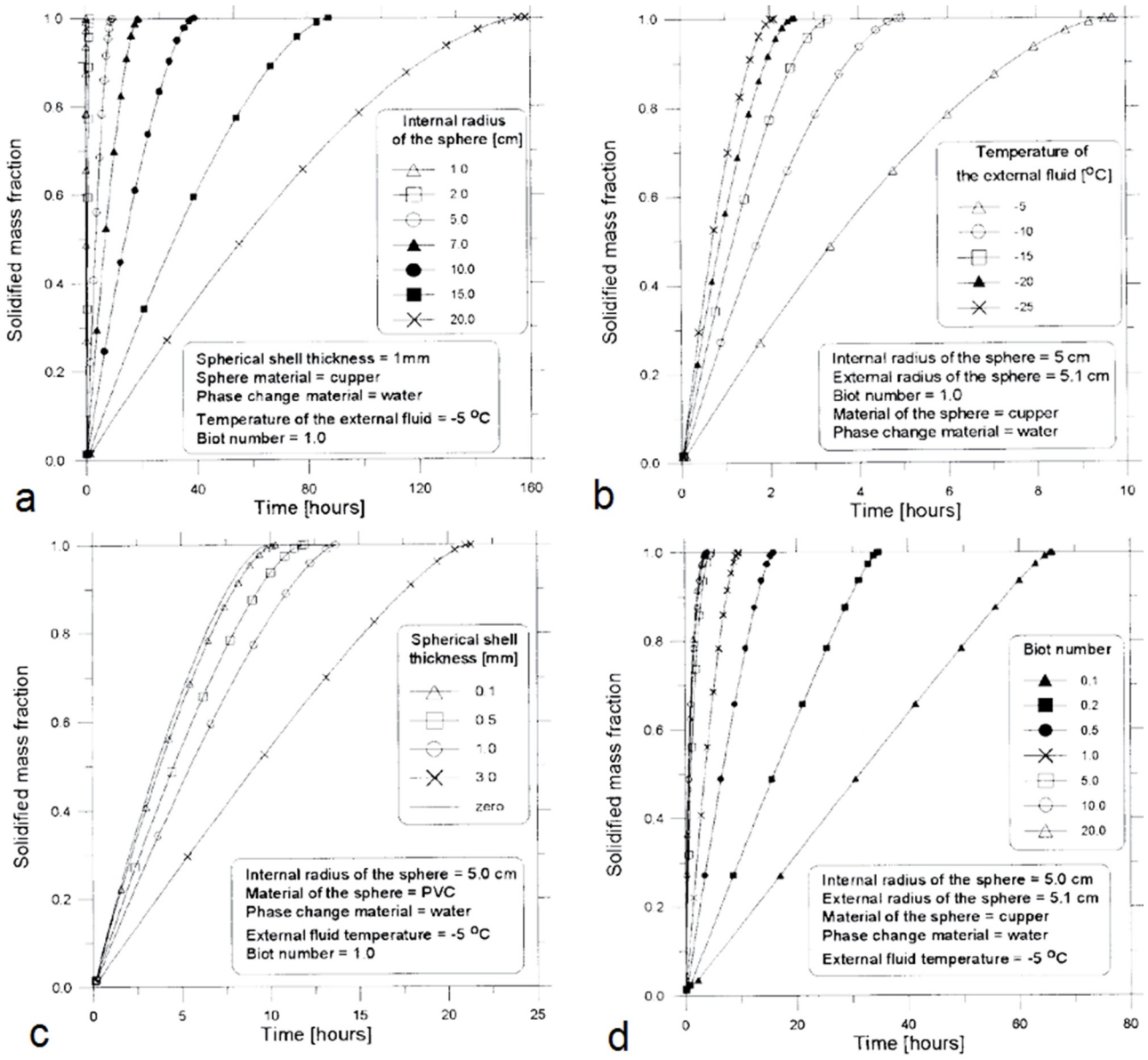

Fig. 36. Effect of various factors on the rate of solidified mass fraction: a – material of spherical shell;b – diameter of sphere; c – temperature of external fluid; d – initial temperature of PCM [95].

effect of different factors on solidification of water inside a spherical capsule. The effects of the internal radius of the sphere, coolant temperature, Biot number and shell thickness are shown in Fig. 36. By numerical simulations, the time of complete solidification related to the coolant temperature can be written as

$$t_f = 1.52977 \times 10^{-4}T^4 - 0.15605T^3 + 59.69380T^2 - 10148.7T + 647014 \quad (37)$$

and to the Biot number as

$$t_f = 13.526Bi^{-0.5685} \quad (38)$$

Authors of [95, 96] concluded that the time for complete solidification increases with the rise in the diameter of the spherical shell and decreases with reduction of the working fluid temperature. The thermal conductivity of the shell materials plays an important role and poor conducting materials causes the delay in starting the solidification process. The increase in the Biot number on the external surface led to a reduction in the time for complete solidification.

Eames and Adref [66, 67] performed an experimental study on the phase change of water in spherical enclosures. The test sphere was filled to 80% of its volume with the de-ionized water. The experiments on freezing were conducted with spheres having diameters of 8.14, 7.00, and 6.27 cm at HTF (chilled water) temperatures of -9.5 and -4.4 °C. From tests, the variations in the solid-liquid interface position were found as

Table 5
Comparison of the complete solidification time, calculated using the correlations of different authors [97].

Ste	Tao (1967)	Quasi-steady	Pedroso (1973)	Riley (1974)	Poots (1962)	Improved quasi-steady
0.1	1.920	1.667	1.805	1.791	0.924	1.773
0.3		0.556	0.686	0.649	0.368	0.668
0.5	0.474	0.333	0.460	0.406	0.257	0.452
0.8		0.208	0.333	0.256	0.195	0.336
1.0	0.284	0.167	0.290	0.200	0.174	0.300
2.0	0.180	0.083	0.204	0.062	0.132	0.247

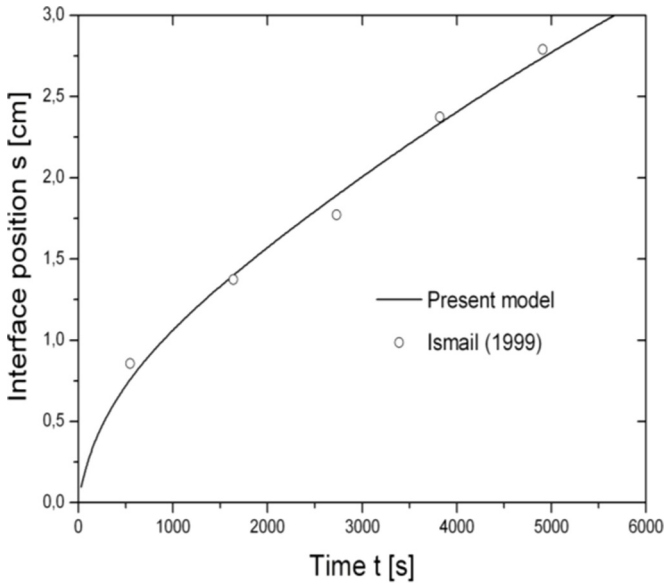

Fig. 37. Comparison of the present model and the experimental results of Ismail and al. [100].

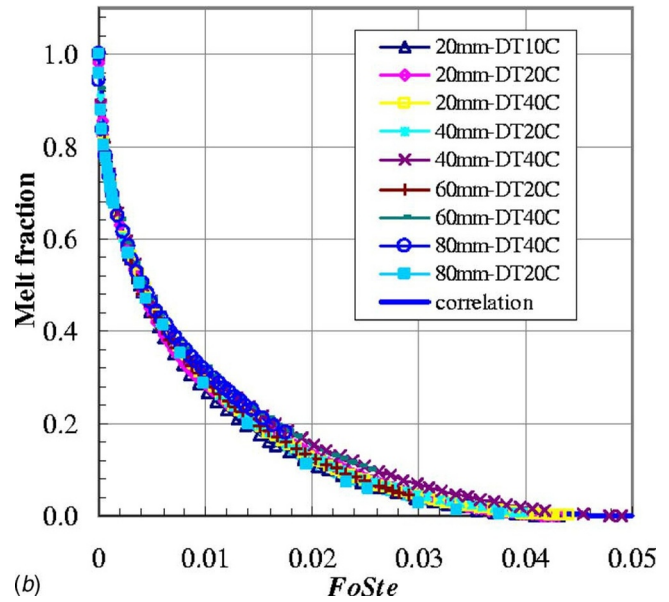

Fig. 38. Generalized results and correlation for the melt fraction [101].

$$r^* = \left(1 - \frac{3}{4\pi r_o}\frac{V_o}{(v_i - v_w)}\left(1 - \frac{P_o}{P_t}\right)\right)^{1/3} \tag{39}$$

where r_o – the inner radius of test sphere; r^* - dimensionless solid-liquid interface radius; V_o – the volume of test sphere; v_i, v_w – the specific volume of ice and water, respectively; P_o and P_t – the absolute pressure of air in test sphere at $t = 0$ and at $t > 0$, respectively.

Variation in the absolute pressure was determined in special tests. Experiments showed that the diameter of spherical container effects significantly on the rate of energy discharge.

Lin and Jiang [97] used an improved quasi-steady analysis for studying the solidification process in solids of a simple geometry. In the analysis based on the known Neumann's solution, an additional term was added to the temperature profile to simulate the transient effect in the temperature distribution in the solid phase. In the spherical case, the location of the solidification front was presented in the form:

$$\frac{1}{3}\left(\frac{r}{r_o}\right)^3 - \frac{1}{2}\left(\frac{r}{r_o}\right)^2 + \frac{1}{6} = \frac{2}{1 + \exp(p_m^2)}FoSte, \tag{40}$$

where p_m is the constant for the spherical enclosure. The time, Fo_f, required for the complete solidification inside the sphere with $r_o = =0$ is

$$Fo_f = t_f = \frac{1 + exp(p_m^2)}{12Ste} \tag{41}$$

In order to validate Eq. (41), the comparison of the dimensionless time with published data was performed, which is presented in Table 5. As it can be seen in Table 5, the good agreement is observed between data of Tao [86], Pedroso & Domoto [88, 89], and the improved quasi-steady analysis method for the Stefan number as high as 1.

Using the governing dimensionless equations of the Stefan problem and the third kind of boundary condition, Bilir and İlken [98] formulated and solved the problem equations numerically. In solving, the enthalpy method with the control volume approach was applied. It was assumed that the solution to be investigated has the form

$$t_f = Fo_f = a \times (Ste)^b \times (Bi)^c \times \theta^d \tag{42}$$

were θ is dimensionless temperature; a, b, c, d are constants.

Assuming that the thermal conductivity and specific heat values for solid and liquid phases of water were constant, the correlation for the time of complete solidification was derived as

$$t_f = Fo_f = 0.5012181 \times Ste^{-0.9070384} \times Bi^{-0.1864788} \times \theta^{-0.9843633} \tag{43}$$

and which is valid for the following range of parameters: $0.01 \leqslant Ste \leqslant 0.5$; $1 \leqslant Bi \leqslant 50$; $0.2 \leqslant \theta \leqslant 1$.

As a result of the experimental investigations conducted by Chan and Tan [99], the effect of three different constant surface temperature conditions (13, 8 and 3 °C) and three different initial superheating of n-hexadecane (8, 2 and 0 °C) were established on the solidification process inside a spherical container. The experiments showed that the lower constant surface temperature led to a longer solidification time, whereas the effect of the initial liquid superheating of the PCM on the solidification process was insignificant.

Teggar and Mezaach [100] investigated inward spherical solidification of a PCM using the finite control volume approach. Fig. 37 presents the numerical modelling results in comparison with literature data.

In 2009, Assis et al. [101] carried out a numerical and experimental study of the process of solidification inside a spherical enclosure. The commercially available paraffin wax RT27 was used as PCM. The spherical shells with diameters of 20, 40, 60, and 80 mm were used for the experimental study at the uniform wall temperature, which varied from 10 to 40 °C below the mean solidification temperature of PCM. Transient numerical simulations were carried out using FLUENT 6.2 software. The experiments were used to validate the results of numerical simulations, as shown in Fig. 37. The statistical analysis of simulation results produced the following correlation for calculation of the molten fraction:

$$MF = [1 - 4.5(FoSte)^{1/2}]^2 \tag{44}$$

Susarla [102] pointed out an error in Eq. (44) due to using the diameter value in the Fourier number calculations instead of the radius in the derivation process, which was confirmed by the authors. Thus, the corrected correlation should be written as

$$MF = [1 - 2.25(FoSte)^{1/2}]^2 \tag{45}$$

Ismail and Moraes [103] reported results of experimental and numerical studies on the solidification of different PCMs, encapsulated into spherical and cylindrical shells. They used glass and plastic spherical shells with diameters of 0.035, 0.076, 0.106 and 0.131 m. The temperature of cooling bath and, consequently, shell surface temperatures were maintained at −5, −10, −12, −15, −18, −20 and -25 °C.

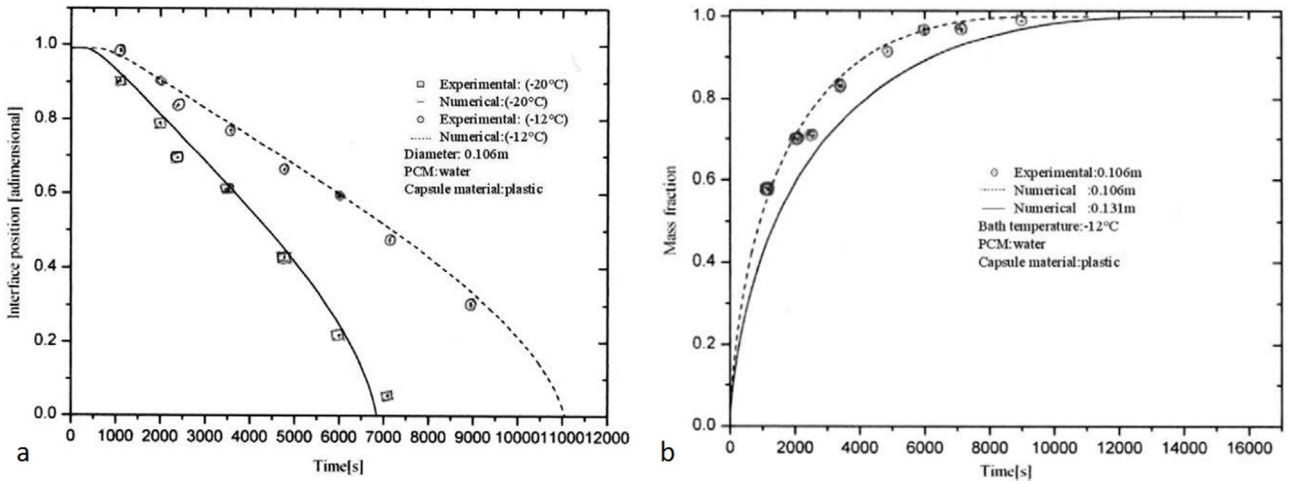

Fig. 39. Experimental data and their comparison: a - variation of the interface position with working temperature; b - variation of the solidified mass fraction with the capsule size [103].

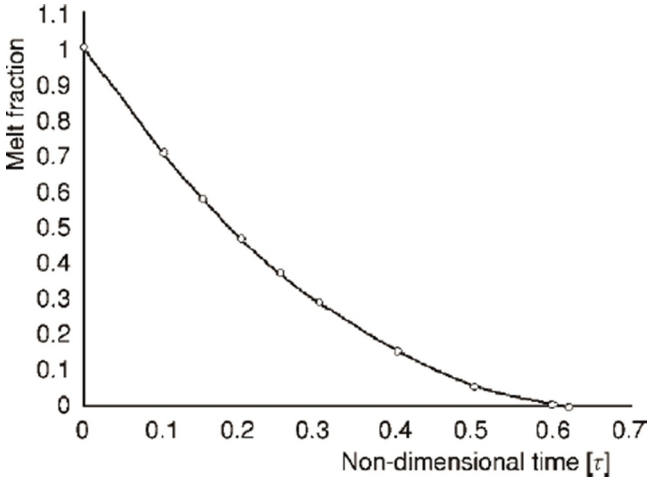

Fig. 40. Fig 40 Molten fraction as a function of dimensionless time ($\tau = \frac{tk\Delta T}{\rho LR^2} = FoSte$) [104].

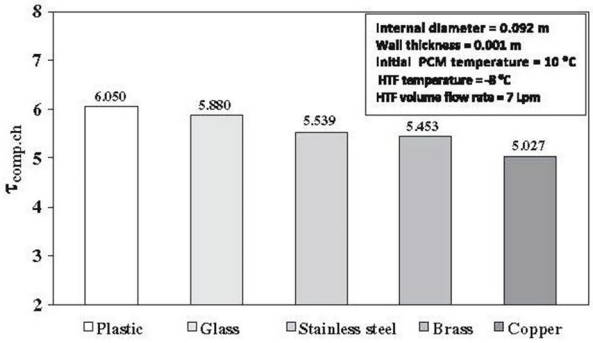

Fig. 41. Effect of the capsule material on the dimensionless time for complete charging [105].

The authors investigated water and mixtures of water with 3.75, 7.5, 15, 25, 30, 40 and 50% Glycol content as PCMs. The main results of their study are summarized in Fig. 38. The study demonstrated that the increase of the glycol content in the mixture reduces the phase change temperature, reaching –15 °C when the Glycol content is 50% and increases the time for complete solidification. Despite the good agreement of numerical and experimental data, see Fig. 39, no correlation for calculation of the solidified fraction was proposed.

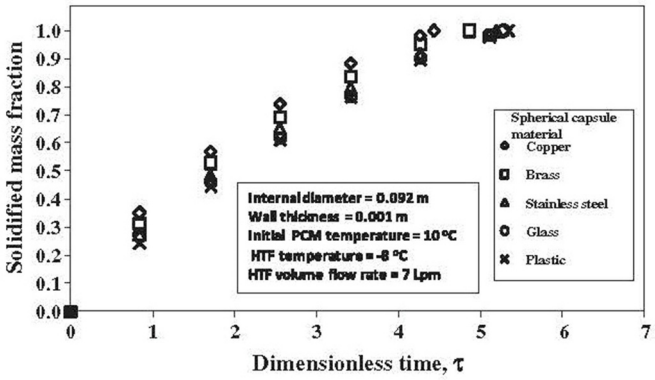

Fig. 42. Variation of the solidified mass fraction with the dimensionless time for different capsule materials [105].

Rajeev and Das [104] proposed a method based on using the time function approximated by Chebyshev series and the operational matrix of integration for the numerical solution of inward solidification of a PCM, contained in cylinder/sphere. It was assumed that the thermal properties of the PCM are constant throughout the analysis for solid and liquid states. The PCM is initially at the fusion temperature, and the solution was achieved using an iterative procedure. The molten fraction of PCM, found by using the proposed method, can be seen in Fig. 40. The theoretical results produced by the authors were not compared to theoretical or experimental data in other studies.

ElGhnam et al. [105] carried out a comprehensive experimental study of freezing and melting of water inside spherical envelopes. Distilled water was chosen as the PCM. In the experiments, they used spherical capsules made of copper, brass, stainless steel, glass and plastic with inner diameters of 42, 70, 92, 110 and 126 mm. The temperature of the HTF, flowing around the sphere with the volumetric rate of 1, 3, 4, 5 and 7 liters per minute, was maintained at -4, -6, -8, -10 and -12 °C. The PCM temperature inside the spherical capsule was measured using 13 thermocouples. Figs. 41–43 present only a part of large volume of experimental data obtained in this work. No correlation was derived for calculation of solidified mass fraction using this data, as it was done by Assis et al. in [101].

Chandrasekaran et al. [106–109] performed the comprehensive experimental investigation of PCM solidification in spherical capsules. Thus, in [106], they analysed the heat transfer in pure water and water/nano copper oxide composition. A low-density polyethylene spherical capsule of 68 mm diameter, filled with the PCM up to 90% of its full

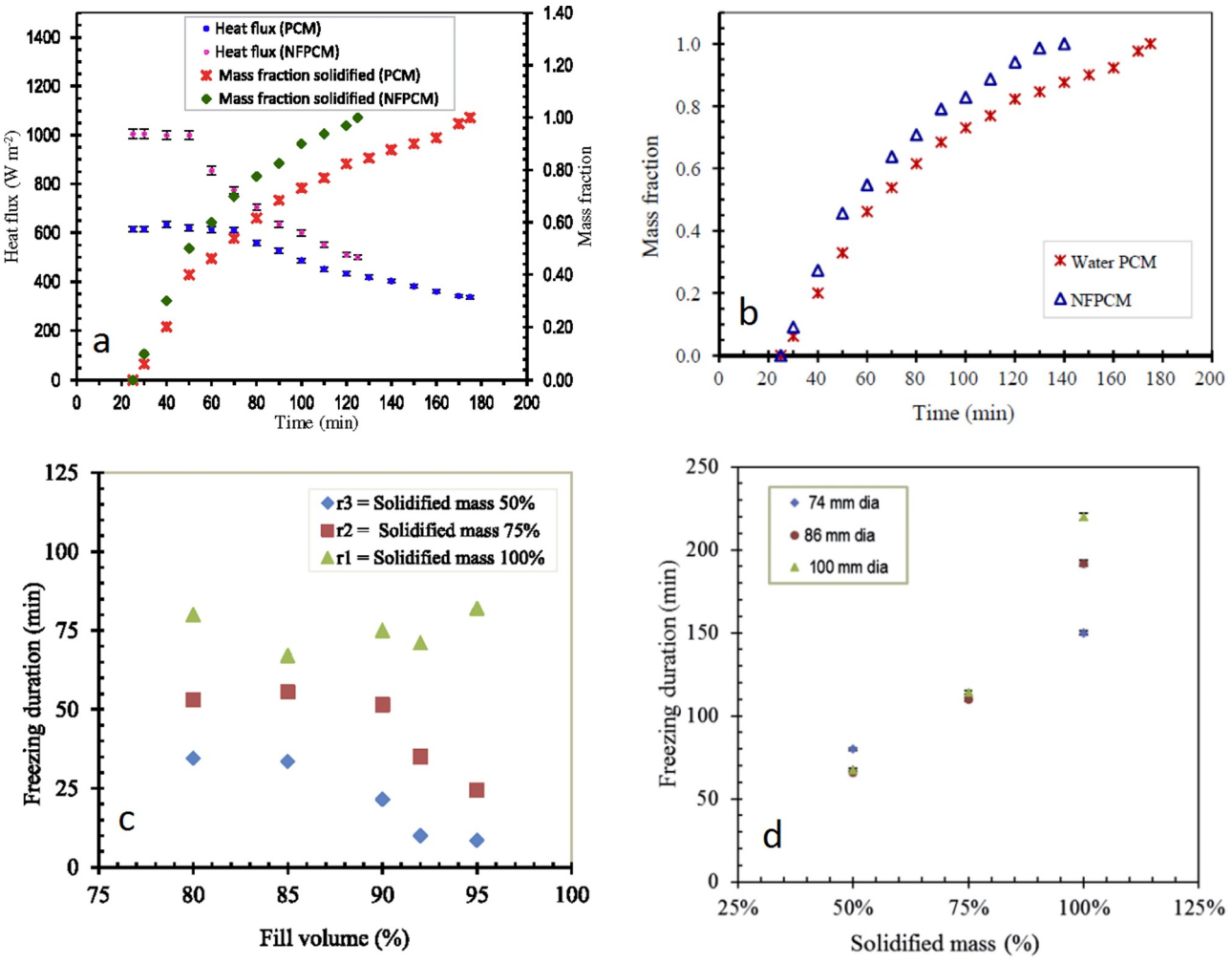

Fig. 43. Typical results obtained by Chandrasekaran et al.: a – solidified mass fraction vs time for t_{bath} = =-2 °C [106]; b – solidified mass fraction vs time for t_{bath} = =-6 °C [107]; c – variation of solidification duration for various volume fills for t_{bath} = =-12 °C [108]; d – variation of solidification duration with solidified PCM mass for t_{bath} = =-6 °C [109].

Table 6
Solidification time of the nanocomposite PCM (t_{bath} = =-9 °C) [110].

GNP concentration (wt.%)	Solidification duration at various radial locations (s)			Reduction in solidification duration at various radial locations (%)		
	r_1* = 30 mm	r_1* = 15 mm	r_3 = 0 (at the centre)	r_1* = 30 mm	r_1* = 15 mm	r_3 = 0 (at the centre)
0	3110	5020	5620			
0.3	2990	4890	5010	3.8	2.6	10.0
0.6	2820	4720	4840	9.4	6.0	13.5
0.9	2710	4590	4650	12.9	8.6	17.2
1.2	2590	4480	4450	16.8	10.8	20.6

* From the centre.

Table 7
Thermophysical properties of composite PCMs to be investigated [111].

Property	Pure TD	TD + 0.5 wt.% NP	TD + 1 wt.% NP
ρ_s (kg/m^3)	893.6	903.8	912.0
ρ_l (kg/m^3)	821.6	824.3	826.9
c_{ps} (kJ/kg•K)	1.689	1.669	1.655
c_{pl} (kJ/kg•K)	2.342	2.313	2.228
k_s (W/m•K)	0.252	0.350	0.451
k_l (W/m•K)	0.159	0.180	0.260
μ (mPa•s)	12.50	22.3	54.00
β (K^{-1})	0.001005	0.001000	0.000995
H_m (kJ/kg)	227.8	219.5	212.2

volume, was used in experiments. Five resistance thermometers were installed to monitor the temperature inside the spherical shell. The solidified mass fraction was determined at the bath temperatures of – 6 and – 2 °C. The typical experimental result is shown in Fig. 43a. The solidification process of water/multiwall carbon nanotubes (MWCNT) composition was investigated in [107]. The deionized water as PCM, sodium dodecyl benzene sulphonate (SDBS) as a surfactant, Pseudomonas as a nucleating agent and MWCNT as a nanomaterial were used for the preparation of the composite PCM. All additive components had 0.1 wt.%. The typical data obtained is shown in Fig. 43b. The thermophysical properties were not measured. In [108], solidification characteristics of water, as the PCM, were investigated to define the effect of volume filled by the PCM in a spherical capsule. In the

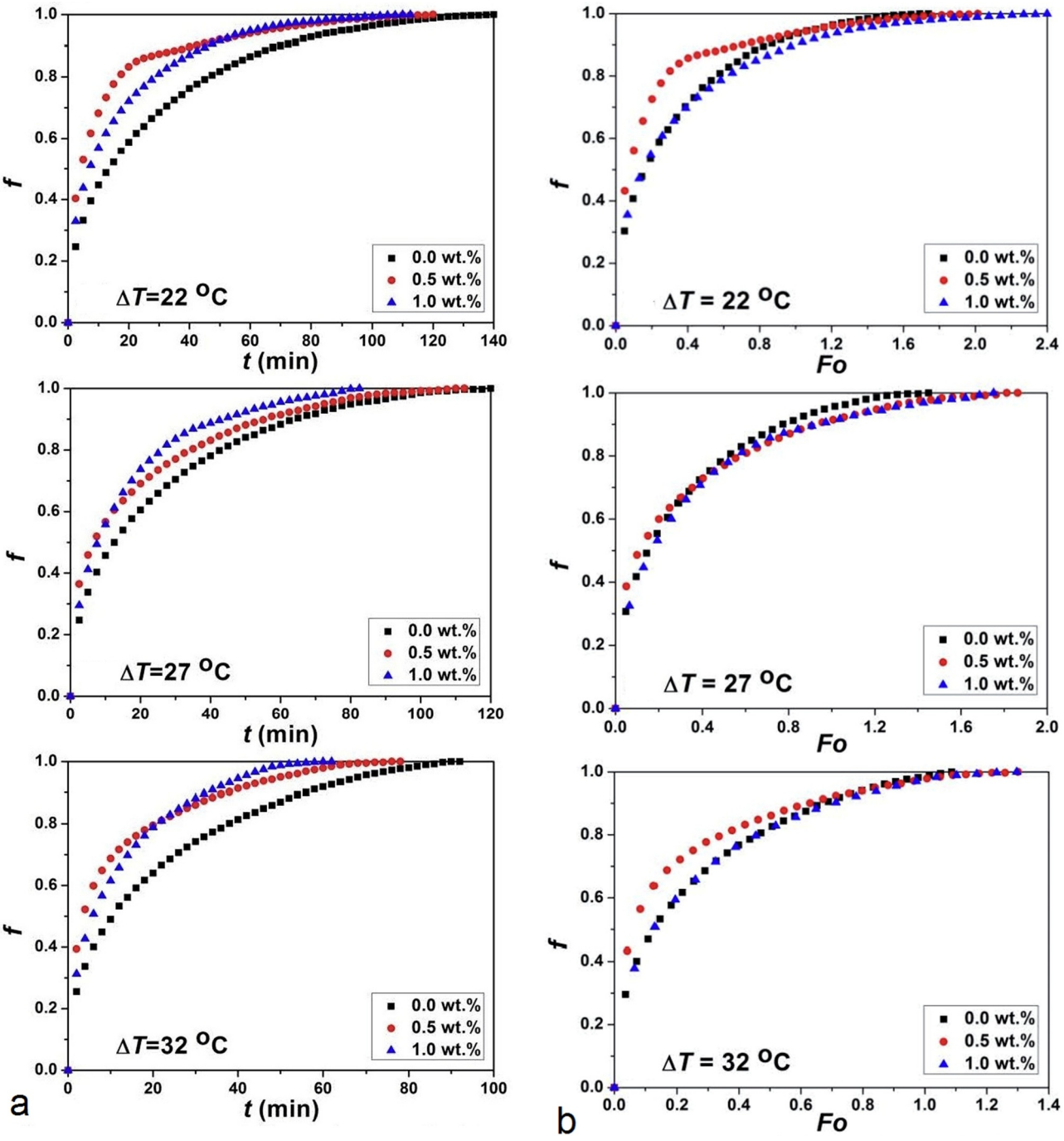

Fig. 44. Instantaneous variation of mass fraction as a function: a - of time at different boundary temperatures; b - dimensionless time *Fo* at different boundary temperatures [111].

experiments, the spherical capsule was filled with water up to 80, 85, 90, 92, and 95 percent of its full volume. The observations showed that an increase in the lled volume led to a significant reduction of the degree of supercooling, and it was eliminated in the case, in which 95% of the total volume was filled, see Fig. 43c. Furthermore, an incremental change in the filled volume had a considerable effect on advancing the commencement of solidification. Finally, in [109], the influence of spherical shell size on solidification characteristics of water were investigated. The authors studied three different sizes of stainless-steel spherical capsules filled with PCM up to 90% of its full volume and maintained at various bath temperatures. The typical dynamics of the solidification process duration with variation of the bath temperature can be seen in Fig. 43c.

Sathishkumar et al. [110] conducted the study of solidification characteristics of water/graphene nanoplatelets (GNP) composition inside a spherical container. Tests were performed using low-density polyethylene spherical container with the outer diameter of 72 mm and the 1-mm wall thickness. Three temperature sensors (resistance thermometers placed along the radius of the container) were used to monitor the solid-liquid interface motion. The solidification process was observed for two temperatures of the bath: -9 °C and -12 °C. Table 6 shows the results of one set of experiments.

Liu et al. [111] performed an experimental study of solidification of the PCM with enhanced thermal conductivity inside a spherical capsule. The compositions of 1-tetradecanol (TD) with melting point of 37 °C and highly conductive graphene nanoplatelets (GNP) were used as the

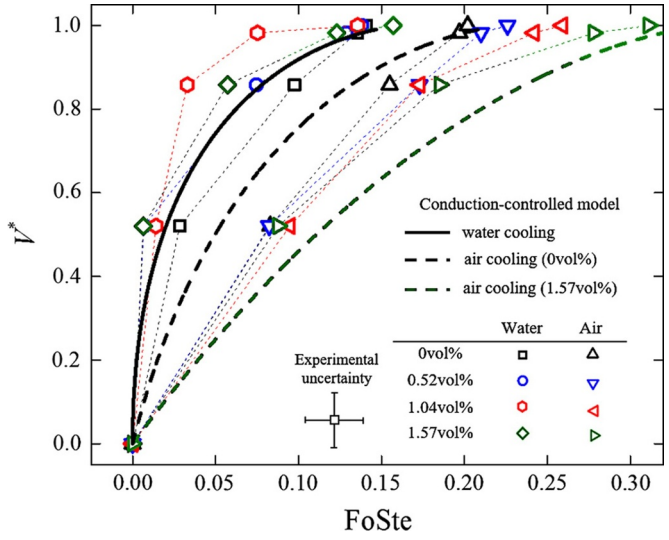

Fig. 45. Comparison of experiments and model predictions for solid fraction, V * as a function of FoSte for solidification of eicosane with xGnP volume fractions of 0%, 0.52%, 1.04% and 1.57% in water at T_{water} = =25 °C and in air at T_{air} = =25 oC and U_{air} = =25 m/s. The model prediction is based on Eq. (11) in the limit of Bi ? 1 for water cooling, and Eq. (11) at U_{air} = =25 m/s for air cooling. [113].

PCM. In experiments, three samples (pure TD, TD + +0.5 wt.% GNP, and TD + +1 wt.% NP) were tested. The results of measurements of thermophysical properties of samples are summarized in Table 7. Tests were carried out in a stainless-steel shell with the inner diameter of 57.6 mm and thickness of the wall equal to 1 mm. The spherical capsule, kept preliminarily for 5 hours at constant temperature of 38 °C, was quickly moved into the water tank, the temperature of which was set to be 5, 10, and 15 °C. The difference between the melting point and boundary temperature ($\Delta T = T_{bath} - T_m$) was 32, 27 and 22 °C, respectively. The results of experiments are shown in Fig. 44. It can be seen in Fig. 44a that curves noticeably differ from each other. In Fig. 44b, the solidified fraction presented as a function of dimensionless time *Fo* and the curves for each boundary temperature are close to each other. No correlations for calculations were derived in this work.

In their next study, Liu et al. [112] used the pure 1-tetradecanol as the PCM in experiments. They used the same experimental rig, which was employed in [111]. Experimental data obtained in [112] was in a good agreement with numerical data of Chandrasekaran et al. [109]. Considering that, the measured variations of solidification fraction were correlated to *FoSte* using the following polynomial equation with a high coefficient of determination equal to 0.9933:

$$f_s = 0.0382 + 3.32(FoSte)^{0.5} - 2.87(FoSte) \quad (46)$$

Table 8
The combined effect of *Bi* and ε on solidification for *Ste* = =0.1 (Narasimhan et al. [116]).

Bi	τ = =*Fo* for complete solidification			% reduction in τ	
	ε = =0	ε = =0.1	ε = =0.3	ε = =0.1	ε = =0.3
0.1	10.75	10.44	8.50	2.88	20.93
1	3.94	3.77	2.69	4.31	31.72
5	3.30	2.84	1.92	13.93	41.81
100	3.17	2.56	1.72	19.24	45.74
500	3.16	2.55	1.7	19.30	46.20

Table 9
The combined effect of *Ste* and ε on solidification for *Bi* = =5 (Narasimhan et al. [112]).

Ste	τ = =*Fo* for complete solidification			% reduction	
	ε = =0	ε = =0.1	ε = =0.3	ε = =0.1	ε = =0.3
0.1	3.06	2.64	1.89	13.56	41.24
0.5	1.9	1.73	1.20	8.94	36.84
0.7	1.84	1.51	1.05	18.09	42.93
1.0	1.56	1.30	0.88	16.66	43.58

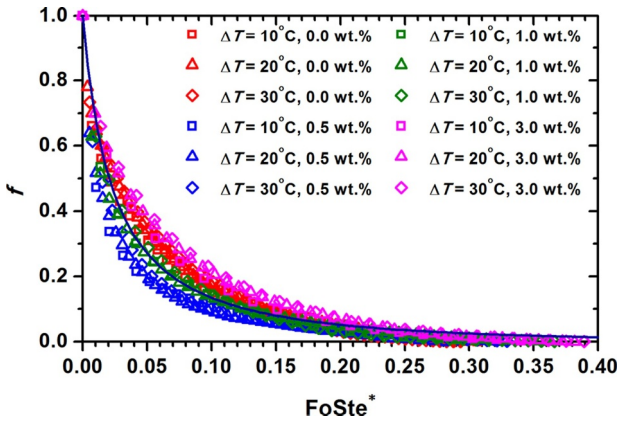

Fig. 47. Variations of the molten fraction as correlated to a combination of scaled dimensionless parameters (FoSte*) for all cases [117].

The regression analysis of data for the dimensionless heat transfer rate, i.e., *Nu* number as a function of *FoSte* produced the equation with an acceptable coefficient of determination of 0.9228:

$$Nu = 3.23\exp[-14.43(FoSte)] \quad (47)$$

The Eq. (47) is valid for $0.015 < FoSte < 0.24$.

Temirel et al. [113] carried out an experimental investigation of solidification of eicosane with and without nano additives inside a

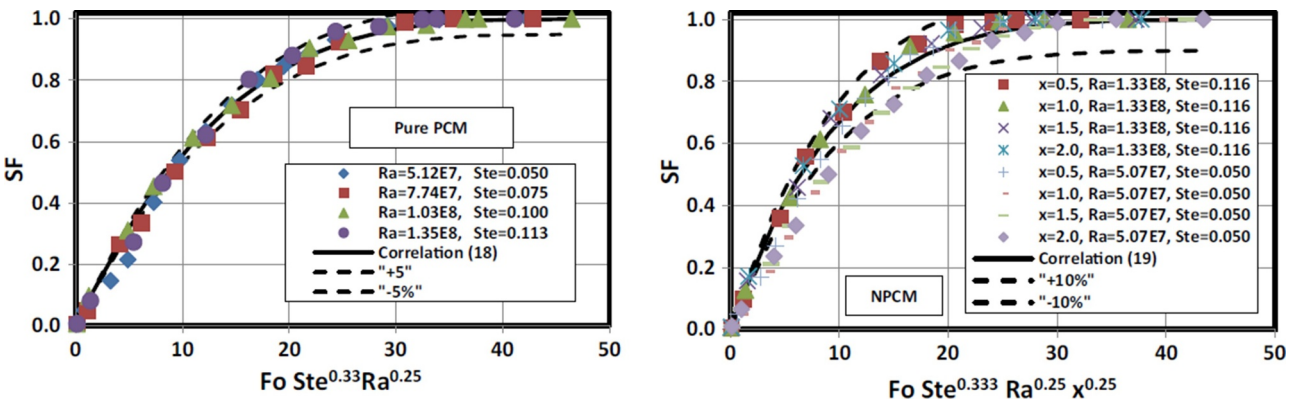

Fig. 46. Variation of solidified mass fraction with dimensionless time, obtained for pure PCM (water) and nano-PCM [115].

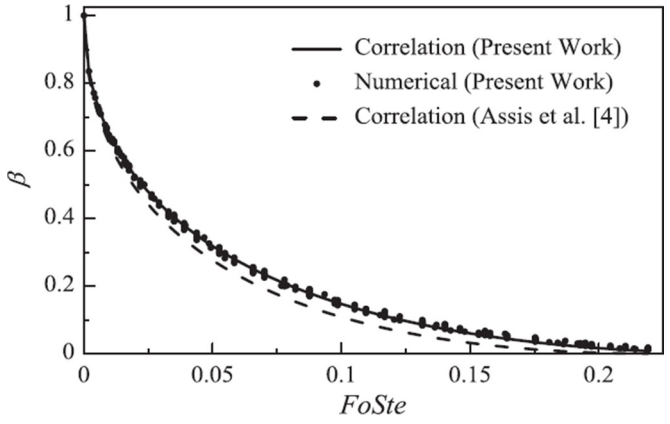

Fig. 48. Comparison of variation of the molten fraction with dimensionless parameter FoSte to data of Assis et al. [101] (Source: [118].

Table 10
Constants as determined by curve fitting for Eq. (51).

GNP content (wt.%)	*A*	*B*	R^2
0.0	30.45	4.71	0.975
0.5	73.86	2.60	0.983
1.0	47.25	3.40	0.981
3.0	24.08	4.41	0.986
0.0 – 3.0	41.61	3.62	0.944

Table 11
Constants as determined by curve fitting for Eq. (52).

GNP content (wt.%)	*A*	*B*	R^2
0.0	18.62	1.11	0.929
0.5	11.36	7.57	0.925
1.0	11.46	3.04	0.962
3.0	10.05	0.03	0.931
0.0 – 3.0	16.68	1.23	0.912

spherical shell. Exfoliated graphite nanoplatelets were used as enhancing additives. In experiments, stainless steel spherical shells were used with inner diameters of 46 and 32 mm and the respective wall thickness of 2 and 3 mm. The solidification tests were performed in water with constant temperature and in the convective air flow. Five thermocouples were installed inside the larger sphere to monitor development of the solid fraction volume. Main results of the study are presented in Fig. 45.

Asker et al. [114] employed the control volume approach and temperature transforming method for the numerical study of inward solidification of a PCM inside the spherical capsule, which initially was not at its melting temperature. Water was considered as the PCM. Validation of the numerical model used in the study was carried out by comparison to experimental and numerical data of Ismail and Henriquez [95]. The variation of the interface position with time was presented as a result of numerical simulations.

Sakr et al. [115] performed the comprehensive experimental study on freezing of pure water and γ-Al2O3/water nano PCM composition. The experimental test rig consisted of a refrigeration cycle working with R404A, which was used to cool an aqua solution of ethylene glycol (as the HTF). Two identical cylindrical tanks with end top and bottom caps, having a diameter of 200 mm and a height of 900 mm, were used as charging and discharging spaces. The γ-Al_2O_3/water nanofluid was prepared with four different nanoparticle volume concentrations of 0.25, 0.5, 0.75 and 1.0%. A low-density polyethylene spherical capsule with an inner diameter of 80 mm and thickness of 2 mm was filled with the PCM, occupying 80% of its inner volume. Eleven calibrated Copper-Constantan (T-type) thermocouples were used to measure the temperature distribution with an accuracy of ± 0.5 °C. A centrifugal pump was employed to circulate the HTF through the piping system to carry out the charging and discharging processes in experiments. Some of results obtained are shown in Fig. 46. Obtained experimental data was presented as following correlations:

$$SF = 1 - \left(1 - \frac{FoSte^{1/3}Ra^{1/4}\chi^{1/4}}{48}\right)^{3.75} \quad (48)$$

2. The complete charging time is correlated to the Rayleigh number for pure water with the maximum deviation of ± 3% as

$$Fo = 27127\,Ra - 0.567 \quad (49)$$

3. The complete charging time for NPCM is correlated to Rayleigh number with the maximum error of ± 12% as

$$Fo = 98293.5\,Ra - 0.646 \quad (50)$$

Additionally, the correlations for the variation of Nusselt number with time for different values of Rayleigh and Stefan numbers were suggested.

Narasimhan et al. [116] performed a numerical investigation of solidification of the PCM impregnated with high conductivity macro particles inside a spherical container. In order to validate the mathematical model results, they carried out the comparison of theoretical value of the nondimensional interface position to data of Hill and Kucera [88]. The good agreement was observed between two these two approaches. The effect of volume particle fraction on the dimensionless interface position was obtained in the graphical form. Study results are presented in Tables 8 and 9.

Recently, Zhu et al. [117] has reported the results of their last experimental study of the inward solidification heat transfer for nano-enhanced PCMs (NePCMs) in a spherical enclosure. 1-Tetradecanol with the additives of graphite nanoplatelets, GNP (0 wt.%, 0.5 wt.%, 1.0 wt.%, and 3.0 wt.%), was used as the PCM. The subcooling degree, i.e., the difference between the melting point and the tank temperature ($\Delta T_{sub} = = T_m - T_{bath}$), was set at 10, 20, and 30 °C. The thermophysical properties of samples were measured prior to conducting tests. Results on the molten fraction change for three boundary temperatures and FoSte converge together at the constant loading (see Fig. 47), and the following correlation was suggested for calculations:

$$f_m = \frac{exp\,[-B\,(FoSte)]}{1 + A\,(FoSte)} \quad (51)$$

where *A* and *B* are coefficients to be determined by curve fitting, as given in Table 10.

The trends in variations of the surface-averaged *Nu* number were similar to that for variations of molten fraction. A slightly different form of exponential function for the correlation was employed after performing curve fitting exercise:

$$Nu = \frac{exp\,[-B\,(FoSte)]}{A\,(FoSte)} \quad (52)$$

where the values for *A* and *B* are listed in Table 11.

Ehms et al. [118] undertook the numerical investigation of the solidification process of erythritol in spheres with dimeters of 10, 20, 30- and 40-mm and with the wall temperature, which is 10, 15, 20, 25, 30, and 40 K below the phase change temperature of the material. The problem was considered as a two-dimensional in geometry and transient in time. The computational domain geometry was spherical; it was filled for 98.5% with the PCM and the remaining volume was filled with air. To maintain constant pressure, the upper part of the sphere was opened, allowing air to enter the sphere. Validation of numerical results was performed by comparison with the numerical and experimental results of Assis et al. [90], using RT27 as PCM, contained in a spherical shell with diameter of 40 mm and $\Delta T = = 20$ K. A good agreement between two sets of data was observed, see Fig. 49. Based on obtained

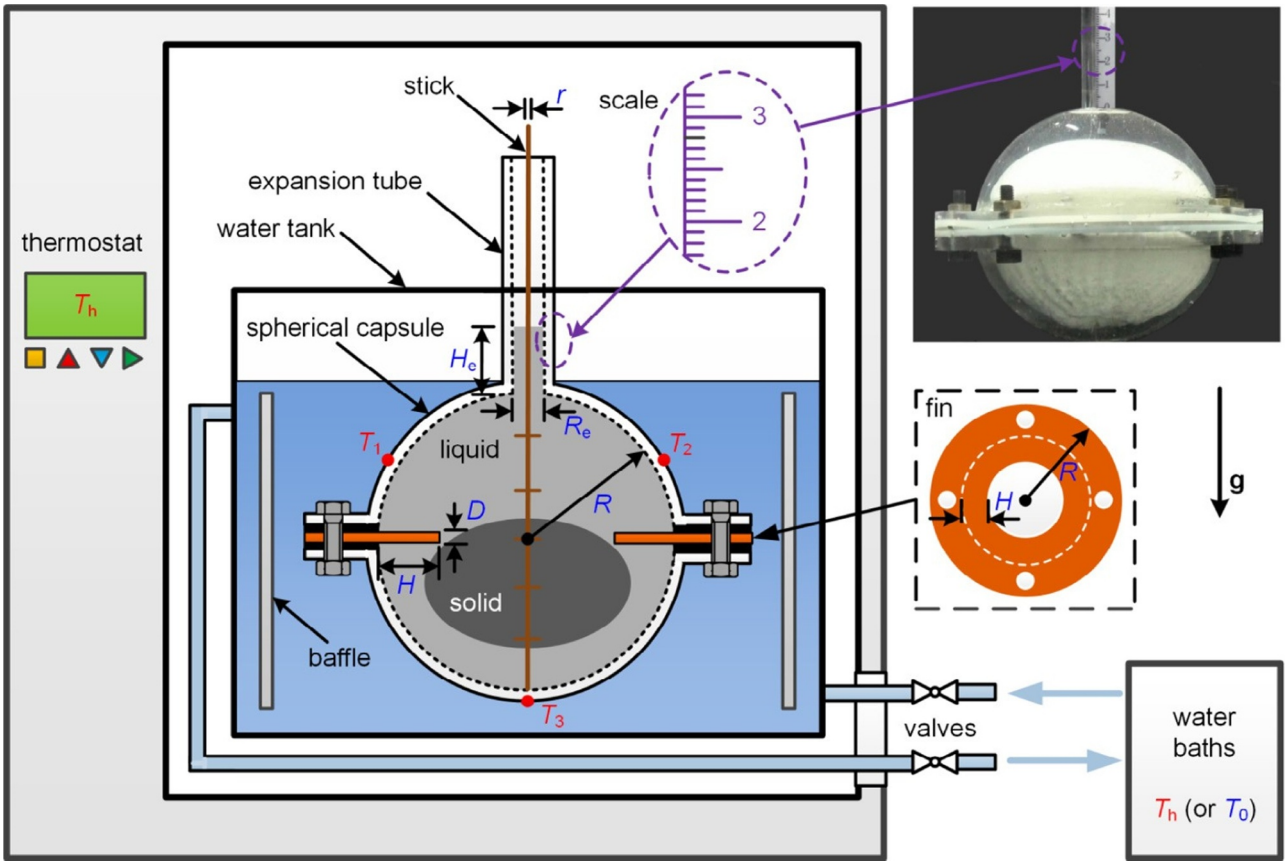

Fig. 49. Experimental spherical capsule rig with an annular fin [119].

numerical results, Ehms et al. [118] suggested the following correlation:

$$\beta = LF = [1 - (3.8FoSte)^{1/2}]^2 \tag{53a}$$

Above in Section 3.2, we considered the results of experimental investigation of the time of complete melting of water and water-polyethylene glycol blends inside a spherical capsule reported by Lago et al. [84]. In this paper, the time of complete solidification has also been studied. The experiment details were described above. Fitting experimental results of PCM solidification duration inside the spherical plastic shell allowed getting the following correlation:

$$t_{complete\ solidification} = 1.09 \times 10^8 D^{2.704} |T_{bath}|^{-1.243} (1 - W)^{-0.781}. \tag{53b}$$

The range of application of correlation (53b) is 0.076 m $\le D \le$ 0.131 m; 0.075 (7.5%) $\le W \le$ 0.5 (50%); -10 °C $\le T_{bath} \le -25$ °C. The comparison of the predicted results with the experimental measurements indicated good agreement and maximum deviation was to be less than 6%.

3.4. Melting and solidification in finned spherical capsules

Fan et al. [119] recently have undertaken an experimental and numerical investigation of the constrained melting of PCM in a

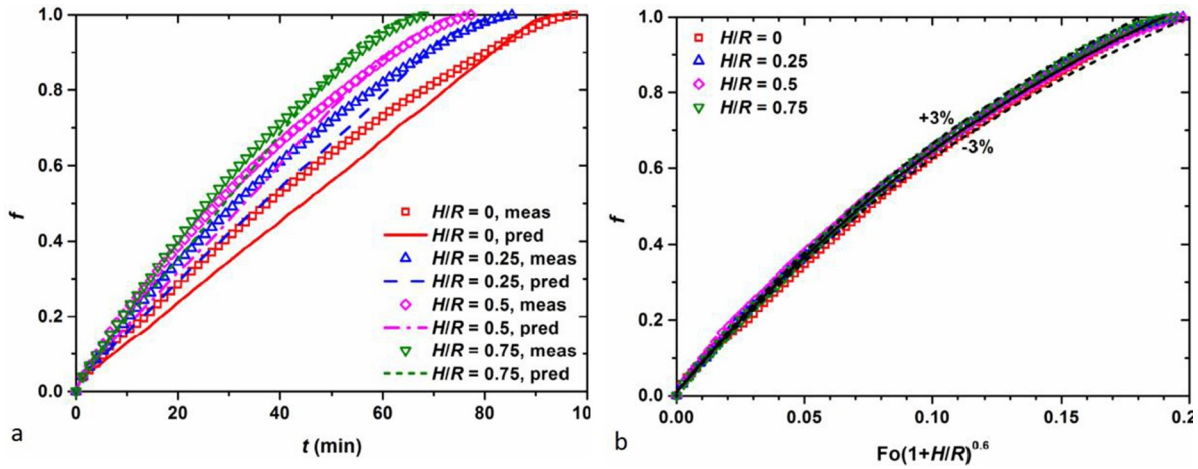

Fig. 50. Variation of the molten fraction with time for various fin heights: a – measured and predicted values versus dimension time; b – measured values versus dimensionless time [119].

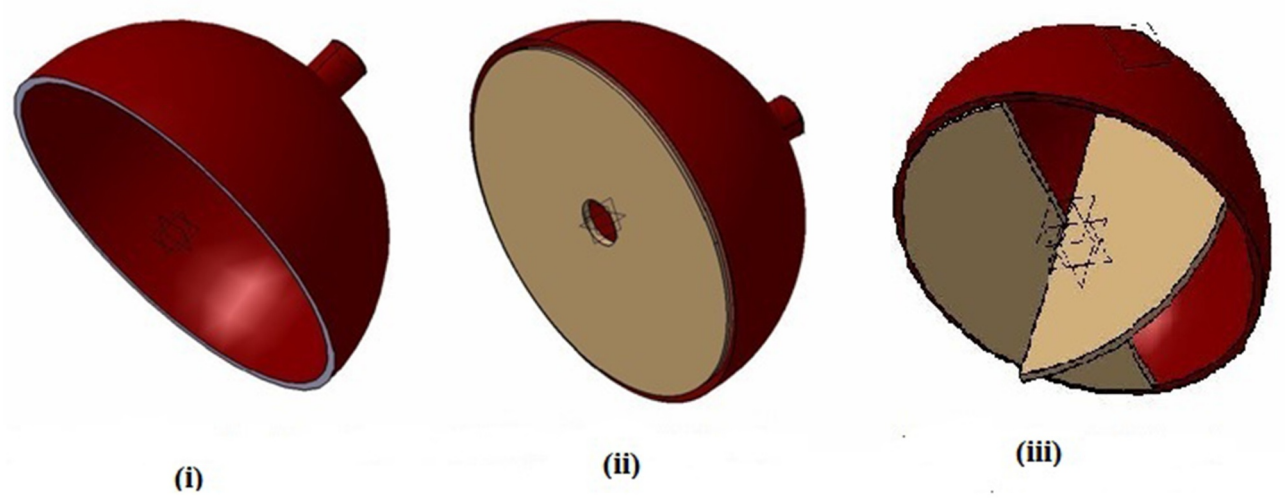

Fig. 51. Cross section of spherical container with different fin configurations i) without fin; ii) circumferentially finned spherical container; iii) orthogonally finned spherical container [121].

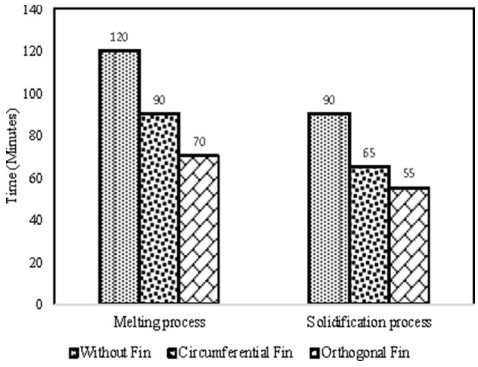

Fig. 52. Comparison of melting and solidification times for different finned spherical capsules [121].

circumferentially finned spherical capsule. The experimental rig, used in work, is shown in Fig. 49. The spherical capsule, as well as water tanks, were made of Plexiglas to provide transparency in the experiment. The aluminum annular-shaped fin was mounted between two hemispherical shells with flanges. The inner diameter of the assembled capsule was 100 mm, with a wall thickness of 2 mm. The fin thickness D was fixed at 2 mm, while the effective fin height H inside the sphere was varied. To maintain the solid PCM at the fixed position, a thin wood stick with a radius of 1 mm was used. The comparison of experimental data and computational results is presented in Fig. 50a. The measured melting duration times are 98, 86, 78, and 69 min for the cases, in which H/R was equal to 0, 0.25, 0.5 and 0.75, respectively. The corresponding predicted values were 94, 84, 75, and 67 min, respectively. The actual melting rate was overestimated by a small margin in the numerical simulations. The relative reduction of the melting time for the finned cases, in which H/R = 0.25, 0.5, and 0.75 with respect to the "no fins" base case was found, in both experimental and numerical studies, to be approximately 11, 20 and 29%, respectively. Thus, the adding a circumferential straight fin with H/R = 0.75, enhanced heat transfer by 30%. Using the approach, suggested by Kamkari and Shokouhmand in [120], Fan et al. [119] proposed the following correlation for calculation of the molten fraction in terms of the modified dimensionless time and fin height

$$f_m = 1.6262 - 1.6166\, exp\left[-\frac{Fo\left(1+\frac{H}{R}\right)^{0.6}}{0.2003}\right] \quad (54)$$

where coefficients were determined by curve fitting of results shown in Fig. 50b.

As it can be seen, the measured changes in the molten fraction almost coincide with the curve, calculated by the above correlation. The coefficient for curve fitting is as high as 0.9989 with a very small relative deviation, being within only ± 3%. Since the Gr and Ste numbers were kept constant in the study, then these are not present in the correlation.

Govindaraj et al. [121] carried out investigation of the melting and solidification processes in a spherical container with the following three configurations: without fin, with circumferential fin and, finally, with orthogonal fin, see Fig. 51. Each capsule has the opening at the top for the filling by PCM and inserting thermocouples vertically. All these stainless-steel spherical capsules had an internal diameter of 88 mm and a wall thickness of 1 mm. The finned spherical capsule had the fin surface area of 5,976 mm^2. Commercial paraffin wax with the phase change temperature ranging between 50.5 and 63 °C was used as the PCM. Fig. 52 compares the total time needed for charging and discharging spherical containers with different orientations. It can be seen in Fig. 52 that the time duration required for complete charging of PCM, was longer compared to the discharging process. The prolonged duration for the charging process is due to the inclusion in the process

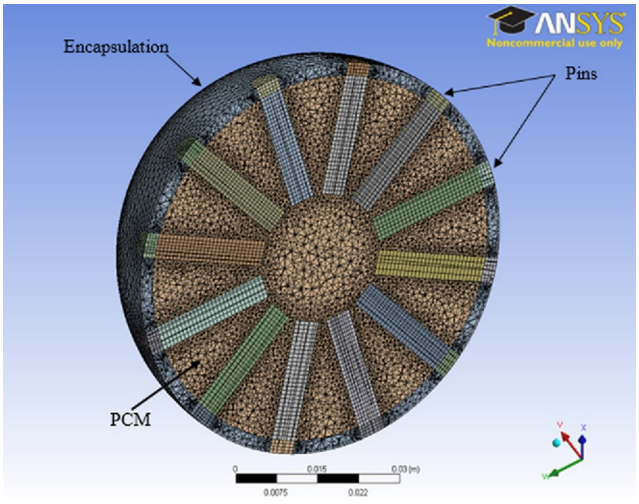

Fig. 53. The cut section of the meshed model of the PCM sphere with pins [121].

Fig. 54. Design modifications of the sphere: (a) a plain plastic sphere, (b) a plain sphere encapsulated with 32 copper pins, and (c) a copper-plated sphere with 32 internally built copper pins [122].

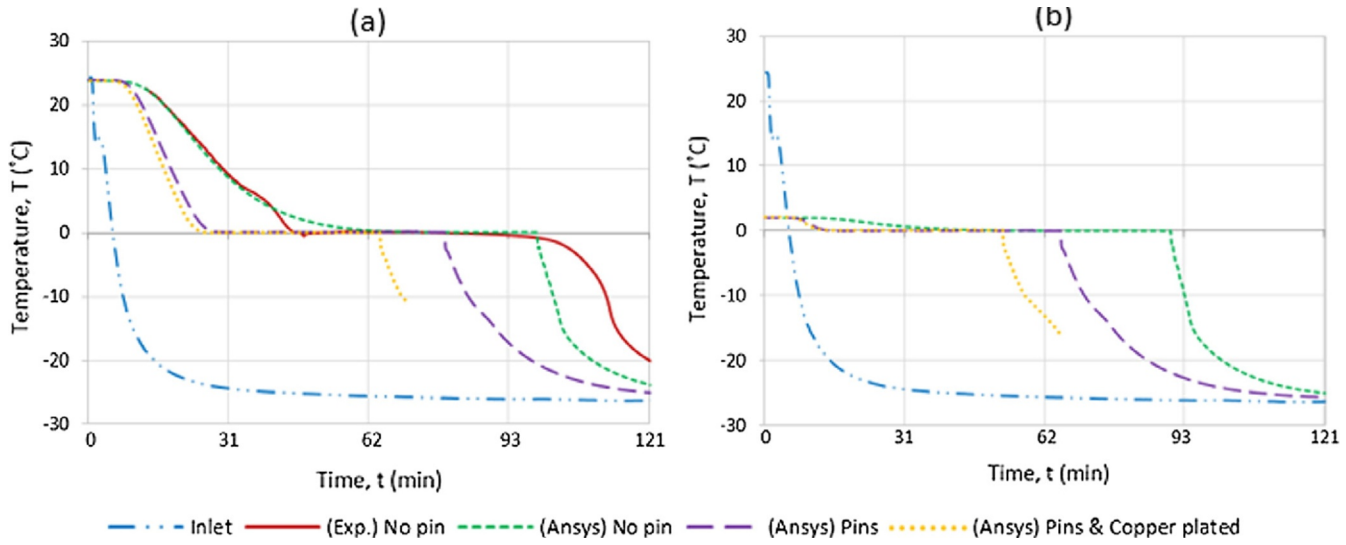

Fig. 55. Comparisons of Ansys CFD software results with various types of encapsulation for HTF with $\dot{m}$ = =0.021 kg/s and T_{in} = = −26 °C and the PCM initial temperatures (a) T_{init} = =24 °C, (b) T_{init} = =2 °C; [122].

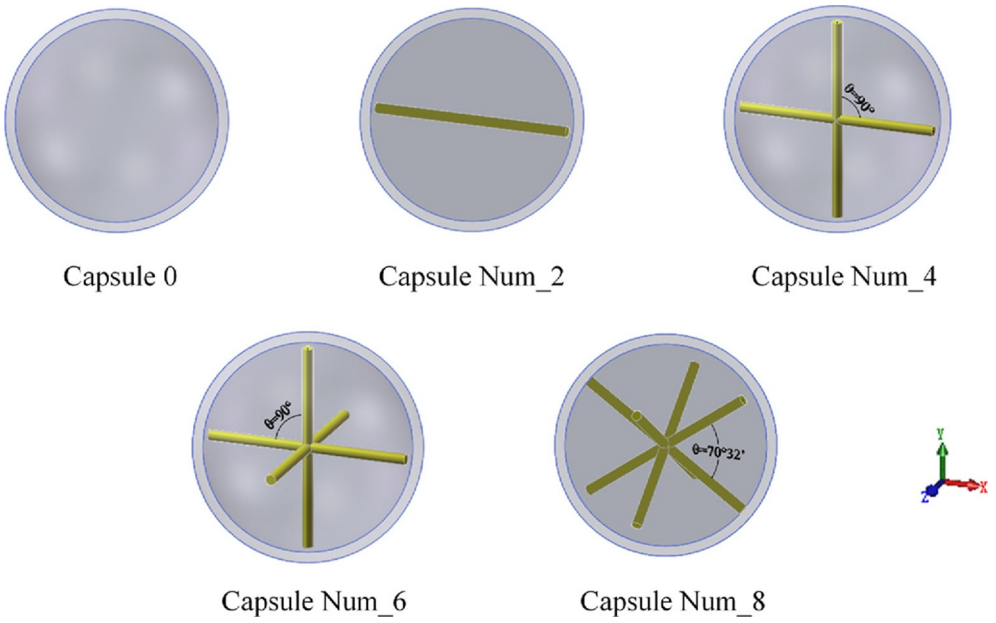

Fig. 56. Configurations of capsules with different fin numbers [123].

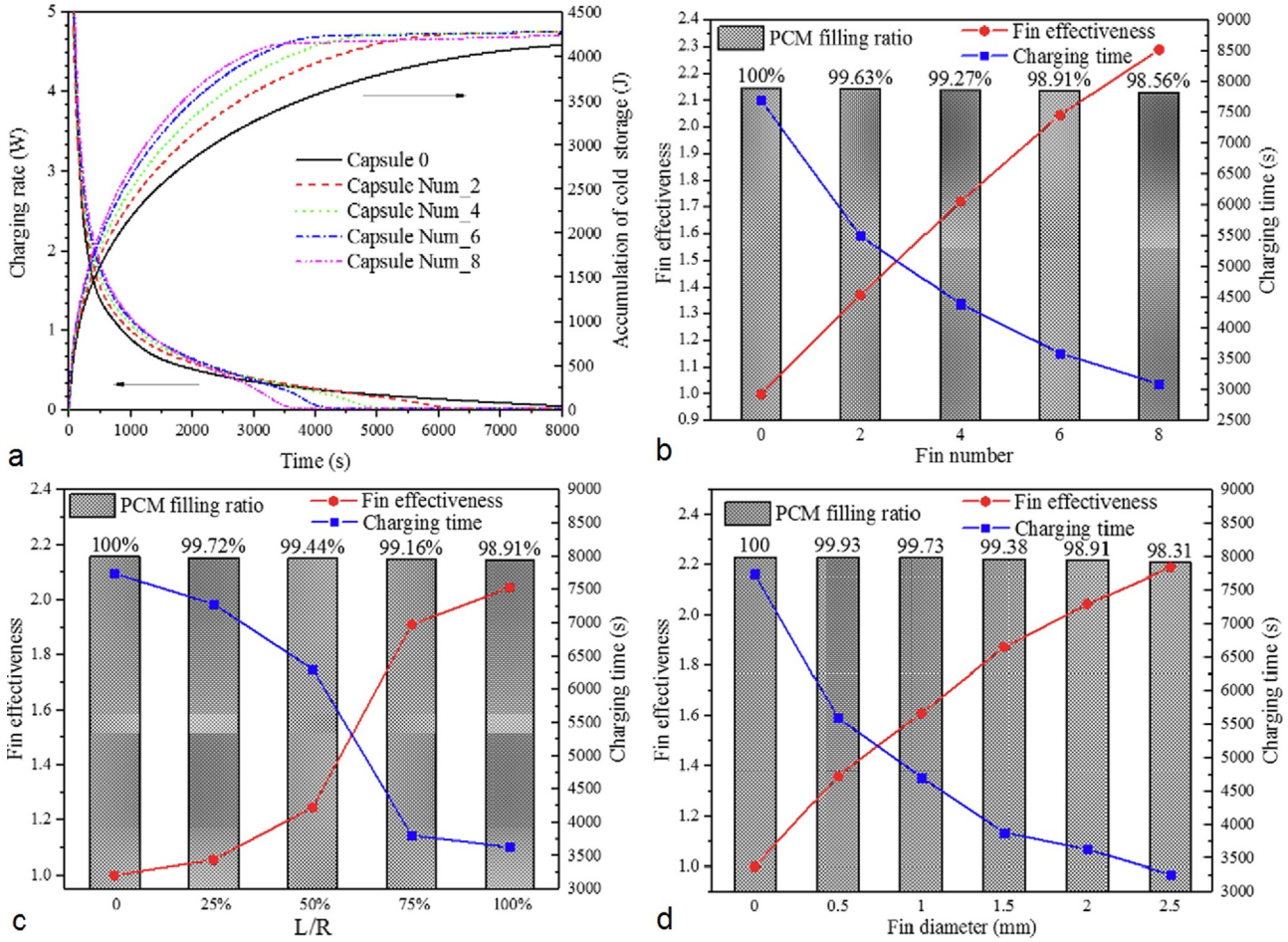

Fig. 57. Results of analysis: a – Charging rate and accumulated cold stored in each capsule; b – influence of pin number on PCM filling ratio, pin effectiveness and charging time; c – influence of L/R on PCM filling ratio, pin effectiveness and charging; d – influence of pin diameter on PCM filling ratio, pin effectiveness and charging time [123].

of sensible heat energy.

Aziz et al. [122] studied the effect of the heat transfer enhancement in the thermal energy storage (TES) system with PCM, encapsulated in a sphere. To enhance the performance, the spherical capsule was modified by deploying pins and copper plating. Computational simulations with the use of Ansys CFX V15 software were compered to data from experimental studies. The tested TES system comprising a single encapsulated PCM sphere (see Fig. 53) with a diameter of 74 mm and containing 32 square copper pins, which are 25.4 mm in length and with a cross-section of 2 × 2 mm, was located in the middle of a well-insulated cylindrical tank. Three configurations of the sphere, see Fig. 54, were used in the study. The first configuration was a sphere with an outer diameter of 74 mm, encapsulated by 2.5 mm-thick medium density polyethylene. The same sphere was modifed for another two configurations using additional conducting pins embedded into the sphere and copper plating.

The PCM, used in the study, was potable water. The HTF was a viscous fluid capable of operating at −40 °C, namely Dynalene HC-40. The range of mass flow rate used in the simulation studies was in the range between 0.031 kg/s and 1.0 kg/s. Typical results obtained are shown in Fig. 55. There was no evaluation of the effect of pin numbers, pin material and its dimensions on the heat transfer characteristics.

Just recently, Jia et al. [123] reported the results of experimental and numerical studies of a spherical PCM container with pin-fins for cold storage and its optimization. In contrast to [122], Jia et al. [123] investigated the effect of circular pin numbers. The influence of the pin length and diameter was also studied to obtain their optimal value. The configurations of the spherical containers with different pin numbers are presented in Fig. 56. The spherical shell, with the inner diameter of 40 mm and wall thickness of 2 mm, was welded to the inner pins so that molten PCM can be placed into the encapsulation between the outer shell and inner pins. The shell and fins are both made of the 6061-aluminum alloy. The capric acid-lauric acid-oleic acid (CA-LA- OA) composite was chosen as the PCM. The simulation of the solidification process was carried out using ANSYS Fluent 18.0 software. The outer wall temperature of the capsule TL for all cases was set to 7 °C, while their initial temperature To was assumed to be 22 °C. The study was run using four different fin numbers of capsules: 0, 2, 4 and 6 (cases Capsule 0, Capsule Num_2, Capsule Num_4 and Capsule Num_6, respectively). The experiment was performed for two different initial temperatures: To = =22 and 25 °C. The experiments were repeated three times to ensure the reproducibility of experimental data. A comparison of the simulated values and experimental data produced a good agreement with deviations less than 6.9%. The main results are shown in Fig. 57. The comprehensive numerical simulation results, which the authors obtained, were not used for deriving the correlation for the dimensionless times as a function of dimensionless parameters, which account for physical properties of the PCM, materials of the spherical shell, number and dimensions of pins and sphere.

3.5. The effective thermal conductivity correlations of the PCM constrained melting in spherical envelopes

Investigations of Bedecarrates et al. [33, 36] have shown the use of

Table 12
Parameters of HTF and PCM during melting tests [124].

HTF mass flow rate (kg/s)	PCM initial temperature (°C)	HTF inlet temperature (°C)	Effective thermal conductivity (W/mK)
0.058	−28	18	1.9
0.052	−27	12	1.3
0.056	−27	11	1.21
0.054	−28	8	1.1

the effective thermal conductivity in modeling the melting heat transfer of water inside spherical capsule permits to simplify the mathematical modelling the packed bad LHSS. These studies stimulated set new research on the effective thermal conductivity of PCMs.

Amin et al. [124] using CFX Ansys 12-1 program developed a CFD simulation model of heat transfer in phase change material contained in a spherical capsule. In the developed model, the buoyancy forces of the PCM are ignored. The PCM was set as a homogeneous binary mixture of water and ice, with the default thermal properties of 0 °C reference temperature. Therefore, the density, thermal conductivity, and other properties of the PCM were assumed constant in the numerical simulations, which only varies marginally over the temperature range considered. For validation of simulation results, the experimental study of charging (solidifying) and discharging (melting) modes in the spherical thermal energy storage capsule of 74 mm in diameter and 2.5 mm thickness has been conducted. Glycol solution was used as heat transfer fluid while the water was served as the PCM. The experimental test results are given in Table 12. Comparing melting tests to the SFD modeling results, it was suggested the following empirical correlation for estimation of the effective thermal conductivity of the PCM (water) in the spherical enclosure:

$$\frac{k_{eff}}{k} = 0.3847 \cdot 10^{-7} \cdot Ra + 1.5859. \tag{55}$$

The equation is valid for $6.8 \times 10^6 < Ra < 4.4 \times 10^7$. The hydraulic diameter of the PCM used for calculation Rayleigh number D_{pcm} is the inner diameter of the sphere.

Liao et al. [125] studied numerically the constrained melting process of the PCM ($NaNO_3$) in a spherical shell (steel) with an inner diameter 50 mm and a shell thickness of 0.2 mm. The numerical modeling results is then validated by comparing with the experimental data obtained by Fan et al. [119] for n-octadecane as the PCM (Fig. 58).

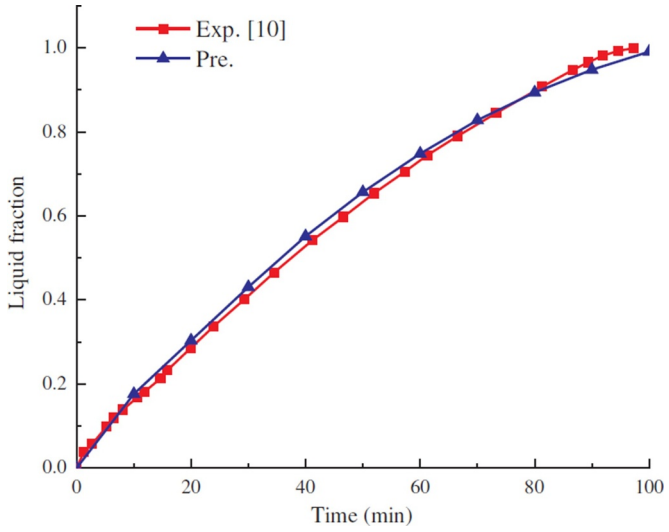

Fig. 58. Comparison of the liquid fraction during the melting process between the Fan et al. [119] result (Exp. [10]) and the simulating result of Liao et al. [125] (Pre.).

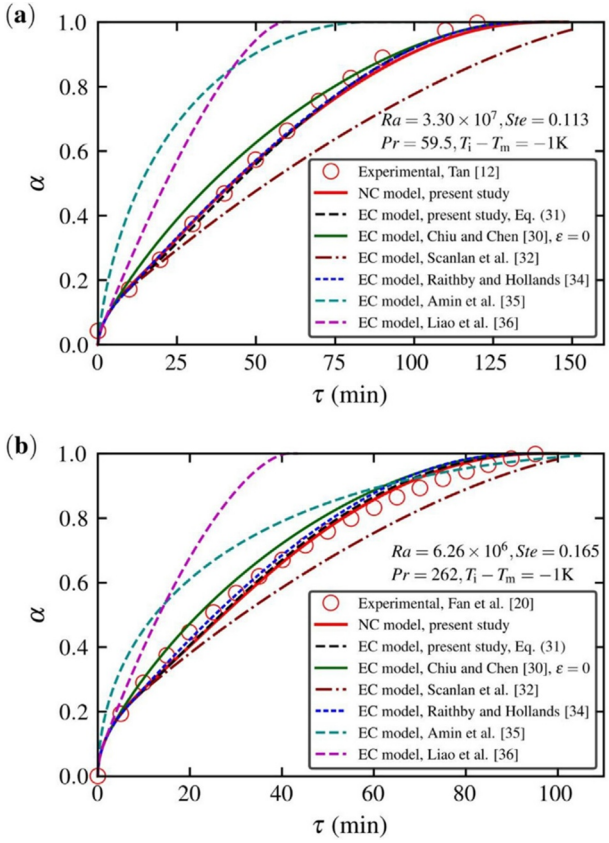

Fig. 59. Comparisons of melting fractions predicted by correlation (57), NC model and the results for the melting inside a sphere obtained in other works [126].

As seen in Fig. 58, the results predicted by the used simulation model agree well with experimental results, and deviation is smaller the 3%. Based on this comparison, it was proposed for estimating the effective thermal conductivity the following empirical correlation:

$$\frac{k_{eff}}{k} = 0.174\, Ra^{0.323}, \quad \text{for } 10^3 < Ra < 5 \times 10^8. \tag{56}$$

Here the characteristic length of the Rayleigh number is the gap spacing δ between the solid-liquid interface and the inner surface of the spherical shell.

Recently, Gao et al. [126] applied a new approach in developing an effective thermal conduction correlation for the prediction of natural convection affected constrained melting process inside a sphere. In contrast to previous studies [124, 125], the present approach is based on considering the melting fraction α (the dimensionless parameter as it was shown in previous sections) is widely used for the melting problem. The used numerical model was validated by comparison of predicted results with experimental data of Tan [48]. Numerical studies result in the following correlation of the effective thermal conduction was proposed

$$\frac{k_{eff}}{k} = 0.129 \alpha^{1.407} Ra^{0.257}. \tag{57}$$

The correlation is valid for $1.5 \times 10^4 \le Ra \le 6.3 \times 10^7$; $17 \le Pr \le 550$; $0.011 \le Ste \le 0.276$. Here the characteristic length is $\delta = = R_o - R_i = = R_o\,(1 - (1 - \alpha)^{1/3})$. Fig. 59 presents the comparison between the predicted results of Gao et al. [126] for the melting fractions inside a sphere and the results obtained with using correlations of other researchers. It is seen that the predictions made by the correlations of Gao et al. [122] and Raithby and Holland [127] are in good agreement with experimental data of Tan [46] and Fan et al. [119]. It is worth noting

that the correlation of Raithby and Holland was obtained for single phase natural convection heat transfer between concentric spheres. The correlations of Amin et al. [124] and Liao et al. [125] are overestimate the molten fractions observed in experiments.

4. Discussion

State of the art on investigations of phase change materials inside spherical shells was analyzed in this paper. Below we discuss the main results of reviewed works.

Constrained melting. As it was shown in Section 3.1, the constrained melting studies were described in eight publications [47-54]. Comparison of the time fixed profiles of PCMs in Fig. 2–Fig. 9 clearly shows that the physics of melting process of the fixed solid PCM is very complex. From experiments, it follows that the sliding of solid takes place during its melting, and the rate of sliding depends on the design of the fixing elements and Stefan number. A comparison of the above figures reveals that not all mathematical models, used for the description of constrained melting, adequately describe the real physical process of melting. As it follows from Fig. 6, that only 3-D numerical simulation, performed by Galione et al. [51], produces results close to experimental observations. Thus, available numerical simulation and experimental results are not fully sufficient to firmly recommend a certain correlation for ultimate evaluation of the complete time of melting and the rate of constrained melting. It essential to emphasize that Li et al. [52] were close to obtaining the correlation, derived from using numerical data (see Fig. 7), for calculation of the molten fraction as a function of dimensionless time. The shortcoming was that generalization of results for unconstrained melting was not performed to the level as in Assis et al. [71], Archibold et al. [74, 78, 79].

Unconstrained melting. Unconstrained melting inside a sphere, as it follows from Section 3.2, was studied to a larger extent compared to the constrained melting. Thus, the unconstrained melting was studied in 26 papers [55-84] with experimental studies being described in eleven works [48, 60, 66-68, 71, 73, 75, 77, 80]. In all these works, except [60, 68, 81], studies on PCM melting were performed in water baths. All obtained data from these experimental investigations was used for verification and validation of the developed mathematical models. Toksoy and İlken [60], Ettouney et al. [68], and Hariharan [81] have studied the charging and discharging processes in the spherical container with the PCM in the airflow. Using produced experimental data, they proposed dimensionless correlations for calculation of the time for complete melting and solidification, as well as heat transfer between the spherical container and the ambient HTF (air). Taking into account the fact that water, salt compositions, and oil (as heat transfer media) are often used in many heat storage systems, it is reasonable to study heat transfer characteristics of PCMs in containers of the spherical form. The time of complete melting of PCMs can be evaluated by using analytical correlations, suggested by Bahrami and Wang [56], Fomin and Saitoh [65], and Veerappan et al. [72]. The accuracy of correlations derived in these works is quite high with errors, not exceeding 20%. The results of all experimental works, which are under discussion, are presented in graphical and tabulated forms for better comparison purposes. The absence of numerical data restricts the range of application of dimensionless correlations and their further usefulness. The application of experimental results for the verification and validation of mathematical models is of paramount importance. It is necessary to mention the experimental work of Eames and Adref [66, 67]. These works are the only works in which the rate of energy stored was found, and having information on such an important parameter is very beneficial for practical purposes. As far as numerical studies are concerned, it is worth pointing out that there is a trend to present results as dimensionless correlations, relating main parameters in the melting of PCMs [71, 74, 77-80]. It necessary to mention that the first correlation (15) obtained by Assis et al. [71] was based on their own experiments. All other numerical simulation results were verified with experimental data presented in [71]. It would also appropriate to highlight the work of Bulunti and Arslantürk [70], who reported main results in the graphical form, and which could be further turned into a dimensionless correlation.

Solidification. As presented in Section 3.3, the process of solidification was studied at least in 34 published papers. The analytical correlations for determination of the time of solidification were obtained in [85, 86, 88-93]. The minimum time required for complete solidification and determined in the above works for the sphere, immersed in the media with a constant temperature, was of the same magnitude and can be expressed by Eq. (25). According to Hill and Kucera [92], the maximum time of complete solidification can be evaluated using the correlation (35).

The experimental studies were performed in [66, 67, 91, 105-113, 115, 117], however, the results obtained in these works do not always correlate with each other. All comments made above on the study of Eames and Adref [66, 67] of melting process, are also relevant and valid for the solidification stage of the process. The comprehensive study of Assis et al. [101] resulted in the correlation (45) for the calculation of the molten fraction during the solidification process. The correlations obtained in other experiments in [115, 117,118] are also used for practical applications. The change in the solidified mass fraction in time, reported in [106, 107], was obtained for two compositions based on water. The absence of measured thermophysical properties and presentation of data only in the graphical form makes results less attractive for practical purposes. It should be noted that the experiments performed by Chinese researchers in [112, 117] are completed with proposed dimensionless correlations (46), (47), (48), and (49). However, most of numerical studies do not produce dimensionless correlations, which could expand the applicability of their investigations. An example of an exception in this list is [101].

Melting and solidification in finned and pinned spherical containers. To our knowledge, there are four works, [119, 121-123], in which the phase change characteristics of PCMs inside finned or pinned spherical enclosures were studied. Fan et al. [119] suggested Eq. (54) for evaluation of the molten fraction as a function of the dimensionless time and height of circumferential fin. The second study of Govindaraj et al. [121] clearly demonstrated that the application of orthogonal fin is preferable compared to circumstance one. The results of [123] after revision by Jia et al. can be presented in the form of a dimensionless correlation.

The effective thermal conductivity correlations of the PCM constrained melting in spherical envelopes. As it was shown, there are only three publications [124-126], in which the correlations of the effective thermal conduction have been proposed. The comparison of these correlations in [126] that results of predictions made with using correlations of Amin et al. [124] and Liao et al. [125] are significantly overestimate of melting rate in comparison with experiments as well as prediction calculated by the correlation of Gao et al. [126]. These significant discrepancies are mainly caused by inadequate choosing the characteristic size δ in the Rayleigh number that reflects the hydraulic gap between the phase change interface and the inner diameter of spherical shell. The range of applicability of the correlation (59) of Gao et al. [126] is restricted by the cases considered in [126] and cannot captured all potential PCMs.

Table 13 summarises the brief data of all reviewed original papers. Results from nine publications have restricted applicability for solving practical issues. The results in most investigations are applicable only in the narrow range of conditions, applied in each case. Applicability of the proposed analytical equations requires rigorous validation by experimental data. The most of experimental, analytical, and numerical studies were performed for the cases in which the spherical capsules were placed in the baths with a constant temperature, though in numerous real applications, a heat transfer fluid flows around the capsules.

Table 13
The generalized data of original studies on phase change heat transfer in spherical capsules containing PCMs.

Researchers	Type of study	Material of PCM	Material of container	Border conditions	Type of presentation of results	Applicability of results for designing spherical TES with other PCM
1	2	3	4	5	6	7
Constrained (fixed) melting						
Khodadadi and Zhang [47]	C & E	Silicon (comp.) Paraffin wax (exp.)	NA Glass	Constant wall temperature	Visual observation. Qualitative description of melting process	Not applicable
Tan [48]	E	N-octadecane	Glass	Water bath with constant temperature	Visual observation. Qualitative description of melting process	Not applicable
Tan et al. [49]	N	N-octadecane	Glass	Constant wall temperature	Graphical comparison of experimental and computational results	Not applicable
Khot [50]	El	Paraffin wax	Glass	Bath constant temperature	Visual observation. Graphical presentation of liquid fraction variation with time for different Stefan number	Not applicable
Galione et al. [51]	Cl	N-octadecane	NA	Constant wall temperature	Graphical presentation of liquid fraction variation with time. The 3-D computational model interface is practically coincides with experimental observations of Tan	Not applicable
Li et al. [52]	N	Paraffin wax	Aluminium, Steel, Plastic	Constant wall temperature	Graphical presentation of molten fraction variation versus time for different diameter, bath temperature, PCM thermal conductivity, and container material	It is applicable for the cases similar to those considered in the study
Sattari et al. [53]	Nl	N-octadecane	Glass	Constant wall temperature	Graphical presentation of molten fraction variation versus time for different bath temperature	It is applicable for the cases similar to those considered in the study
Soni et al. [54]	N	N-octadecane	NA	Constant wall temperature	Graphical comparison of experimental and computational results	Not applicable
Unconstrained melting						
Moore and Bayazitoglu [55]	C	N-octadecane	Glass	Water bath with constant temperature	Graphical comparison of the dimensionless interface position with *Fo* for low *Ste*	It is applicable for the cases similar to those considered in the study
Bahrami and Wang [56]	T	NA	NA	Constant wall temperature	$\tau = (\frac{Ste}{PrA\gamma})^{1/4}(\frac{\rho s}{\rho l})(1.56\xi + 0.279\xi^2 + 0.261\xi^3 - 0.0686\xi^4)$	This equation can be used for determination of the time of complete melting for any PCM
Roy and Sengupta 57]	N	NA	NA	Constant wall temperature	Graphical presentation of variation of the dimensionless drop of interface with dimensionless time	It is applicable for the cases similar to those considered in the study
Toksoy and İlken [60]	E	$CaCl_2$•$6H_2O$	Glass	Air flow with constant temperature	The results presented in tabular and graphical forms. Tabular data can be used for validation of numerical studies	Tabular data can be used for validation of numerical studies
Saitoh et al. [63]	T	Water	NA	Constant wall temperature	Graphical presentation of molten mass fraction with dimensionless time	It is applicable for water as PCM. It overestimates in comparison with data of Bahrami & Wang [73]
Hu & Shi [64]	N	NA	NA	Constant wall temperature	Graphical comparison obtained results for the dimensionless interface position with dimensionless time wit data of 72,73]	It is applicable for the cases similar to those considered in the study
Fomin and Saitoh [65]	A & N	NA	NA	Constant wall temperature	$\tau_m = \frac{(\sqrt{2}+A)}{2} + \frac{(\sqrt{2}+A+B)Ste}{8}$	Analytical solution can be used for the estimation of the time complete melting for any PCM
Eames and Adref [66,67]	El	Water	Glass	Constant wall temperature	$Q = -1.44k_iT_c(0.12\frac{t^*}{R_0} - 1)$ and $Q = 4k_wT_c(0.3\frac{t^*}{R_0} - 1)^2$	The empirical equations derived from experimental results can be used for designing the ice storage systems
Ettouney et al. [68]	E	Paraffin wax	Copper	Air flow with constant temperature	$Fo_m = 0.199\ Ste^{-0.56}Bi^{-0.212}$ And $Fo_s = 0.344\ Ste^{0.62}Bi^{-2.01}$	The empirical equations derived from experimental results can be used for designing the latent storage systems with air as HTF
Regin et al. [69]	E & N	Paraffin wax	HDPE	Water bath with constant temperature	Graphical presentation of the molten fraction with time and the time of complete melting with radius of the sphere for various Stefan numbers	It is applicable for the cases similar to those considered in the study
Buluntu & Arslantürk [70]	Nl	NA	NA	Convective and radiation heating	Graphical presentation of the dimensionless interface location with Fourier number and the time of complete melting with Stefan number	It is applicable for the cases similar to those considered in the study

(*continued on next page*)

Table 13 (*continued*)

1	2	3	4	5	6	8
Assis et al. [71]	N & E	Parrafin wax RT27	Glass	Water bath with constant temperature	$MF = 1 - (1 - \frac{FoSte^{\frac{1}{3}}Gr^{\frac{1}{4}}}{1.9})^{\frac{3}{2}}$	The empirical formula allows to calculate mass molten fraction with time and consequently the time of complete melting
Tan [47]	E	N-octadecane	Glass	Water bath with constant temperature	Visual observation. Graphical presentation of variation of the liquid fraction with time for various Stefan number	Not applicable
Veerappan et al. [72]	A	NA	NA	Constant wall temperature	Analytical correlations	The derived correlations can be used
Koizumi [73]	N & E	N-octadecane	Plastic	Water bath with constant temperature	Visual observation. Graphical presentation of variation of the liquid fraction with time for different diameter of the sphere	Not applicable
Archibold et al. [74]	N	Sodium nitrate	Aluminium	Constant wall temperature	$LMF = 1 - (1 - \frac{FoSte^{\frac{1}{3}}Gr^{\frac{1}{4}}}{2.9})^2$	The empirical correlation can be used for the evaluation of main characteristics of a spherical storage unit
Rizan et al. [75]	E	N-octadenane	Pyrex flask	Constant heat flux	The results of experiments presented in graphical and tabular forms for	The tabular data can be used for validation of the numerical modelling of PCM
Hosseinzadeh et al. [76]	N	Paraffin wax RT27 + copper nano particles	NA	Constant wall temperature	Graphical presentation of the molten fraction variation with time for different content of nano-particles	Not applicable
Hosseinzadeh et al. [77]	N & E	N-octadenane	Glass	Water bath with constant temperature	$MF = 6.64\ \theta^{1.07}\exp(-22\theta)\ \ln Gr$	The empirical correlation can be used for the evaluation of main characteristics of a spherical storage unit
Archibold et al. [78]	N	Sodium nitrate	Nickel alloy	Constant wall temperature	$MF = 1 - [1 - \frac{FoSte^{0.37}Gr^{0.25}}{2.8}]^{2.35}$	The empirical correlation can be used for the evaluation of main characteristics of a spherical storage unit
Archibold et al. [79]	N	Sodium nitrate Parrafin wax RT27	Nickel alloy	Constant wall temperature	$MF = 1 - [1 - \frac{FoSte^{0.33}Gr_R^{0.27}Pr^{0.37}\chi^{0.72}\xi^{-0.02}}{9.5}]^{1.8}$	The empirical correlation can be used for the evaluation of main characteristics of a spherical storage unit
Fan et al. [80]	E	1-dodecanol	Stainless steel	Constant wall temperature	$MF = 1.102 - 1.101exp(-\frac{FoSte^{0.33}Gr^{0.1}}{0.129})$	The empirical correlation can be used for the evaluation of main characteristics of a spherical storage unit
1	2	3	4	5	6	8
Hariharan [81]	C & E	Paraffin	NA	Air flow with constant temperature	Graphical presentation of variation of the PCM temperature with time	Not applicable
Gosh and Guha [82]	N & E	Parrafin wax RT27	Aluminum Copper, Glass	Water bath with constant temperature	Visual observation. Grafical presentation of variation of the melt fraction for different material of the spherical capsule	Not applicable
Gao et al. [83]	E	Paraffin	Glass	WBCT	$\alpha = 0.374Fo^{0.712}Ste^{0.243}Ra^{0.166}S_i^{-0.094}\varepsilon^{-0.192.}$	The empirical correlation can be used for the evaluation of characteristics of a spherical storage unit
Lago et al. [84]	E	Water and water-PEG	Plastic	Thermal bath	$t_{complete\ melting} = 4.7 \times 10^5 D^{0.99}(1 - W)^{2.34}\lvert T_{inl}\rvert^{0.033}T_{bath}{}^{-0.53}$	The empirical correlation can be used for the evaluation of the time of complete melting of ice, ice-polyethylene glycol mixtures
Solidification						
London and Seban [85]	A	Water	NA	Constant wall temperature	$\tau_f = FoSte = \frac{1}{6} + \frac{1}{3Bi}$	The formula can be used for evaluation of the time of complete freesing of water
Tao [86]	A & N	NA	NA	Constant wall temperature	$\tau_f = FoSte = \frac{1}{6} + \frac{1}{3Bi}$	The formula can be used for evaluation of the time of complete freezing of any liquid

(*continued on next page*)

Table 13 (*continued*)

1	2	3	4	5	6	8
Shih and Chou [87]	Analitic-al iteration method	NA	NA	Constant wall temperature	The formulas for analytical calculation of the solidification time versus dimensionless parameters	The use of formulas give the results that sufficiently differ from numerical results
Pedroso and Domoto [88, 89]	A	NA	NA	Constant wall temperature	$\tau = FoSte = \frac{3(r^*-1)^2+2(r^*-1)^3}{6} + \frac{(r^*-1)^3 Ste}{6} - \frac{1}{45}\frac{(r^*-1)^2 Ste^2}{r^*}$	The formula can be used for evaluation of the time of complete freezing of any liquid
Riley [90]	Analyti-cal	NA	NA	CWT	$\tau_f = FoSte = \frac{1}{6} + \frac{Ste}{6} - \frac{Ste^{\frac{3}{2}}}{3(2\pi)^{\frac{1}{2}}} + \ldots$	The formula can be used for evaluation of the time of complete freezing of any liquid
Kern and Wells [91]	A	NA	NA	Constant wall temperature	$Fo_f(Ste \to 0) = \frac{1}{Ste}(\frac{1}{3Bi} + \frac{1}{6})$	The formula can be used for evaluation of the time of complete freezing of any liquid
Hill and Kucera [92]	Semi-analy-tical	NA	NA	Constant wall temperature	$t^*_{fmin} = Fo_{fmin} = (\frac{2}{Bi} + 1)/6Ste$ and $t^*_{fmax} = Fo_{fmax} = (\frac{1}{Ste} + 1)(\frac{2}{Bi} + 1)/6$	The formula can be used for evaluation of the time of complete freezing of any liquid
Milanez and Ismail [93]	A	NA	NA	Constant wall temperature	$\tau_f = Fo_f Ste = \frac{1}{6} + \frac{1}{3Bi}$	The formula can be used for evaluation of the time of complete freezing of any liquid
Caldwell and Chan [94]	N	NA	NA	Constant wall temperature	Graphical presentation of variation of the solid-liquid interface position with dimensionless time	Not applicable
Ismail and Henriquez [95, 96]	N	NA	NA	Constant wall temperature	Graphical presentation of variation of solidifaied mass fraction with time for different sphere radius, temperature of external HTF and different Bio numbers	The result can be used only for cases considered in the study

1	2	3	4	5	6	8
Lin and Jiang [97]	Quasi-steady analysis	NA	NA	Constant wall temperature	$Fo_f = t_f = \frac{1+\exp(p_m^2)}{12Ste}$	The formula can be used for evaluation of the time of complete freezing of any liquid
Bilir and İlken [98]	N	NA	NA	Constant wall temperature	$t_f = Fo_f = 0.5012181 \times Ste^{-0.9070384} \times Bi^{-0.1864788} \times \theta^{-0.9843633}$	The formula can be used for evaluation of the time of complete freesing of water
Chan and Tan [99]	E	N-hexadecade	Fluminum	Water bath with constant temperature	Graphical presentation of variation of solidifaied fraction with time for three different bath temperature	The result can be used only for cases considered in the study
Teggar et al. [100]	N	NA	NA	Constant wall temperature	Graphical presentation of variation of the solidification front with dimensionless time	Not applicable
Assis et al. [101]	N & E	Parrafin wax RT27	Thin plastic	Water bath with constant temperature	$MF = [1 - 2.25(FoSte)^{1/2}]^2$	The formula can be used for evaluation of the time of complete freezing of any liquid
Ismail and Moraes [103]	N & E	Water and its glycol mixtures	Glass plastic	Water bath with constant temperature	Graphical presentation of results	The result can be used only for cases considered in the study
Rajeev and Das [104]	N	NA	NA	Constant wall temperature	Graphical presentation of the molten fraction variation with dimensionless time	The result can be used only for cases considered in the study
ElGhnam et al. [105]	E	Water	Copper, glass, brass, stainless steel, plastic	HTF flow with constant temperature	Graphical presentation of results	The result can be used only for cases considered in the study
Chandrasekaran et al. [106-109]	E	Water, water nano-compositions	LDPE	Water-ethylene glycol bath with constant temperature	Graphical presentation of results	The result can be used only for cases considered in the study
Satishkumar et al. [110]	E	Water/GNP	LDPE	Water-ethylene glycol BCT	Tabular and graphical presentation of results	Tabular data can be used for validation of numerical simulation results

(*continued on next page*)

Table 13 (*continued*)

1	2	3	4	5	6	8
Liu et al. [111]	E	1-tetradecanol	Stainless steel	Water bath with constant temperature	Graphical presentation of variation of the solidified fraction in time	The result can be used only for cases considered in the study
Liu et al. [112]	E	1-tetradecanol	Stainless steel	Water bath with constant temperature	$f_s = 0.0382 + 3.32(FoSte)^{0.5} - 2.87(FoSte)$	The formula can be used for evaluation of the time of complete solidification
Temirel et al. [113]	E	Eicosane and eicosane/GNP	Stainless steel	Water bath with constant temperature	Graphical presentation of variation of the solidified volume fraction in time	The result can be used only for cases considered in the study
Asker et al. [114]	N	Water	NA	Constant wall temperature	Graphical presentation of variation of the interface position in time	Not applicable
1	2	3	4	5	6	8
Sakr et al. [115]	E	Water/ γ-Al_2O_3	LDPE	Water bath with constant temperature	$SF = 1 - (1 - \frac{FoSte^{1/3}Ra^{1/4}\chi^{1/4}}{48})^{3.75}$	The formula can be used for evaluation of the time of complete solidification
Narasimhan et al. [116]	N	NA	NA	Constant wall temperature	The results are presented in graphical and tabular forms	Tabular data can be used for the cases similar to considered
Zhu et al. [117]	E	1-tetradecanol/ GNP	Stainless steel	Water bath with constant temperature	$f_m = \frac{\exp[-B(FoSte)]}{1 + A\ (FoSte)}$	Correlations for melting fraction and Nusselt number can be used for prediction of performances of spherical TES
Nazzi Ehms et al. [118]	N	Erythritol	NA	Constant wall temperature	$\beta = LF = [1 - \ (3.8FoSte)^{1/2}]^2$	The formula can be used for evaluation of the time of complete solidification
Lago et al. [84]	E	Water and water-polyethylene glycol	Plastic	Thermal bath	$t_{complete\ solidification} = 1.09 \times 10^8 D^{2.704} \lvert T_{bath} \rvert^{-1.243} (1 - W)^{-0.781}$	The empirical correlation can be used for the evaluation of the time of complete solidification of water, water-polyethylene glycol mixtures
Melting and solidification in finned and pinned spherical capsules						
Fan et al. [119]	E &N	N-octadecane	Plexiglas	Water bath with constant temperature	$f_m = 1.6262 - 1.6166\ exp[-\frac{Fo(1 + \frac{H}{R})^{0.6}}{0.2003}]$	Correlations for melting fraction and Nusselt number can be used for prediction of performances of spherical TES
Govindaraj et al. [121]	E	:Paraffin wax	Stainless steel	Water bath with constant temperature	The results are presented in graphical form	The results can be used only for cases considered in the study
Aziz et al. [122]	C & E	Water	Plastic	Water bath with constant temperature	Graphical presentation of variation of the PCM temperature with time	The results can be used only for the case considered in the study
Jia et al. [123]	E & N	CA-LA-OA blend	Aluminum	Water bath with constant temperature	Graphical presentation of variation of the solidification time with pin number, pin diameter and length	The results can be used only for cases considered in the study
The effective thermal conductivity correlations of the PCM constrained melting in spherical envelopes						
Amin et al [124]	N & E	Water	Medium density polyethylene	Glycol based liquid flow with constant temperature	$\frac{k_{eff}}{k} = 0.3847 \cdot 10^{-7} \cdot Ra + 1.5859.$	The correlation can be used in simulating the melting process
Liao et al [125]	N	$NaNO_3$	Steel	CWT	$\frac{k_{eff}}{k} = 0.174\ Ra^{0.323}$	The correlation allow to estimate the effective thermal conduction
Gao et al. [126]	N	N-octadecane, 1-Dodecanol		WBCT	$\frac{k_{eff}}{k} = 0.129\alpha^{1.407} Ra^{0.257}$	The melting fraction estimated with using the present correlation gives a better prediction than using the previously reported correlations [124, 125]

Type of study: A – analytical; C – computational; E –experimental; N—Numerical; T –theoretical. Type of phase change: M- melting; S – Solidification; Border conditions: BCT – bath with constant temperature; CWT-constant wall temperature; WBCT – water bath with constant temperature. Other abbreviations: GNP – graphite nanoplatelets; LDPE – low density polyethylene; NA – not available.

5. Conclusions

It is well known that the thermal processes, involving convective heat transfer are difficult to be described without using criterial equations with dimensionless parameters due to the large amount of solid, liquid, and gaseous matters participating in the process of heat transfer. Melting and solidification of PCMs are not exceptions from this rule. As highlighted, research groups of E. M. Sparrow and R. Viskanta carried out fundamental investigations on heat transfer in PCMs in the USA. However, these studies had mainly of an academic character. The rapid development of technology and creation of a large amount of perspective PCMs, which can be efficiently and feasibly used in practice, stimulated a new round of intensive investigations on the heat transfer in PCMs. These studies were aimed at determination of the duration of complete melting or solidification processes and the rate of energy storing or releasing in the process of phase change. This review shows that the most studies on the PCM melting and solidification were performed at a fixed HTF temperature, which is the simplest case for describing outside thermal conditions. Such approach does not ensure high accuracy calculation of the practical heat transfer characteristics for available PCMs. There is an obvious shortage in comprehensive and systematic experimental studies of the heat transfer during PCM melting and solidification, covering a wide range of phase change materials, heat transfer fluids, types of heat exchangers and initial and boundary conditions. Therefore, the following recommendations can be made for future work in this field:

1 For PCMs, the heat transfer characteristics of which are being investigated, their thermophysical properties should be reliably measured including the melting point, heat of fusion, thermal conductivity, density, specific heat in the solid and liquid state as well as viscosity in the temperature region close to the melting point.
2 When melting and solidification behaviour of the mixtures or compositions is investigated, then their thermophysical properties should be also accurately measured. Particularly it concerns the viscosity in the mushy zone, which may vary by several orders of magnitude. Practice shows that incorrect value of this parameter significantly contributes to the departure of numerical simulation results from experimental data.
3 To simplify verification of numerical data, it is advisable to present experimental results in both tabular and graphical forms.
4 The experimental or numerical results of investigations are recommended to present in the dimensionless form.
5 Along with the presentation of correlations for calculation of the change in liquid fraction, it would be useful to produce correlations for calculation of the energy storing/releasing rates, the rate of melting/solidification, and the time required for complete melting/solidification.
6 Further investigations of phase change behaviour of PCMs inside a spherical capsule, exposed to the flow of typical heat transfer fluids, are necessary.
7 Systematic comparison of all known correlations with the use of all available experimental database would be very beneficial for practical applications.

Declaration of competing interest

None.

Acknowledgments

This study was funded by European Union's Horizon 2020 Research and Innovation Program (Project Grant Agreement 723596 - INNOVA MICROSOLAR) and H2020-MSCA-IF-2015 Program (Project Grant Agreement 705944 - THERMOSTALL).

Supplementary materials

Supplementary material associated with this article can be found, in the online version, at doi:10.1016/j.est.2019.101082.

References

[1] G.A. Lane, Solar heat storage: latent heat materials, Background and Scientific Principles 1 CRC Press Inc, Boca Raton, 1983.
[2] H. Mehling, L.F. Cabeza, Heat and cold storage with PCM, An Up to Date Introduction Into Basics and Applications, Springer, Berlin, 2008.
[3] A.M. Khudhair, M.M. Farid, A review on energy conservation in building applications with thermal storage by latent heat using phase change materials, Energy Convers. Manage. 45 (2) (2004 Jan 1) 263–275.
[4] S. Jegadheeswaran, S.D. Pohekar, Performance enhancement in latent heat thermal storage system: a review, Renewable Sustainable Energy Rev. 13 (9) (2009 Dec 1) 2225–2244.
[5] F. Agyenim, N. Hewitt, P. Eames, M. Smyth, A review of materials, heat transfer and phase change problem formulation for latent heat thermal energy storage systems (LHTESS), Renewable Sustainable Energy Rev. 14 (2) (2010 Feb 1) 615–628.
[6] T. Nomura, N. Okinaka, T. Akiyama, Technology of latent heat storage for high temperature application: a review, ISIJ Int. 50 (9) (2010 Sep 15) 1229–1239.
[7] Climator Sweden A.B.https://www.climator.com/en/pcm-climsel/product-data-sheets.
[8] Cristopia Energy Systems. http://cristopia.com/EN/Public/fr-FR/catalogue.pdf.
[9] Entropy Solutions Inc.http://www.puretemp.com/stories/puretemp-technical-data-sheets.
[10] Microtek Laboratories, Inc.https://www.microteklabs.com/product-data-sheets.
[11] PCM Products Ltd.https://www.pcmproducts.net.
[12] RGEES, LLC.https://rgees.com/products.php.
[13] Rubitherm GmbH.https://www.rubitherm.eu/en/index.php/productcategory/organische-pcm-rt.
[14] PCM Energy P. Ltd.https://www.teappcm.com.
[15] M. Kenisarin, K. Mahkamov, Solar energy storage using phase change materials, Renewable Sustainable Energy Rev. 11 (9) (2007 Dec 31) 1913–1965.
[16] S.E. Kalnæs, B.P. Jelle, Phase change materials and products for building applications: a state-of-the-art review and future research opportunities, Energy Build. 94 (2015 May 1) 150–176.
[17] R Viskanta, Phase-change heat transfer. chapter 5, in: G.A. Lane (Ed.), Solar Heat storage: Latent heat materials. Volume 1. Background and Scientific Principles, CRC Press Inc, Boca Raton, 1983, pp. 153–222 Ed..
[18] L.S. Yao, J. Prusa, Melting and freezing, Adv. Heat Transf. 19 (1989) 1–95.
[19] M. Toksoy, B.Z. İlken, Phase change heat transfer in cylindrical domain: modelling and its importance in the thermal energy storage, in: B. Kılkış, S. Kakaç (Eds.), Energy Storage Systems, Kluwer Academic Publishers, 1989, pp. 191–229.
[20] S. Sengupta, S.K. Roy, Gravity-assisted melting in enclosures, in: B. Kılkış, S. Kakaç (Eds.), Energy Storage Systems, Kluwer Academic Publishers, 1989, pp. 383–413.
[21] S. Fukusako, M. Yamada, Melting heat transfer inside ducts and over external bodies, Exp. Therm. Fluid Sci. 19 (2) (1999 Feb 1) 93–117.
[22] B. Zalba, J.M. Marín, L.F. Cabeza, H. Mehling, Review on thermal energy storage with phase change: materials, heat transfer analysis and applications, Appl. Therm. Eng. 23 (3) (2003 Feb 28) 251–283.
[23] S. Liu, Y. Li, Y. Zhang, Review on heat transfer mechanisms and characteristics in encapsulated PCMs, Heat Transf. Eng. 36 (2014) 880–901.
[24] N.S. Dhaidan, J.M. Khodadadi, Melting and convection of phase change materials in different shape containers: a review, Renewable Sustainable Energy Rev. 43 (2015) 449–477 Mar 31.
[25] C.Y. Zhao, Review on thermal transport in high porosity cellular metal foams with open cells, Int. J. Heat Mass Transf. 55 (13–14) (2012 Jun 1) 3618–3632.
[26] J.M. Khodadadi, L. Fan, H. Babaei, Thermal conductivity enhancement of nanostructure-based colloidal suspensions utilized as phase change materials for thermal energy storage: a review, Renewable Sustainable Energy Rev. 24 (2013 Aug 31) 418–444.
[27] A.F. Regin, S.C. Solanki, J.S. Saini, Heat transfer characteristics of thermal energy storage system using PCM capsules: a review, Renewable Sustainable Energy Rev. 12 (2008) 2438–2451.
[28] J.P. Bedecarrats, F. Strub, B. Falcon, J.P. Dumas, Phase-change thermal energy storage using spherical capsules: performance of a test plant, Int. J. Refrig. 19 (3) (1996 Jan 1) 187–196.
[29] K. Cho, S.H. Choi, Thermal characteristics of paraffin in a spherical capsule during freezing and melting processes, Int. J. Heat Mass Transf. 43 (2000) 3183–3196.
[30] K.A.R. Ismail, J.R. Henriquez, Numerical and experimental study of spherical capsules packed bed latent heat storage system, Appl. Therm. Eng. 22 (2002) 1705–1716.
[31] J.P. Bédécarrats, J. Castaing-Lasvignottes, F. Strub, J.P. Dumas, Study of a phase change energy storage using spherical capsules. Part I: experimental results, Energy Convers. Manage.. 50 (10) (2009 Oct 1) 2527–2536.
[32] P. Galione, O. Lehmkuhl, J. Rigola, A. Oliva, I.M Rodríguez, Numerical Simulations of Thermal Energy Storage Systems with Phase Change Materials, ISES Solar World Congress, 2011, pp. 1–12.
[33] M. Wu, C. Xu, Y.L. He, Dynamic thermal performance analysis of a molten-salt packed-bed thermal energy storage system using PCM capsules, Appl. Energy 121 (2014 May 15) 184–195.

[34] M.J. Li, B. Jin, Z. Ma, F. Yuan, Experimental and numerical study on the performance of a new high-temperature packed-bed thermal energy storage system with macroencapsulation of molten salt phase change material, Appl. Energy 221 (2018 Jul 1) 1–5.

[35] E. Alptekin, M. Özer, M. Top, F.E. Yavuz, M.A. Ezan, A numerical study on phase change inside a spherical capsule, Exergetic Energetic Environ. Dimensions (2018) 613–625.

[36] Cristopia Energy Systems – The STL Technology. Available at http://www.cristopia.com/EN/la-technologie-stl.html.

[37] M.N. Fard, H.T. Jokari, Experimental and numerical simulation of phase change material melting and solidification inside sphere capsule for thermal energy storage, 9th International Conference on Electrical, Computer, Mechanical and Mechatronics Engineering, Istanbul, Turkey, ICE-2018, 2018September 6-7.

[38] M. Bechiri, K. Mansouri, N. Hamlet, S Amirat, Numerical solution of NEPCM melting inside spherical enclosure, 3rd International Conference on Control, Engineering & Information Technology (CEIT), IEEE, 2015 May 25, pp. 1–4.

[39] K. Rachedi, A.I. Korti, Numerical simulation of melting and solidification of different kinds of phase change materials (pcm) encapsulated in spherical nodules in a water flow, Comput. Therm. Sci. 9 (4) (2017) 297–310.

[40] W. Li, Y.H. Wang, C.C. Kong, Experimental study on melting/solidification and thermal conductivity enhancement of phase change material inside a sphere, Int. Commun. Heat Mass Transf. 68 (2015) 276–282.

[41] M. Hlimi, S. Hamdaoui, M. Mahdaoui, T. Kousksou, A.A. Msaad, A. Jamil, A. El Bouardi, Melting inside a horizontal cylindrical capsule, Case Stud. Therm. Eng. 8 (2016 Sep 1) 359–369.

[42] R. Prabakaran, J.P. Kumar, D.M. Lal, C. Selvam, S. Harish, Constrained melting of graphene-based phase change nanocomposites inside a sphere, J. Therm. Anal. Calorim. (2019) In Press. Available at https://link.springer.com/article/10.1007/s10973-019-08458-4.

[43] H. Yang, J. Song, B. He, G Ding, Numerical study on charging characteristics of heat pipe-assisted cylindrical capsule for enhancing latent thermal energy storage, Solar Energy 190 (2019 Sep 15) 147–155.

[44] L.M Jiji, Heat Conduction, Third ed., Springer Verlag Berlin Heidelberg, 2009.

[45] E.M. Sparrow, R.R. Schmidt, J.T. Ramsey, Experiments on the role of natural convection in the melting of solids, J. Heat Transf. 100 (1) (1978 Feb 1) 11–16.

[46] N.W. Hale Jr, R. Viskanta, Photographic observation of the solid-liquid interface motion during melting of a solid heated from an isothermal vertical wall, Lett. Heat Mass Transf. 5 (6) (1978 Nov 1) 329–337.

[47] J.M. Khodadadi, Y. Zhang, Effects of buoyancy-driven convection on melting within spherical containers, Int. J. Heat Mass Transf. 44 (8) (2001 Apr 1) 1605–1618.

[48] F.L. Tan, Constrained and unconstrained melting inside a sphere, Int. Commun. Heat Mass Transf. 35 (4) (2008 Apr 1) 466–475.

[49] F.L. Tan, S.F. Hosseinizadeh, J.M. Khodadadi, L. Fan, Experimental and computational study of constrained melting of phase change materials (PCM) inside a spherical capsule, Int. J. Heat Mass Transf. 52 (15–16) (2009 Jul 1) 3464–3472.

[50] S.A. Khot, N.K. Sane, B.S. Gawali, Experimental investigation of phase change phenomena of paraffin wax inside a capsule, Int. J. Eng. Trends Technol. 2 (2) (2011).

[51] P.A. Galione, O. Lehmkuhl, J. Rigola, A. Oliva, Fixed-grid numerical modeling of melting and solidification using variable thermo-physical properties–application to the melting of n-octadecane inside a spherical capsule, Int. J. Heat Mass Transf. 86 (2015) 721–743.

[52] W. Li, S.G. Li, S. Guan, Y. Wang, X. Zhang, X. Liu, Numerical study on melt fraction during melting of phase change material inside a sphere, Int. J. Hydrogen Energy 42 (29) (2017 Jul 20) 18232–18239.

[53] H. Sattari, A. Mohebbi, M.M. Afsahi, A.A. Yancheshme, CFD simulation of melting process of phase change materials (PCMs) in a spherical capsule, Int. J. Refrig. 73 (2017) 209–218.

[54] V. Soni, A. Kumar, V.K. Jain, Modeling of PCM melting: analysis of discrepancy between numerical and experimental results and energy storage performance, Energy 150 (2018) 190–204.

[55] F.E. Moore, Y. Bayazitoglu, Melting within a spherical enclosure, J. Heat Transf. 104 (1) (1982 Feb 1) 19–23.

[56] P.A. Bahrami, T.G. Wang, Analysis of gravity and conduction-driven melting in a sphere, J. Heat Transf. 109 (3) (1987 Aug 1) 806–809.

[57] S.K. Roy, S. Sengupta, The melting process within spherical enclosures, J. Heat Transf. 109 (1987) 460–462.

[58] M. Bareiss, H. Beer, An analytical solution of the heat transfer process during melting of an unfixed solid phase change material inside a horizontal tube, Int. J. Heat Mass Transf. 27 (5) (1984 May 1) 739–746.

[59] F.E. Moore, Melting within a Spherical Enclosure, M. S. thesis Rice University, 1981.

[60] M. Toksoy, B.Z İlken, Melting in a spherical enclosure: an experimental study, in: B. Kılkış, S. Kakaç (Eds.), Energy Storage Systems, Kluwer Academic Publishers, 1989, pp. 735–742.

[61] B. Carlsson, G. Wettermark, Heat-transfer properties of a heat-of-fusion store based on $CaCl_2$•$6H_2O$, Solar Energy 24 (3) (1980 Jan 1) 239–247.

[62] A.D. Solomon, Melt time and heat flux for a simple PCM body, Solar Energy 22 (3) (1979 Jan 1) 251–257.

[63] T.S. Saitoh, H. Kato, H Hoshina, Theoretical analysis for combined close-contact and natural convection melting in ice storage spherical capsule, IECEC 96. Proceedings of the 31st Intersociety Energy Conversion Engineering Conference, 3 IEEE, 1996 Aug 11, pp. 2104–2108.

[64] Y. Hu, M. Shi, Close-contact melting in a spherical enclosure, Sci. China Ser. E 41 (1) (1998 Feb 1) 82–87.

[65] S.A. Fomin, T.S. Saitoh, Melting of unfixed material in spherical capsule with non-isothermal wall, Int. J. Heat Mass Transf. 42 (22) (1999 Nov 1) 4197–4205.

[66] I.W. Eames, K.T. Adref, Freezing and melting of water in spherical enclosures of the type used in thermal (ice) storage systems, Appl. Therm. Eng. 22 (7) (2002 May 1) 733–745.

[67] K.T. Adref, I.W. Eames, Experiments on charging and discharging of spherical thermal (ice) storage elements, Int. J. Energy Res. 26 (11) (2002 Sep 1) 949–964.

[68] H. Ettouney, H. El-Dessouky, A. Al-Ali, Heat transfer during phase change of paraffin wax stored in spherical shells, J. Solar Energy Eng. 127 (3) (2005 Aug 1) 357–365.

[69] A. Regin, S.C. Solanki, J.S Saini, Experimental and numerical analysis of melting of PCM inside a spherical capsule, 9th AIAA/ASME Joint Thermophysics and Heat Transfer Conference, 2006, p. 3618.

[70] B. Bulunti, C. Arslanturk, Analysis of inward melting of spheres subject to convection and radiation, J. Therm. Sci. Techonology. 26 (2) (2006) 11–16.

[71] E. Assis, L. Katsman, G. Ziskind, R. Letan, Numerical and experimental study of melting in a spherical shell, Int. J. Heat Mass Transf. 50 (9–10) (2007 May 1) 1790–1804.

[72] M. Veerappan, S. Kalaiselvam, S. Iniyan, R Goic, Phase change characteristic study of spherical PCMs in solar energy storage, Solar Energy 83 (8) (2009 Aug 1) 1245–1252.

[73] H. Koizumi, Time and spatial heat transfer performance around an isothermally heated sphere placed in a uniform, downwardly directed flow (in relation to the enhancement of latent heat storage rate in a spherical capsule), Appl. Therm. Eng. 24 (17–18) (2004) 2583–2600.

[74] A.R. Archibold, M.M. Rahman, D.Y. Goswami, E.L Stefanakos, Parametric investigation of the melting and solidification process in an encapsulated spherical container, ASME 2012 6th International Conference on Energy Sustainability collocated with the ASME 2012 10th International Conference on Fuel Cell Science, Engineering and Technology, 2012 Jul 23, pp. 573–584. American Society of Mechanical Engineers.

[75] M.Z. Rizan, F.L. Tan, C.P. Tso, An experimental study of n-octadecane melting inside a sphere subjected to constant heat rate at surface, Int. Commun. Heat Mass Transf. 39 (10) (2012 Dec 1) 1624–1630.

[76] S.F. Hosseinizadeh, A.R. Darzi, F.L. Tan, J.M. Khodadadi, Unconstrained melting inside a sphere, Int. J. Therm. Sci. 63 (2013 Jan 1) 55–64.

[77] S.F. Hosseinizadeh, A.R. Darzi, F.L. Tan, Numerical investigations of unconstrained melting of nano-enhanced phase change material (NEPCM) inside a spherical container, Int. J. Therm. Sci. 51 (2012 Jan 1) 77–83.

[78] A.R. Archibold, J. Gonzalez-Aguilar, M.M. Rahman, D.Y. Goswami, M. Romero, E.K. Stefanakos, The melting process of storage materials with relatively high phase change temperatures in partially filled spherical shells, Appl. Energy 116 (2014 Mar 1) 243–252.

[79] A.R. Archibold, M.M. Rahman, D.Y. Goswami, E.K. Stefanakos, Analysis of heat transfer and fluid flow during melting inside a spherical container for thermal energy storage, Appl. Therm. Eng. 64 (1–2) (2014 Mar 1) 396–407.

[80] L.W. Fan, Z.Q. Zhu, Y. Zeng, Q. Ding, M.J. Liu, Unconstrained melting heat transfer in a spherical container revisited in the presence of nano-enhanced phase change materials (NePCM), Int. J. Heat Mass Transf. 95 (2016 Apr 1) 1057–1069.

[81] K. Hariharan, G.S. Kumar, G. Kumaresan, R. Velraj, Investigation on phase change behavior of paraffin phase change material in a spherical capsule for solar thermal storage units, Heat Transf. Eng. 39 (9) (2018 May 28) 775–783.

[82] D. Ghosh, C. Guha, Numerical and experimental investigation of paraffin wax melting in spherical cavity, Heat Mass Transf. 55 (5) (2019 May 1) 1427–1437.

[83] Z. Gao, Y. Yao, H. Wu, A visualization study on the unconstrained melting of paraffin in spherical container, Appl. Therm. Eng. 155 (2019 Jun 5) 428–436.

[84] T.G. Lago, K.A. Ismail, F.A. Lino, A Arabkoohsar, Experimental correlations for the solidification and fusion times of PCM encapsulated in spherical shells, Experimental Heat Transfer (2019 Aug 31) 1–15, https://doi.org/10.1080/08916152.2019.1656301.

[85] A.L. London, R.A. Seban, Rate of ice formation, Trans. ASME 65 (7) (1943 Oct) 771–779.

[86] L.C. Tao, Generalized numerical solutions of freezing a saturated liquid in cylinders and spheres, AIChE J. 13 (1) (1967 Jan 1) 165–169.

[87] Y.P. Shih, T.C. Chou, Analytical solutions for freezing a saturated liquid inside or outside spheres, Chem. Eng. Sci. 26 (11) (1971 Nov 1) 1787–1793.

[88] R.I. Pedroso, G.A. Domoto, Inward spherical solidification—solution by the method of strained coordinates, Int. J. Heat Mass Transf. 16 (5) (1973 May 1) 1037–1043.

[89] R.I. Pedroso, G.A. Domoto, Perturbation solutions for spherical solidification of saturated liquids, J. Heat Transf. 95 (1) (1973 Feb 1) 42–46.

[90] D.S. Riley, F.T. Smith, G. Poots, The inward solidification of spheres and circular cylinders, Int. J. Heat Mass Transf. 17 (12) (1974 Dec 1) 1507–1516.

[91] J. Kern, G.L. Wells, Simple analysis and working equations for the solidification of cylinders and spheres, Metall. Trans. B 8 (1) (1977 Mar 1) 99–105.

[92] J.M. Hill, A. Kucera, Freezing a saturated liquid inside a sphere, Int. J. Heat Mass Transf. 26 (11) (1983 Nov 1) 1631–1637.

[93] L.F. Milanez, K.A. Ismail, Solidification in spheres, theoretical and experimental investigation, Multi-Phase 3rd International Conference on Multi-Phase and Heat Transfer, Miami, 1984.

[94] J. Caldwell, C.C. Chan, Spherical solidification by the enthalpy method and the heat balance integral method, Appl. Math. Modell. 24 (1) (2000 Jan 1) 45–53.

[95] K.A. Ismail, J.R. Henrıquez, Solidification of PCM inside a spherical capsule, Energy Convers. Manage. 41 (2) (2000 Jan 1) 173–187.

[96] K.A. Ismail, J.R. Henriquez, T.M. Da Silva, A parametric study on ice formation inside a spherical capsule, Int. J. Therm. Sci. 42 (9) (2003 Sep 1) 881–887.

[97] S. Lin, Z. Jiang, An improved quasi-steady analysis for solving freezing problems in a plate, a cylinder and a sphere, J. Heat Transf. 125 (6) (2003 Dec 1) 1123–1128.
[98] L. Bilir, Z. İlken, Total solidification time of a liquid phase change material enclosed in cylindrical/spherical containers, Appl. Therm. Eng. 25 (10) (2005 Jul 1) 1488–1502.
[99] C.W. Chan, F.L. Tan, Solidification inside a sphere—an experimental study, Int. Commun. Heat Mass Transf. 33 (3) (2006 Mar 1) 335–341.
[100] M. Teggar, E. Mezaache, Study of inward spherical solidification of phase change materials for low temperature use, 4th International Conference on Advances in Mechanical Engineering and Mechanics, Sousse, Tunisia, 2008 16-18 December2008 Dec.<.
[101] E. Assis, G. Ziskind, R. Letan, Numerical and experimental study of solidification in a spherical shell, J. Heat Transf. 131 (2) (2009 Feb 1) 024502.
[102] Susarla S. Discussion on: Assis, E., Ziskind, G., and Letan, R., 2009, Numerical and Experimental Study of Solidification in a Spherical Shell, ASME J. Heat Transfer 2009;131:024502. J. Heat Transfer. 2014 Jan 1;136(1):015501.
[103] K.A. Ismail, R.I. Moraes, A numerical and experimental investigation of different containers and PCM options for cold storage modular units for domestic applications, Int. J. Heat Mass Transf. 52 (19–20) (2009 Sep 1) 4195–4202.
[104] K. Rajeev, S. Das, A numerical study for inward solidification of a liquid contained in cylindrical and spherical vessel, Therm. Sci. 14 (2) (2010) 365–372.
[105] R.I. ElGhnam, R.A. Abdelaziz, M.H. Sakr, H.E. Abdelrahman, An experimental study of freezing and melting of water inside spherical capsules used in thermal energy storage systems, Ain Shams Eng. J. 3 (1) (2012 Mar 1) 33–48.
[106] P. Chandrasekaran, M. Cheralathan, V. Kumaresan, R Velraj, Enhanced heat transfer characteristics of water based copper oxide nanofluid PCM (phase change material) in a spherical capsule during solidification for energy efficient cool thermal storage system, Energy 72 (2014) 636–642.
[107] P. Chandrasekaran, M. Cheralathan, V. Kumaresan, R. Velraj, Solidification behaviour of water based nanofluid phase change material with a nucleating agent for cool thermal storage system, Int. J. Refrig. 41 (2014 May 1) 157–163.
[108] P. Chandrasekaran, M. Cheralathan, R Velraj, Effect of fill volume on solidification characteristics of DI (deionized) water in a spherical capsule–An experimental study, Energy 90 (2015 Oct 1) 508–515.
[109] P. Chandrasekaran, M. Cheralathan, R Velraj, Influence of the size of spherical capsule on solidification characteristics of DI (deionized water) water for a cool thermal energy storage system–An experimental study, Energy 90 (2015 Oct 1) 807–813.
[110] A. Sathishkumar, V. Kumaresan, R. Velraj, Solidification characteristics of water based graphene nanofluid PCM in a spherical capsule for cool thermal energy storage applications, Int. J. Refrig. 66 (2016 Jun 1) 73–83.
[111] M.J. Liu, Z.Q. Zhu, L.W. Fan, Z.T Yu, An experimental study of inward solidification of nano-enhanced phase change materials (NePCM) inside a spherical capsule, ASME 2016 Heat Transfer Summer Conference collocated with the ASME 2016 Fluids Engineering Division Summer Meeting and the ASME 2016 14th International Conference on Nanochannels, Microchannels, and Minichannels, ASME, 2016 Jul 10V002T08A016-V002T08A016.
[112] M.J. Liu, L.W. Fan, Z.Q. Zhu, B. Feng, H.C. Zhang, Y. Zeng, A volume-shrinkage-based method for quantifying the inward solidification heat transfer of a phase change material filled in spherical capsules, Appl. Therm. Eng. 108 (2016 Sep 5) 1200–1205.
[113] M. Temirel, H. Hu, H. Shabgard, P. Boettcher, M. McCarthy, Y. Sun, Solidification of additive-enhanced phase change materials in spherical enclosures with convective cooling, Appl. Therm. Eng. 111 (2017 Jan 25) 134–142.
[114] M. Asker, H. Ganjehsarabi, M.T. Coban, Numerical investigation of inward solidification inside spherical capsule by using temperature transforming method, Ain Shams Eng. J. 9 (4) (2018) 537–547.
[115] R.Y. Sakr, A.A. Attia, A.A. Altohamy, I.M. Elsemary, M.A. Rabbo, Heat transfer enhancement during freezing process of nano phase change material (NPCM) in a spherical capsule, Appl. Therm. Eng. 125 (2017 Oct 1) 1555–1564.
[116] N.L. Narasimhan, V. Veeraraghavan, G. Ramanathan, B.S. Bharadwaj, M. Thamilmani, Studies on the inward spherical solidification of a phase change material dispersed with macro particles, J. Energy Storage 15 (2018 Feb 28) 158–171.
[117] Z.Q. Zhu, M.J. Liu, N. Hu, Y.K. Huang, L.W. Fan, Z.T. Yu, J. Ge, Inward solidification heat transfer of nano-enhanced phase change materials in a spherical capsule: an experimental study, J. Heat Transf. 140 (2) (2018 Feb 1) 022301.
[118] J.N. Ehms, R.D. Oliveski, L.O. Rocha, C. Biserni, Theoretical and numerical analysis on phase change materials (PCM): a case study of the solidification process of erythritol in spheres, Int. J. Heat Mass Transf. 119 (2018 Apr 30) 523–532.
[119] L.W. Fan, Z.Q. Zhu, S.L. Xiao, M.J. Liu, H. Lu, Y. Zeng, Z.T. Yu, K.F. Cen, An experimental and numerical investigation of constrained melting heat transfer of a phase change material in a circumferentially finned spherical capsule for thermal energy storage, Appl. Therm. Eng. 100 (2016 May 5) 1063–1075.
[120] B. Kamkri, H. Shokouhmand, Experimental investigation of phase change material melting in rectangular enclosures with horizontal partial fins, Int. J. Heat Mass Transf. 78 (2014 Nov 30) 839–851.
[121] K. Govindaraja, P. Panchabikesan, D.C. Denkenberger, V. Ramalingam, Effect of fin orientations in a spherically encapsulated phase change materials for effective heat transfer enhancement, Chem. Eng. Trans. 62 (2017) 277–282.
[122] S. Aziz, N.A. Amin, M.A. Majid, M. Belusko, F. Bruno, CFD simulation of a TES tank comprising a PCM encapsulated in sphere with heat transfer enhancement, Appl. Therm. Eng. 143 (2018 Oct 1) 1085–1092.
[123] X. Jia, X. Zhai, X. Cheng, Thermal performance analysis and optimization of a spherical PCM capsule with pin-fins for cold storage, Appl. Therm. Eng. (2018 Nov 24).
[124] N.A. Amin, F. Bruno, M. Belusko, Effective thermal conductivity for melting in PCM encapsulated in a sphere, Appl. Energy 122 (2014 Jun 1) 280–287.
[125] Z. Liao, C. Xu, Y. Ren, F. Gao, X. Ju, X. Du, A novel effective thermal conductivity correlation of the PCM melting in spherical PCM encapsulation for the packed bed TES system, Appl. Therm. Eng. 135 (2018 May 5) 116–122.
[126] Z. Gao, Y. Yao, H. Wu, Validation of a melting fraction-based effective thermal conductivity correlation for prediction of melting phase change inside a sphere, Int. J. Therm. Sci. 142 (2019) 247–257.
[127] G.D. Raithby, K.G. Hollands, A general method of obtaining approximate solutions to laminar and turbulent free convection problems, Adv. Heat Transf. 11 (1975 Jan 1) 265–315.